

**Zeitschrift:** Eclogae Geologicae Helvetiae  
**Herausgeber:** Schweizerische Geologische Gesellschaft  
**Band:** 92 (1999)  
**Heft:** 1

**Artikel:** Structural and metamorphic evolution of the northern Himachal Himalaya, NW India (Spiti-eastern Lahul-Parvati valley traverse)  
**Autor:** Wyss, Martin / Hermann, Jörg / Steck, Albrecht  
**DOI:** <https://doi.org/10.5169/seals-168645>

### **Nutzungsbedingungen**

Die ETH-Bibliothek ist die Anbieterin der digitalisierten Zeitschriften auf E-Periodica. Sie besitzt keine Urheberrechte an den Zeitschriften und ist nicht verantwortlich für deren Inhalte. Die Rechte liegen in der Regel bei den Herausgebern beziehungsweise den externen Rechteinhabern. Das Veröffentlichen von Bildern in Print- und Online-Publikationen sowie auf Social Media-Kanälen oder Webseiten ist nur mit vorheriger Genehmigung der Rechteinhaber erlaubt. [Mehr erfahren](#)

### **Conditions d'utilisation**

L'ETH Library est le fournisseur des revues numérisées. Elle ne détient aucun droit d'auteur sur les revues et n'est pas responsable de leur contenu. En règle générale, les droits sont détenus par les éditeurs ou les détenteurs de droits externes. La reproduction d'images dans des publications imprimées ou en ligne ainsi que sur des canaux de médias sociaux ou des sites web n'est autorisée qu'avec l'accord préalable des détenteurs des droits. [En savoir plus](#)

### **Terms of use**

The ETH Library is the provider of the digitised journals. It does not own any copyrights to the journals and is not responsible for their content. The rights usually lie with the publishers or the external rights holders. Publishing images in print and online publications, as well as on social media channels or websites, is only permitted with the prior consent of the rights holders. [Find out more](#)

**Download PDF:** 12.12.2025

**ETH-Bibliothek Zürich, E-Periodica, <https://www.e-periodica.ch>**

# Structural and metamorphic evolution of the northern Himachal Himalaya, NW India

## (Spiti-eastern Lahul-Parvati valley traverse)

MARTIN WYSS<sup>1</sup>, JÖRG HERMANN<sup>2</sup> & ALBRECHT STECK<sup>1</sup>

**Keywords:** Himalayan tectonics, nappe tectonics, fold superposition, synorogenic extension, nappe extrusion, inverted metamorphic field gradient.

### ABSTRACT

The Himalayan orogen is the result of the collision between the Indian and Asian continents that began 55–50 Ma ago, causing intracontinental thrusting and nappe formation. Detailed mapping as well as structural and microfabric analyses on a traverse from the Tethyan Himalaya southwestward through the High Himalayan Crystalline and the Main Central Thrust zone (MCT zone) to the Lesser Himalayan Sequence in the Spiti-eastern Lahul-Parvati valley area reveal eight main phases of deformation, a series of late stage phases and five stages of metamorphic crystallization. This sequence of events is integrated into a reconstruction of the tectonometamorphic evolution of the Himalayan orogen in northern Himachal Pradesh.

The oldest phase D<sub>1</sub> is preserved as relics in the High Himalayan Crystalline. Its deformational conditions are poorly known, but the metamorphic evolution is well documented by a prograde metamorphism reaching peak conditions within the upper amphibolite facies. This indicates that D<sub>1</sub> was an important tectonometamorphic event including considerable crustal thickening. The structural, metamorphic and sedimentary record suggest that D<sub>1</sub> most probably represents an early stage of continental collision.

The first event clearly attributed to the collision between India and Asia is documented by two converging nappe systems, the NE-verging Shikar Beh Nappe and the SW-verging north Himalayan nappes. The D<sub>2</sub> Shikar Beh Nappe is characterized by isoclinal folding and top-to-the NE shearing, representing the main deformation in the High Himalayan Crystalline. D<sub>2</sub> also caused the main metamorphism in the High Himalayan Crystalline that was of a Barrovian-type, reaching upper amphibolite facies peak conditions. The Shikar Beh Nappe is interpreted to have formed within the Indian crust SW of the subduction zone. Simultaneously with NE-directed nappe formation, incipient subduction of India below Asia caused stacking of the SW-verging north Himalayan Nappes, that were thrust from the northern edge of the subducted continent toward the front of the Shikar Beh Nappe. As a result, the SW-verging folds of the D<sub>3</sub> Main Fold Zone formed in the Tethyan Himalaya below the front of the north Himalayan nappes. D<sub>3</sub> represents the main deformation in the Tethyan Himalaya, associated with a greenschist facies metamorphism. Folding within the Main Fold Zone subsequently propagated toward SW into the High Himalayan Crystalline, where it overprinted the pre-existing D<sub>2</sub> structures.

After subduction at the base of the north Himalayan nappes, the subduction zone stepped to the base of the High Himalayan Crystalline, where D<sub>4</sub> folds were crosscut by SW-directed D<sub>4</sub> thrusting. During D<sub>4</sub>, the Crystalline Nappe, comprising the Main Fold Zone and relics of the Shikar Beh Nappe was thrust toward SW over the Lesser Himalayan Sequence along the 4 to 5 kms thick Main Central Thrust zone. Thrusting was related to a retrograde greenschist facies overprint at the base of the Crystalline Nappe and to pro-

grade greenschist facies conditions in the Lesser Himalayan Sequence. Simultaneously with thrusting at the base of the Crystalline Nappe, higher crustal levels were affected by NE-directed D<sub>5</sub> normal extensional shearing and by dextral strike-slip motion, indicating that the high-grade metamorphic Crystalline Nappe was extruded between the low-grade metamorphic Lesser Himalayan Sequence at the base and the north Himalayan nappes at the top. The upper boundary of the Crystalline Nappe is not clearly delimited and passes gradually into the low-grade rocks at the front of the north Himalayan nappes.

Extrusion of the Crystalline Nappe was followed by the phase D<sub>6</sub>, characterized by large-scale, upright to steeply inclined, NE-verging folds and by another series of normal and extensional structures D<sub>7</sub>+D<sub>8</sub> that may be related to ongoing extrusion of the Crystalline Nappe. The late stage evolution is represented by the phases D<sub>A</sub> and D<sub>B</sub> that indicate shortening parallel to the axis of the mountain chain and by D<sub>C</sub> that is interpreted to account for the formation of large-scale domes with NNW-SSE-trending axes, an example of which is exposed in the Larji-Kullu-Rampur tectonic window.

### ZUSAMMENFASSUNG

Die Gebirgsbildung im Himalaja ist das Resultat der Kollision zwischen dem indischen und dem asiatischen Kontinent, welche vor 55–50 Millionen Jahren begann. Eine detaillierte Kartierung sowie Struktur- und Texturanalysen entlang einer Traverse durch den Tethyan Himalaya (unmetamorphe bis tiefmetamorphe Zone im NE des Himalaja), das High Himalayan Crystalline (mittel- bis hochmetamorphe Zone im Zentrum des Himalaja), den Main Central Thrust (zentrale Hauptüberschiebung) und die Lesser Himalayan Sequence (unmetamorphe bis tiefmetamorphe Einheiten südwestlich der Hauptüberschiebung) im Gebiet des Spititales, von Ostlahul und des Parvatitales im nördlichen Himachal Pradesh zeigen eine mehrphasige tektonische und metamorphe Entwicklung. Es können acht Hauptdeformationsphasen, einige Spätphasen und fünf Stadien metamorpher Kristallisation unterschieden werden. Auf der Basis dieser Beobachtungen wird versucht, die tektonische Entwicklung des Himalaja in Nord-Himachal Pradesh zu rekonstruieren.

Relikte einer ersten Phase D<sub>1</sub> treten im High Himalayan Crystalline auf. Die Deformationsbedingungen dieser Phase sind kaum bekannt, die metamorphe Entwicklung hingegen ist gut dokumentiert und erreichte die obere Amphibolitfazies. Dies bedeutet, dass D<sub>1</sub> zu einer starken Krustenverdickung führte und deshalb als eine wichtige Phase betrachtet werden muss, die sehr wahrscheinlich einem frühen Stadium der Kontinentalkollision zugeordnet werden kann.

Das Hauptereignis der Kontinentalkollision ist durch zwei konvergierende Deckensysteme dokumentiert, die NE-vergente Shikar-Behdecke und die

<sup>1</sup> Institut de Minéralogie et Pétrographie, Université de Lausanne, BFSH 2, CH–1015 Lausanne, Switzerland

<sup>2</sup> Institut für Mineralogie und Petrographie, ETH-Zentrum, CH–8092 Zürich, Switzerland



SW-vergenten Nordhimalajadecken. Isoklinale Falten und NE-gerichtete Scherbewegungen der D<sub>2</sub>-Shikar-Behdecke sind die Hauptstrukturen im High Himalayan Crystalline. Die dazu gehörende Hauptmetamorphose war prograd und erreichte Bedingungen im Bereich der oberen Amphibolitfazies. Die Shikar-Behdecke bildete sich innerhalb der indischen Kontinentalkruste südwestlich der Subduktionszone. Gleichzeitig mit der Überschiebung der Shikar-Behdecke entstanden auch die Nordhimalajadecken, welche während eines frühen Stadiums der Subduktion vom Nordostrand des subduzierten indischen Kontinents südwestwärts gegen die Front der Shikar-Behdecke geschoben wurden. An der Front der Nordhimalajadecken bildete sich eine SW-vergente Faltenzone, die D<sub>3</sub>-Hauptfaltenzone (Main Fold Zone), welche die Hauptdeformation im Tethyan Himalaya repräsentiert. Die Hauptfaltenzone propagierte in der Folge nach Südwesten, wo die Strukturen der D<sub>2</sub>-Shikar-Behdecke im High Himalayan Crystalline von SW-vergenten D<sub>3</sub>-Falten überprägt wurden. Die dazugehörige Metamorphose erreichte grünschieferfazielle Bedingungen im Tethyan Himalaya und Amphibolitfazies im High Himalayan Crystalline.

Nach der Bildung der D<sub>2</sub>- und D<sub>3</sub>-Decken sprang die Subduktionszone von der Basis der Nordhimalajadecken nach Südwesten zum 4-5 km breiten Main Central Thrust. Während der Phase D<sub>4</sub> wurde die hochmetamorphe Kristallindecke (Crystalline Nappe), welche die Hauptfaltenzone und Relikte der

Shikar-Behdecke enthält, nach Südwesten über die tiefmetamorphen Einheiten der Lesser Himalayan Sequence überschoben. Die Basis der Kristallindecke wurde dabei retrograd von einer grünschieferfaziellen Metamorphose überprägt. Gleichzeitig mit der SW-gerichteten Überschiebung entlang des Main Central Thrust entstanden in höheren Krustenbereichen D<sub>5</sub>-Extensionsstrukturen in Form von NE-gerichteten Abschiebungen und Falten-Reorientierungen sowie dextrale Blattverschiebungen. Das gleichzeitige Auftreten von SW-gerichteten Überschiebungen und NE-gerichteten Abschiebungen deutet darauf hin, dass die Kristallindecke zwischen der Lesser Himalayan Sequence an der Basis und den Nordhimalajadecken extrudiert wurde. Die Abschiebungen und Blattverschiebungen sind diffus verteilt. Aus diesem Grund ist die Kristallindecke gegen oben nicht klar begrenzt und geht fließend in die Basis der Nordhimalajadecken über.

Nach der Extrusion der Kristallindecke folgten NE-vergente D<sub>6</sub>-Rückfaltungen und Dombildungen sowie weitere Phasen mit Extensionsstrukturen D<sub>7</sub> und D<sub>8</sub>, welche höchstwahrscheinlich die Fortführung der Extrusion der Kristallindecke anzeigen. Die späte Entwicklung des Nordwesthimalaja ist geprägt durch die Phasen D<sub>A</sub>, D<sub>B</sub> und D<sub>C</sub>. D<sub>A</sub> und D<sub>B</sub> weisen auf eine Verkürzung parallel zur Achse des Orogens hin und D<sub>C</sub> bildete späte Dome mit NNW-SSE gerichteten Achsen.

## 1. Tectonic overview

The Himalayan orogen is the result of the continental collision between the Indian and the Eurasian plates that began between the latest Paleocene and early Eocene (Patriat & Achache 1984; Garzanti et al. 1987; Garzanti et al. 1996). The orogen is traditionally subdivided into five laterally continuous major tectonometamorphic units (Gansser 1964, Fig. 1). These are from north to south: (1) The Indus-Tsangpo Suture Zone (ITSZ) that is composed of ophiolites and oceanic sediments, representing the remnants of the Neotethys ocean and foreland arcs that separated India from the Cimmerian microcontinents (Tibetan Block) during the Mesozoic. (2) The Tethyan Himalaya (TH), consisting of a nearly complete stratigraphic section of generally low-grade metamorphic to non-metamorphic Upper Precambrian to Lower Eocene sediments that were deposited on the northern margin of the Indian plate (Gaetani et al. 1983, 1990). (3) The High Himalayan Crystalline (HHC), formed of medium- to high-grade metamorphic Precambrian to Jurassic sediments and Ordovician to Tertiary plutonic complexes (Frank et al. 1973, 1977; Steck et al. 1993a, b). (4) The Lesser Himalayan Sequence (LHS), mainly made up of the Proterozoic and Paleozoic Gondwanian sedimentary cover of the Indian continent and of Proterozoic metavolcanics, diabbases and granites (Frank et al. 1977, 1995; Bhat & LeFort 1992) that were overthrust by the High Himalayan Crystalline along the Main Central Thrust (MCT). (5) The Subhimalaya (SH) is composed of Tertiary molasse sediments (Siwaliks), resulting from erosion of the Himalayan chain during its uplift. It is separated from the Lesser Himalayan Sequence by the Main Boundary Thrust (MBT) and from the alluvial deposits of the Indo-Gangetic plain by the Himalayan Frontal Thrust.

Locally, wedged between the High Himalayan Crystalline and the Lesser Himalayan Sequence, a sixth unit, the Lesser

Himalayan Crystalline (LHC) occurs that consists of medium- to high-grade metamorphic metasediments and Proterozoic intrusions (for review see Vannay & Grasemann 1998).

According to paleomagnetic data (Besse et al. 1984), approximately 1000 km of the Indian plate margin has been underthrust below and/or accreted to the Asian continent after the closing of the Neotethys ocean at the Indus Suture Zone. This shortening caused a complex folding and mainly SW-propagating nappe formation within the leading edge of the subducted Indian plate. In the NW Himalaya, nappe structures can be observed in the Tethyan Himalaya, in the High Himalayan Crystalline and in the Lesser Himalayan Crystalline (Frank et al. 1973; Bassoulet et al. 1980; Steck et al. 1993a, b; Vannay & Grasemann 1998).

## 2. Introduction

This study deals with a transect from the Tethyan Himalaya through the High Himalayan Crystalline and the Main Central Thrust zone to the Lesser Himalayan Sequence. The major part of the transect is situated in regions where no detailed previous work had been carried out. The Tethyan Himalaya has been studied in the Taktshi valley, a tributary of the Spiti valley and in the northeastern upper Chandra valley in eastern Lahul. The High Himalayan Crystalline has been studied in the southwestern upper Chandra valley in eastern Lahul, in the Sara Umga valley, the Tos valley and the Parvati valley. The Main Central Thrust zone and the Lesser Himalayan Sequence have been investigated in the Brahmaganga- and Parvati valleys (Fig. 2, Plate 1). The study is part of a geological research program in the NW Himalaya that has been carried out by the Earth Sciences Department of the University of Lausanne since 1979. During this project, the geology of continuous traverses from the Indus-Tsangpo Suture Zone east of Leh in Ladakh to the Main Boundary Thrust near Mandi in the Beas

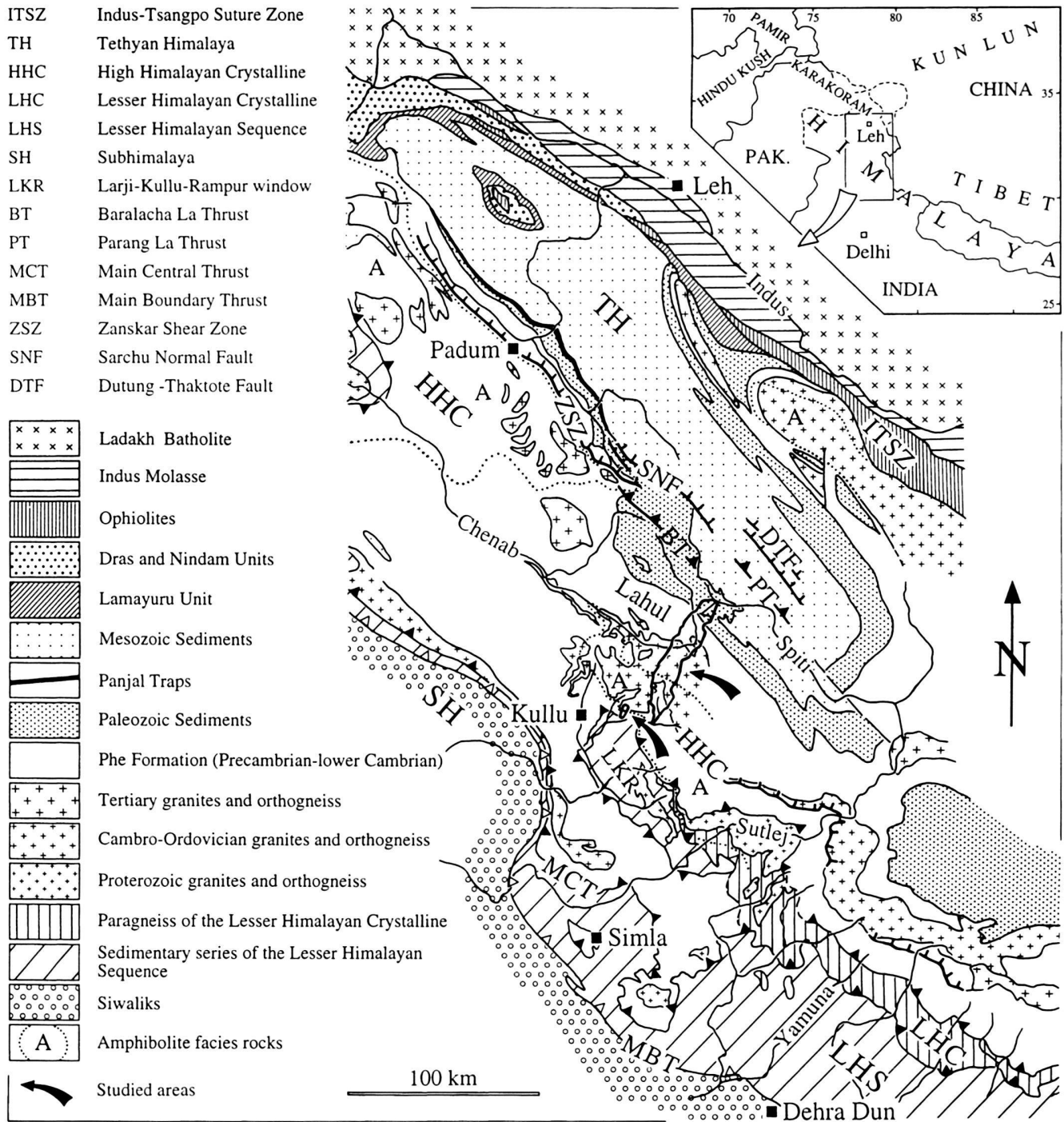


Fig. 1. Geological map of the NW Himalaya between Dehra Dun and Leh. Compiled after Hayden (1904), Frank et al. (1973), Thöni (1977), Steck et al. (1993a), Vannay (1993), Frank et al. (1995), Steck et al. (1998), Vannay & Grasemann (1998), Dèzes et al. (in press) and own data.

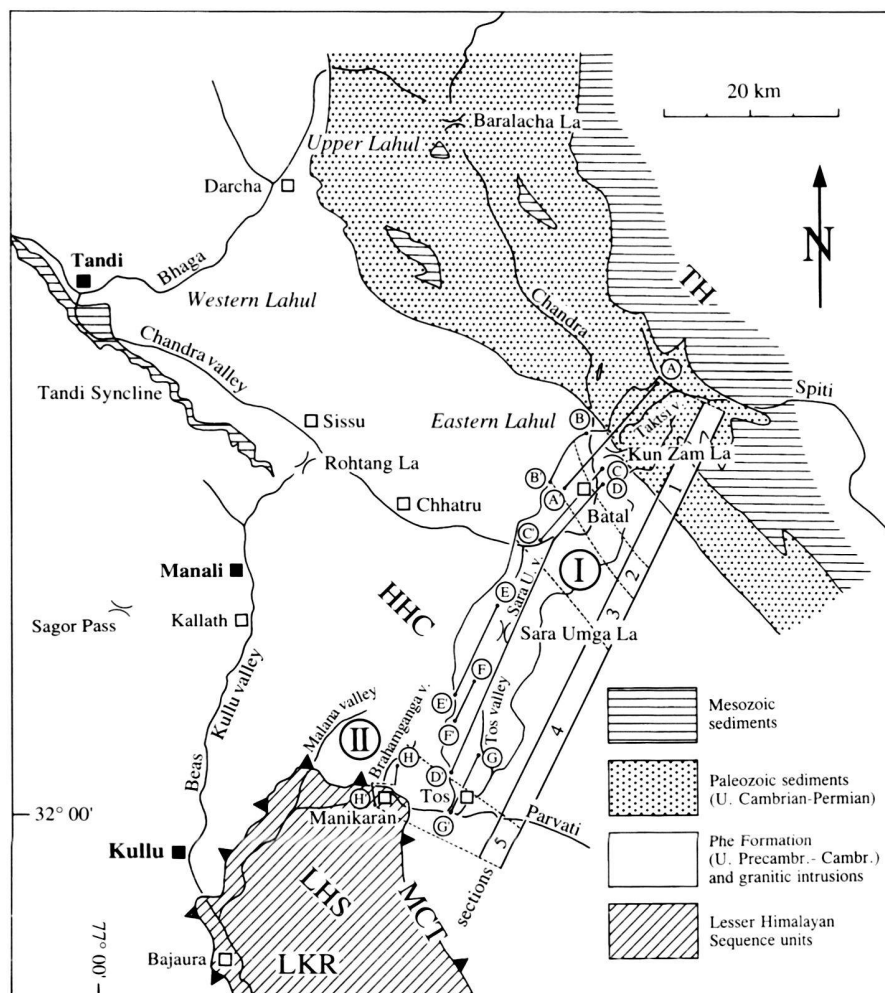


Fig. 2. General map of the traverses presented on Plate 1 and adjacent areas. Traverse I is about 60 km long, including the Tethyan Himalaya and the High Himalayan Crystalline. It is shown on a map together with the cross sections A-A' to G-G' on Plate 1. Traverse II is about 6 km long, including the High Himalayan Crystalline and the Lesser Himalayan Sequence with the Main Central Thrust zone in between. It is represented by the cross section H-H' on Plate 1. The contour line surrounding traverse I corresponds to the contour of the map on Plate 1. The studied area is subdivided into the sections 1-5 that are characterized by different metamorphic conditions, different styles and intensities of deformation and different sequences of deformational phases. TH = Tethyan Himalaya, HHC = High Himalayan Crystalline, LHS = Lesser Himalayan Sequence, MCT = Main Central Thrust, LKR = Larji-Kullu-Rampur tectonic window.

valley has been investigated (for review see Steck et al. 1993a, b; Epard et al. 1995; Steck et al. 1998).

The aim of this study is to provide detailed field data about the petrography and the structural and metamorphic evolution of the Spiti-eastern Lahul-Parvati valley transect. Mapping on a 1:25000 scale, structural analyses on a map- and outcrop scale and microtextural analyses of thin sections permit a detailed description of the deformational and metamorphic evolution. New data are presented emphasizing (a) an important tectonometamorphic event that predates the first known Tertiary Himalayan nappe formation, (b) early NE-verging nappe stacking, (c) a large SW-verging fold zone below the front of the SW-verging north Himalayan nappes, (d) two phases of NE-directed normal movement working simultaneously with SW-directed thrusting, (e) dextral strike-slip shearing and (f) shortening parallel to the mountain chain. Features (a), (c), (d) and (f) were previously undocumented in this part of the Himalaya.

#### Presentation of the data

The studied transect passes through different tectonostratigraphic levels of the Himalayan orogen that are characterized by different metamorphic conditions, different styles and intensities of deformation and different sequences of deformational phases. To take these differences into consideration, the transect is subdivided into five sections that are from NE to SW: (1) Taktsi valley-Kun Zam La, (2) northeastern upper Chandra valley, (3) southwestern upper Chandra valley, (4) Tos- and Sara Umga valleys and (5) Parvati- and Brahamganga valleys (Fig. 2, Plate 1). Section 1 represents the stratigraphically lowermost part of the Tethyan Himalaya, section 2 is situated at the transition between the Tethyan Himalaya and the High Himalayan Crystalline, the sections 3 and 4 are situated within the High Himalayan Crystalline and section 5 comprises the tectonostratigraphically lowermost part of the High Himalayan Crystalline and the uppermost part of the Lesser Himalayan Sequence, including the Main Central Thrust zone.

In chapter 4, the petrography is summarized for all five sections. In chapter 5, the deformational phases and stages of metamorphic crystallization are presented individually for each section. In chapter 6, the individual sequences of deformational phases observed in the five sections are correlated with each other and with the stages of metamorphic crystallization in order to establish an overall sequence of tectonometamorphic phases valid for the transect as a whole. Finally, in chapter 7, a model for the tectonometamorphic evolution is presented. Readers only interested in a structural overview or in the model should skip the chapters 4 and 5 and pass on to the chapters 6 and 7.

### 3. Geological setting and previous work

The traverse is presented in the direction of increasing tectonostratigraphic depth from the Tethyan Himalaya in the NE through the High Himalayan Crystalline to the Lesser Himalayan Sequence in the SW. In the studied area few previous investigations have been carried out. Previous studies were restricted to its northeastern and southwestern parts. In the northeastern part they mainly dealt with stratigraphy and structural geology, whereas in the southwestern part petrography was their main focus. For locations, see Figures 1 and 2.

#### Stratigraphy and petrography

The stratigraphy of the studied transect is summarized in Table 1. In the Taktsi valley, a tributary of the upper Spiti valley, low-grade sediments of the Tethyan Himalaya crop out, the stratigraphy of which is comparable to the stratigraphy established by Vannay (1993) for upper Lahul. The first map of this region was drawn by Hayden (1904). The several kms thick, pelitic Precambrian to Lower Cambrian Phe Formation is the stratigraphically lowest formation observed in the Taktsi valley. It constitutes not only the base on which the sediments of the Tethyan Himalaya were deposited, but also the major part of the medium- to high-grade High Himalayan Crystalline metasediments in the Chandra-, Tos- and Parvati valleys (Frank et al. 1973; Vannay 1993), indicating that the High Himalayan Crystalline is the stratigraphic continuation of the Tethyan Himalaya downsection. The rock types occurring in the Tethyan Himalaya and in the High Himalayan Crystalline are summarized in Table 1 and will be presented in detail in chapter 4. In the upper Chandra valley, in the Sara Umga valley and in the Tos valley, the Phe Formation metasediments were intruded by the Hanuman Tibba intrusives of Ordovician age ( $495 \pm 16$  Ma, Rb/Sr whole rock isochron, Frank et al. 1977) that were generally transformed to orthogneiss.

The Lesser Himalayan Sequence that is exposed in the Larji-Kullu-Rampur tectonic window mainly consists of Proterozoic sediments and metagranites (Frank et al. 1973; Frank et al. 1977; Thöni 1977). According to Thöni (1977) the massive quartzites of the Berinag Group are the tectonostratigraphically highest rocks of the Lesser Himalayan Sequence in this area.

Tab. 1. Stratigraphy and petrography of the Tethyan Himalaya (TH), the High Himalayan Crystalline (HHC) and the Lesser Himalayan Sequence (LHS) in the Taktsi valley-Eastern Lahul-Tos valley-Parvati valley area. Note the gradual transition between the Tethyan Himalaya and the High Himalayan Crystalline reflected by a continuous stratigraphy and by gradually increasing metamorphic conditions.

Age	Formation	Petrography	Section
Upper Permian	Kuling	Siltstones, shales, sandstones, limestones, marls	1
Upper Permian	Ganmachidam	Conglomerates, sandstones	
Middle to Upper Carboniferous	Po	Siltstones, shales, sandstones, limestones, marls	
Lower Carboniferous	Lipak	Limestones, dolomites, marls, sandstones, shales, gypsum	
Middle Devonian	Muth	Quartzsandstones	
Middle Ordovician	Thaple	Sandstones, siltstones, shales, dolomites	2
Lower Cambrian	Angular unconf.		
	Karsha	<b>Lower chlorite zone:</b> Siltstones, greywackes, sandstones, dolomites	
Precambrian to Lower Cambrian	Phe	<b>Lower chlorite zone:</b> Siltstones, greywackes, sandstones	
		<b>Upper chlorite zone:</b> Slates	
		<b>Biotite zone:</b> Slates, phyllites	
Lower Ordovician	Hanuman Tibba intrusion	<b>Garnet zone:</b> Phyllites, garnet-bearing two-mica schists, biotite schists	3
		<b>Kyanite zone:</b> Garnet-, kyanite- and/or sillimanite-bearing two-mica gneiss and schists	4
Granites, gneiss			5
Main Central Thrust			
Precambrian	Mélange zone	Quartzite, calcschists, phyllites	5
	Berinag Group	Quartzite, biotite-chlorite schists, phyllites	
			LHS

#### Nappe tectonics

The Himalayan orogen is dominated by SW-verging nappe structures. North and northeast of the studied area, SW-verging nappes were reported from the Tethyan Himalaya by Steck et al. (1993a, b) and Steck et al. (1998), referred to as the Nyimaling-Tsarap Nappe and Mata Nappe, respectively. In this study, these nappes are integrated into the north Himalayan nappe system. In the High Himalayan Crystalline of the lower Tos- and upper Parvati valleys, the Crystalline Nappe was thrust toward SW along the Main Central Thrust over the



rocks of the Lesser Himalayan Sequence (Frank et al. 1973; Frank et al. 1977; Thöni 1977). Thrusting along the Main Central Thrust is of Miocene age (biotite Rb/Sr cooling ages, Frank et al. 1977).

In the Tandi area in western Lahul and in the Kullu valley-Rohtang La area, an early NE-verging folding was described by Steck et al. (1993a, b), Vannay (1993), Epard et al. (1995) and Vannay & Steck (1995) that predated formation of the Crystalline Nappe. According to these authors, this folding was related to a nappe stack thrust towards NE, termed the Shikar Beh Nappe.

In the lower Parvati valley, Frank et al. (1973), Frank et al. (1977) and Thöni (1977) defined the thin, SW-verging Bajaura Nappe, consisting of variable rock types (containing mainly phyllites, graphitic calcschists and augengneiss) that are wedged between the Lesser Himalayan Berinag Quartzite and the Crystalline Nappe. Frank et al. (1987) referred to this unit as the Lower Crystalline Nappe.

#### *Normal faults and late stage phases*

In the Zaskar- and Sarchu regions NW of the studied area, the transition between the Tethyan Himalaya and the High Himalayan Crystalline is dominated by large-scale normal-and/or dextral strike-slip shear zones, referred to as the Zaskar Shear Zone (Searle 1986; Herren 1987; Searle et al. 1988; Kündig 1989; Searle & Rex 1989; Gapais et al. 1992; Searle et al. 1992; Patel et al. 1993; Dèzes et al. *in press*) and the Sarchu Normal Fault, respectively (Srikantia & Bhargava 1982; Spring & Crespo-Blanc 1992; Spring et al. 1993; Steck et al. 1993a, b). Normal shearing and/or dextral strike-slip movement are generally referred to as the North Himalayan Shear Zone (Pêcher et al. 1991) or the South Tibetan Detachment System (Burchfiel et al. 1992). In order to link the shear zones in the Zaskar- and Sarchu regions with a series of similar shear zones observed SE of the studied area in Garhwal (Pêcher & Scaillet 1989; Pêcher 1991; Metcalfe 1993), in central Nepal (Pêcher 1991; Pêcher et al. 1991) and in southern Tibet (Burg et al. 1984; Brun et al. 1985; Burchfiel & Royden 1985; Burchfiel et al. 1992) Searle (1986) and Searle et al. (1988) proposed that they continue towards SE across the upper Chandra valley (corresponding to the sections 2 and 3 in this study). The situation in the investigated area, however, is particular in that the transition between these domains is gradual. According to Hayden (1904), Frank et al (1973), Frank et al (1977), Fuchs (1987), Vannay (1993) and Vannay & Steck (1995) there exists neither a stratigraphic nor a tectonometamorphic discontinuity between the Tethyan Himalaya and the High Himalayan Crystalline in the upper Chandra valley area.

Vannay & Steck (1995) described late stage dextral shearing in the lower Chandra valley area, referred to as the Chandra Dextral Shear Zone. Steck et al. (1993a, b), Epard et al. (1995) and Vannay and Steck (1995) reported a late stage backfolding- and doming phase west of the studied transect.

#### *Metamorphism*

The metamorphic grade of the pelitic, Precambrian to Lower Cambrian Phe Formation sediments increases from the lower chlorite zone in the Taktsi valley southwestwards to the biotite zone (Steck et al., 1993a, b) and garnet zone in the upper Chandra valley. In the Tos- and upper Parvati valleys, the metamorphic grade reaches the kyanite- and sillimanite zones, indicating a Barrovian-type metamorphism with southwestwards increasing metamorphic conditions (Frank et al. 1973; Frank et al. 1977). These authors conclude that this metamorphism was caused by the formation of the SW-verging Crystalline Nappe. According to Epard et al. (1995) it was rather the result of the NE-verging stacking of the Shikar Beh Nappe, that predated formation of the Crystalline Nappe. Metamorphic conditions related to the Shikar Beh Nappe decrease from upper amphibolite facies in the Kullu valley- Rohtang La area W of the studied area to lower greenschist facies in upper western Lahul (Baralacha La area). According to Epard et al. (1995), the evolution of the regional metamorphism was biphasic in the Himachal Himalaya. The main metamorphism was related to the NE-verging Shikar Beh Nappe, whereas the metamorphism associated with the subsequent SW-directed stacking of the Crystalline Nappe occurred under slightly retrograde conditions.

The rocks of the Lesser Himalayan Sequence reached lower greenschist facies conditions only (Frank et al. 1973; Frank et al. 1977; Thöni 1977). This leads to an unusual situation in that the upper amphibolite facies High Himalayan Crystalline rocks overlie these low-grade rocks, a feature that is referred to as an inverted metamorphic field gradient between the Lesser Himalayan Sequence and the High Himalayan Crystalline. In addition, Frank et al. (1973), Frank et al. (1977) and Thöni (1977) postulated an inversion of the metamorphic isograds inside the High Himalayan Crystalline due to SW-directed folding and overthrusting of the Crystalline Nappe along the Main Central Thrust. In the Kullu valley-Rohtang La area, Epard et al. (1995) reported a SW-verging open folding of the Shikar Beh Nappe isograds due to formation of the Crystalline Nappe.

#### **4. Petrography**

In section 1, sediments of the Precambrian to Lower Cambrian Phe Formation, the Lower Cambrian Karsha Formation, the Middle Ordovician Thaple Formation, the Middle Devonian Muth Formation and the Lower Carboniferous Lipak Formation make up most of the rocks (Table 1, Plate 1). In the sections 2, 3 and 4, sediments of the Phe Formation and orthogneiss of the Ordovician Hanuman Tibba intrusion occur. In section 5, sediments of the Phe Formation and of the Proterozoic Lesser Himalayan Sequence predominate.

### *Karsha-, Thaple-, Muth- and Lipak formations*

The Karsha Formation consists of alternations of sandstones, greywackes and siltstones with intercalated dolomite beds. The Thaple Formation is made up of sandstones intercalated with siltstones, shales and dolomites. The Muth Formation consists of massive, mature quartz sandstones. The Lipak Formation displays a wide variety of lithologies comprising sandstones, limestones, arenitic limestones, marls, dolomites, black shales and gypsum. For a detailed stratigraphy of these formations, see Vannay (1993).

### *Phe Formation*

The Phe Formation is a 7-9 kilometers thick deposit consisting generally of monotonous alternations of subarkosic to arkosic sandstones, greywackes and siltstones with a millimeter- to meter-scale bed thickness, that underwent low-grade to high-grade metamorphic recrystallization. On the basis of metamorphic mineral assemblages, the Phe Formation rocks are referred to as low-Al pelites (Spear, 1993). Locally, carbonaceous graphitic quartzites and thin marly layers are intercalated. In the Tos valley, small mafic intrusions occur in the lowermost Phe Formation. The metamorphic grade of the Phe Formation metapelites increases from section 1 southwards to section 5 from lower chlorite zone conditions over biotite- and garnet zone conditions to kyanite- and sillimanite zone conditions (Table 1). In section 5, the kyanite zone mineral assemblage was retrogressively overprinted by greenschist facies conditions.

### *Metapelites*

In section 1, due to their low metamorphic grade (Table 1), the metapelites of the Phe Formation display all characteristics of sedimentary rocks. Metasiltstones are slates displaying a strong schistosity, whereas more arenitic layers display only a weak schistosity or lack a schistosity. The rocks mainly consist of detrital monocrystalline grains of quartz (over 70%), plagioclase and sericitised K-feldspar. White mica is abundant as buckled detrital grains and also occurs in the matrix as a fine-grained product of recrystallization of the original detrital pelitic fraction. It is often observed as intergrowths with chlorite. Some beds contain abundant pyrite. Detrital rutile, titanite, tourmaline, zircon, apatite, epidote-clinozoisite and opaque minerals are accessories. Graded bedding, cross stratifications and rhythmities of alternating sandstones and siltstones are often observed. On bed surfaces ripple marks, desiccation cracks, synaeresis cracks and trace fossils are abundant.

The metapelites in section 2 consist of slates and phyllites displaying components of detrital quartz and feldspar in a matrix generally made up of white mica, chlorite and locally also of graphite. The grain size of white mica increases considerably from NE to SW, where additional rare biotite occurs. Coarse-grained white mica wedged between the components is considered to be of detrital origin. The ratios between quartz

and feldspar and between the components and the matrix are strongly variable, representing the primary sedimentary bedding that still dominates the aspect of the rocks. Sedimentary structures, however, are rarely preserved.

In section 3 the metapelites are mainly phyllites, two-mica schists and biotite schists, depending on grain size and mineral content. The primary sedimentary bedding is well preserved on all scales. The rocks consist of quartz, plagioclase, biotite, white mica, chlorite and rare garnet poikiloblasts. Locally, graphite is abundant.

The metapelites in section 4 are generally medium- to coarse-grained garnet-bearing two-mica gneisses and schists with additional kyanite and/or sillimanite, consisting of quartz, plagioclase, biotite, white mica, garnet, kyanite, sillimanite, tourmaline and rare K-feldspar. Staurolite, apatite, rutile, ilmenite, zircon and monazite are accessories. Generally, these rocks display a strong metamorphic mineral segregation separating quartz- and plagioclase-rich microlithons from biotite- and white mica-rich cleavage domains. Lenses and layers of pure quartz are a common feature in section 4. The primary sedimentary bedding is recorded in the form of different mineral ratios. Towards the contact with the Hanuman Tibba intrusion, the grain size of the rocks decreases. Within the contact aureole, that reaches a thickness of 30 meters, a fine-grained sillimanite- and garnet-bearing biotite schist occurs, consisting of biotite, white mica, quartz, plagioclase, garnet, fibrolitic sillimanite and rare K-feldspar. In the direct vicinity of the intrusion, pseudomorphs of white mica and quartz after andalusite occur, that are characterized by remnants of chiastolite crosses.

In section 5, the metapelites display the same mineral composition as in section 4, but the rocks are more fine-grained, white mica is more abundant and K-feldspar and sillimanite are lacking. In addition, towards the base of the High Himalayan Crystalline, biotite was partly overgrown by chlorite, garnet rims were transformed to chlorite and kyanite was transformed to white mica.

### *Marls*

In the sections 2, 3 and 4, thin marly layers are intercalated with the pelitic beds. In section 2 these layers consist of fine-grained actinolite, quartz, albite and zoisite. In section 3 actinolite, quartz, albite, clinozoisite, epidote, garnet and biotite occur, and in section 4 the marly layers are medium-grained garnet-, hornblende-, diopside-, plagioclase- and quartz-bearing granofelses with accessory scapolite, dolomite, calcite, epidote, clinozoisite, sphene and apatite.

### *Carbonaceous graphitic quartzites*

Within the Phe Formation, a 5 to 30 meters thick layer containing various carbonaceous graphitic quartzites occurs, that can be followed throughout sections 3 and 4. This layer represents an important marker horizon to trace structures on a large scale. It consists of various beds half a meter to two me-

Tab. 2. Mineral abbreviations.

Ank = Ankerite	Ky = Kyanite
Bt = Biotite	Pl = Plagioclase
Chl = Chlorite	Qtz = Quartz
Gr = Graphite	Sil = Sillimanite
Grt = Garnet	St = Staurolite
Hbl = Hornblende	Wm = White mica
Kfs = K-feldspar	(mostly muscovite)

Tab. 3. Abbreviations used for the structural and microtextural analyses.

D = Deformational phase	L = Stretching lineation
M = Stage of metamorphic crystallization	S = Schistosity or cleavage
F = Fold	B = Sedimentary bedding
FA = Fold axis	SZ = Shear zone
AS = Axial surface	SB = Shear band
	LS = Leucosome

ters thick, that are characterized by the overall presence of graphite. The stratigraphic column of the carbonaceous graphitic quartzites is variable. The main components of these rocks are quartz, graphite, calcite and dolomite. In section 3, additional tremolite, albite, and pyrite occur. Sphene, zircon and hematite are accessory minerals. In section 4, fuchsite, tremolite, green and black hornblende, pyrite and sphene occur in addition, and K-feldspar, zircon and clinozoisite are accessories. In section 4, the carbonaceous graphitic quartzites are always associated to metapelites with a high content of marly layers and bulky quartz-feldspar nodules with inclusions of cm-scale hornblende crystals.

#### *Orthogneiss of the Hanuman Tibba intrusion*

The orthogneiss displays mainly a syenogranitic to monzogranitic composition. It is characterized by phenocrysts of K-feldspar and by a high content of tourmaline. Small bodies of granodioritic to tonalitic composition and fine-grained microgranites also occur, and in the Sara Umga valley, the orthogneiss is crosscut by rare dolerite dikes. Generally, the orthogneiss shows a schistosity marked by biotite and white mica. Locally, the intrusives are massive and display no signs of deformation, with the exception of magmatic flow fabrics. In sections 3 and 4 minor garnet also occurs.

The Hanuman Tibba intrusion is only observed in contact with the Phe Formation sediments. In the sections 2 and 3 the contact is discordant. The country rocks are crosscut by various sills and dikes. Locally, xenoliths of metasediments occur within the intrusives. In section 4 the contact is mostly concordant and characterized by a series of sills that intruded the sillimanite- and garnet-bearing biotite schist in the contact aureole.

#### *Metasediments of the uppermost Lesser Himalayan Sequence*

The two tectonostratigraphically highest units of the Proterozoic Lesser Himalayan Sequence exposed in the studied area are the massive Berinag Quartzites and a mélange zone made up of calcschists, phyllites and isolated lenses of Berinag Quartzite (Table 1) that is wedged between the Berinag Quartzite and the High Himalayan Crystalline.

The white Berinag Quartzite consists of quartz with an equigranular-polygonal fabric. Locally, a weak sedimentary banding marked by graphite and white mica, as well as lenses of fuchsite, are observed. Zircon and ore minerals are accessories. In the Berinag Quartzite, rare conglomerate zones occur, the matrix of which consist of quartz, graphite, ore minerals and white mica.

The calcschists and phyllites occur mainly in the mélange zone. Isolated layers of phyllites also occur inside the Berinag Quartzite. The calcschists consist of fine-grained calcite, dolomite, white mica, quartz, chlorite, biotite, sericitized plagioclase, K-feldspar, graphite and ore minerals. Detrital tourmaline, monazite and zircon are accessory minerals. The phyllites are made up of very fine-grained white mica, chlorite, biotite, graphite and ribbons of equigranular-polygonal quartz.

### **5. Deformational phases and metamorphism in the sections 1 to 5**





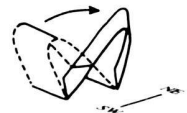
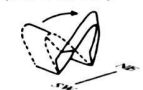

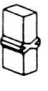


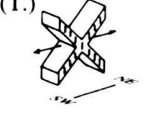
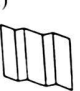

#### *Introduction*

The structural and metamorphic evolution of each section is analysed and subdivided into several deformational phases and stages of metamorphic crystallization, respectively. Deformational phases are revealed by structural elements such as folds of a certain style and vergence with axes and axial surfaces of a certain orientation, as well as by schistositities, shear bands, thrusts, veins and fractures. Each individual deformational phase is characterized by one or several structural elements, that affect older structural elements and/or that are superposed by younger structural elements. Stages of metamorphic crystallization are assigned to deformational phases that are associated with the crystallization of new minerals. Different stages of metamorphic crystallization may occur under similar metamorphic conditions. Mineral abbreviations are summarized in Table 2.

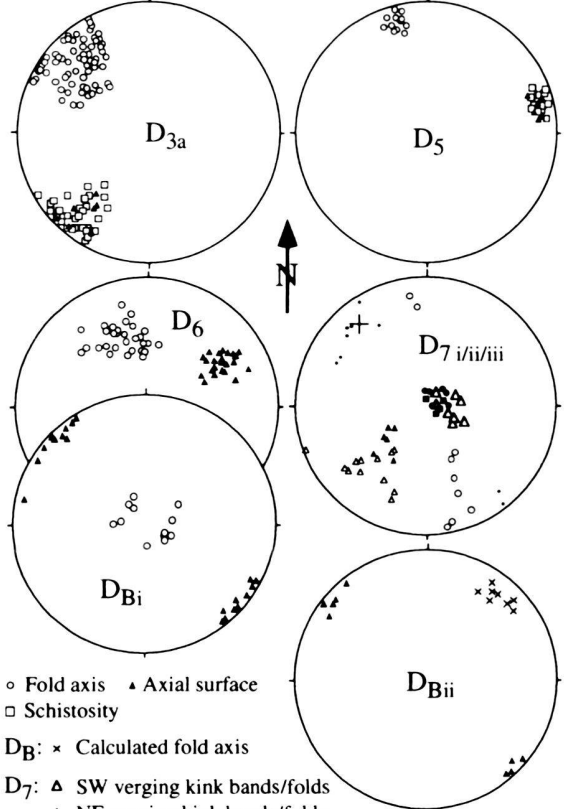
The low-Al pelites of the Precambrian to Lower Cambrian Phe Formation are the most important rocks for structural and microtextural analyses in the studied transect, as they occur in all five sections and recorded a great number of deformational phases and stages of metamorphic crystallization. In contrast, the orthogneiss of the Hanuman Tibba intrusion recorded only few deformational phases and the mineral assemblages are difficult to assign to distinct stages of metamorphic crystallization. Therefore, they are of lesser importance in deciphering the structural and metamorphic history. Other rock types, such as the sediments of the Lower Cambrian Karsha Formation, the Middle Ordovician Thaple Formation, the Middle Devon-

Tab. 4. Deformational phases and stages of metamorphic crystallization occurring in section 1, presented in their sequential order. Geometry and orientations of structures, foliations and mineral assemblages are shown for the Precambrian to Lower Cambrian Phe Formation. For the Middle Ordovician to Lower Carboniferous Thaple (T.)-, Muth (M.)- and Lipak (L.) Formations, the geometry of the structures is shown. Minerals in bold are related to the respective stage of metamorphic crystallization and/or foliation.

The deformational phase D<sub>5</sub> did not create new fold axes, but reoriented pre-existing F<sub>3</sub> fold axes. S<sub>5</sub> axial surface schistositities by contrast developed during D<sub>5</sub>. In general, the D<sub>3</sub>- and D<sub>5</sub> structures are only locally overprinted by the subsequent phases D<sub>6</sub>, D<sub>7</sub> and D<sub>B</sub>. On a large scale, their influence upon the orientation of D<sub>3</sub>- and D<sub>5</sub> structures is not documented.

Phase	Phe Formation			Thaple-, Muth-, Lipak Fms.
	Geometry	Foliation	Mineral assembl.	Geometry
D <sub>2</sub>		Cleavage S <sub>2</sub>	Qtz, pl, Kfs, <b>w</b> m, <b>chl</b>	
D <sub>3a</sub> M <sub>3</sub>		Slaty cleavage S <sub>3a</sub>	Qtz, pl, Kfs, <b>w</b> m, <b>chl</b>	(T., M., L.) 
D <sub>3b</sub>				(T., M., L.) 
D <sub>5</sub>		Slaty -/ crenulation cleavage, cleavage bundles S <sub>5</sub>	Qtz, pl, Kfs, <b>w</b> m, <b>chl</b>	(T., M., L.) 
D <sub>6</sub>			Qtz, pl, Kfs, <b>w</b> m, <b>chl</b>	
D <sub>7</sub>	i)  ii)  iii) 		Qtz, pl, Kfs, <b>w</b> m, <b>chl</b>	(T.) 
D <sub>B</sub>	i)  ii) 		Qtz, pl, Kfs, <b>w</b> m, <b>chl</b>	

Orientation of structural elements, projected on the lower hemisphere of the Schmidt equal area stereonet



○ Fold axis    ▲ Axial surface  
 □ Schistosity  
 D<sub>B</sub>: × Calculated fold axis  
 D<sub>7</sub>: ▲ SW verging kink bands/folds  
      ▲ NE verging kink bands/folds  
      ■ Bisector of the angle between the AS of box folds  
      • Bisector of the angle between conjugated kink bands  
      + Calculated intersection between conjugated kink bands  
      • Kink axis

ian Muth Formation and the Lower Carboniferous Lipak Formation as well as the metasediments of the Lesser Himalayan Sequence are of local importance only due to their limited regional distribution in the studied transect.

#### Phase numbering

Abbreviations for deformational phases, structural elements and stages of metamorphic crystallization are summarized in Table 3. Each deformational phase and each stage of metamorphic crystallization observed in the Tethyan Himalaya and in the High Himalayan Crystalline bears an Arabic number,

e.g. D<sub>1</sub>, M<sub>1</sub>. Added small letters, e.g. D<sub>3a</sub>, M<sub>1a</sub>, refer to interfering subphases or to substages of metamorphic crystallization, respectively. Indices such as i, ii, e.g. D<sub>1i</sub>, are used to indicate different structures related to the same phase of deformation which do not interfere. Roman numbers e.g. D<sub>I</sub> are used in the Lesser Himalayan Sequence, where not all phases clearly correspond with the phases observed above the Main Central Thrust zone. Late stage deformations, that can be related to each other only rarely, are indicated by capital letters, e.g. D<sub>A</sub>.

The sequences of deformational phases and the sequences of stages of metamorphic crystallization are different in the individual sections, e.g. one phase may occur in one section only



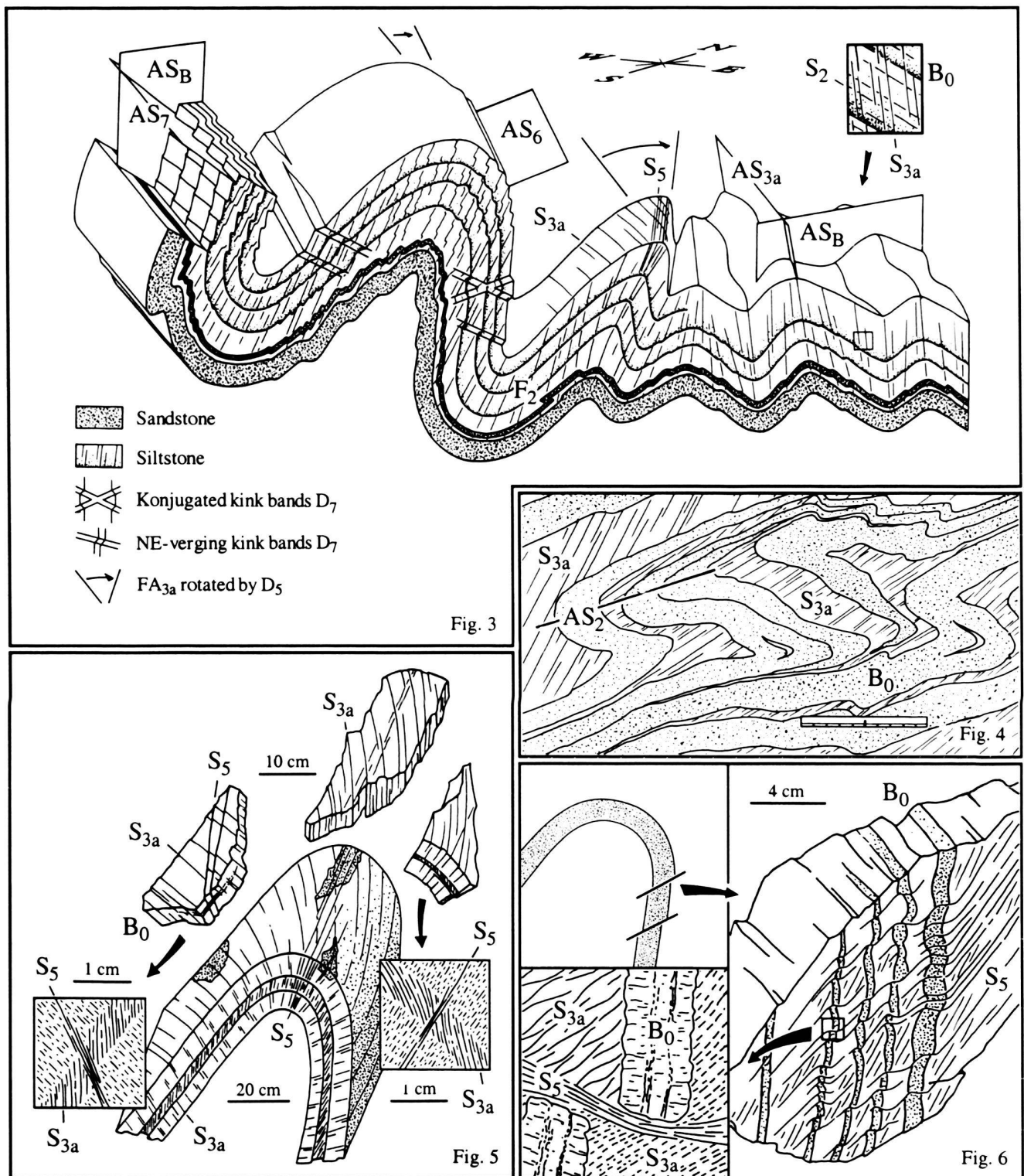


Fig. 3. Block diagram, summarizing the style of the main phases of deformation and their relationships in section 1, observed in the Phe Fm. (not to scale, for abbreviations see Table 3).

Fig. 4. Relic of a  $F_2$  fold, overprinted by the main schistosity  $S_{3a}$  (Phe Fm., measuring rod for scale: 10 cm, SW is on the left hand side).

Fig. 5.  $F_{3a}$  fold, reoriented by  $D_5$ . The intersection between  $S_{3a}$  and the sedimentary bedding  $B_0$  is wrapped around the  $D_5$ -reoriented  $F_{3a}$  fold axis (Phe Fm., SW is on the left hand side).

Fig. 6. Sandstone layers within siltstone, dismembered by pressure solution along  $S_5$  cleavage bundles on the inverted limb of a  $F_{3a}$  fold that was reoriented by  $D_5$  (Phe Fm., SW is on the left hand side, left below: simplified drawing from a thin section.).

or another phase may be missing in one or more sections. We do not, however, introduce individual phase numberings for each section, in order to maintain correlations between numbering schemes in the different sections. The phases are numbered according to chapter 6, where the correlation of the sequences of deformational phases of all sections is discussed. Therefore, the sequence of phases for an individual section may be e.g. D<sub>2</sub> - D<sub>3</sub> - D<sub>6</sub> - D<sub>7</sub>.

Structural terms are used according to Ramsay & Huber (1987a, b) and terms for textures are used according to Passchier & Trouw (1996). Mineral zones for metapelites are used after Spear (1993) and metamorphic facies are used after Spear (1993) and Bucher & Frey (1994).

### Section 1: Taktsi valley-Kun Zam La

#### Deformation

In the Taktsi valley-Kun Zam La section, seven deformational phases (D<sub>2</sub>, D<sub>3a</sub>, D<sub>3b</sub>, D<sub>5</sub>, D<sub>6</sub>, D<sub>7</sub> and D<sub>B</sub>) are observed (Table 4). The related structures are best documented in the sediments of the Precambrian to Lower Cambrian Phe Formation (Fig. 3). In general, the main deformation is the folding F<sub>3a</sub>. D<sub>5</sub> is also mostly a penetrative phase, D<sub>2</sub>, D<sub>6</sub>, D<sub>7</sub> and D<sub>B</sub> in contrast occur only locally. Some of the phases observed in the Phe Formation show similar structures in the rocks of the Thaple-, Muth- and Lipak formations.

The oldest structural element is the weak cleavage S<sub>2</sub>, marked by detrital white mica oriented subparallel to the sedimentary bedding in the siltstones of the Phe- and Karsha formations. This cleavage is probably related to an early phase of F<sub>2</sub> folding, rare relic structures of which occur near Kun Zam La (Fig. 4), but it can also represent a "sedimentary cleavage" that was formed due to the preferential sedimentary orientation of micas parallel to the bedding.

Generally, the slaty cleavage S<sub>3a</sub> is the dominant structural element. It appears preferentially in the Phe- and Karsha formations, where it overprints S<sub>2</sub>, and in the siltstone beds of the Thaple Formation. S<sub>3a</sub> is related to the open to isoclinal F<sub>3a</sub> folds that are observed on a meter- to kilometer-scale, representing the main phase of deformation D<sub>3</sub>.

The axial surfaces AS<sub>3</sub> of meter- to ten meter-scale F<sub>3a</sub> folds and S<sub>3a</sub> dip either to NE or to WSW. Folds with axial surfaces dipping to NE are mostly open and display axes that plunge to NW, and folds with axial surfaces dipping to WSW are mostly close or tight with axes plunging to NNW. NE and SW of section 1, AS<sub>3a</sub> and S<sub>3a</sub> dip to NE and therefore, F<sub>3a</sub> folds are considered to verge originally to SW. As a consequence, in section 1, axial surfaces of mostly close to tight F<sub>3a</sub> folds are interpreted to be reoriented from their original NE-dipping orientation to a WSW-dipping orientation, combined with a clockwise rotation of 20-40° of the FA<sub>3</sub> fold axes by the deformation D<sub>5</sub>. In most of the F<sub>3a</sub> fold hinges that were overturned by D<sub>5</sub>, S<sub>3a</sub> is overprinted by the WSW-dipping slaty cleavage S<sub>5</sub> and the intersections between S<sub>3a</sub> and the sedimen-

tary bedding are wrapped around the D<sub>5</sub>-reoriented axis of F<sub>3a</sub> folds (Fig. 5). On the fold limbs, S<sub>5</sub> appears as a crenulation cleavage or as cleavage bundles. In cm-scale rhythmites of alternating sandstones and siltstones, on many of the D<sub>5</sub>-reoriented F<sub>3a</sub> fold limbs, arenitic layers and S<sub>3a</sub> are dismembered and displaced along the surfaces of S<sub>5</sub> cleavage bundles due to pressure solution during D<sub>5</sub> (Fig. 6).

The sedimentary bedding, S<sub>2</sub> and S<sub>3a</sub>/S<sub>5</sub> were subsequently overprinted by two phases of coaxial open folding and kinking D<sub>6</sub> and D<sub>7</sub>. Neither of these deformations developed a cleavage in the rocks. D<sub>6</sub> appears as an open folding on a decimeter- to meter-scale (Fig. 7), rarely also as a millimeter- to centimeter-scale open crenulation. The local vergence of many F<sub>6</sub> folds is towards SW, however, frequently they do not reveal a clear vergence.

D<sub>7</sub> appears as decimeter-scale single kink bands and conjugate kink bands (i on Table 4), as kink folds (ii) and as box folds (iii). The NE-verging single kink bands display a gently NE-dipping kink plane subparallel to the axial surface of the kink folds. The bisector of the angle between the conjugate kink bands generally dips gently to NE and is subparallel to the bisector of the angle between the axial surfaces of the box folds. The kink bands locally overprint F<sub>6</sub> folds (Fig. 7). In the Thaple Formation arenites, conjugate sets of "en-echelon" quartz-filled veins with subhorizontal bisectors of the angle between the vein sets are observed that are interpreted to be related to D<sub>7</sub>.

F<sub>7</sub> kink folds interfere with F<sub>B</sub> folds that display steep axes (D<sub>B</sub>i: on Table 4, Fig. 8). The vergence of F<sub>B</sub> folds depends on the pre-existing geometry. Open F<sub>3a</sub> folds are overprinted by open folds that display axes and axial planes perpendicular to F<sub>3a</sub> (D<sub>B</sub>ii on Table 4), resulting in dome-basin (type 1) interference patterns (Figs 9, 10). These two structures, interfering with F<sub>7</sub> folds and with F<sub>3a</sub> folds, are considered to represent the same deformational phase D<sub>B</sub>, because the related directions of shortening, perpendicular to the axial surfaces, are similar for both structures (Table 4).

#### Veins

Two types of complex composite quartz-ankerite vein systems occur, displaying two different interference patterns. Their integration in the sequence of phases remains unclear.

*Type 1:* series of primary parallel composite quartz-ankerite veins with a thickness of some millimeters, oriented parallel to S<sub>3a</sub>, reaching in total a thickness of some centimeters to decimeters or, in a few cases, even up to a meter, are crosscut perpendicularly by secondary fibrous "stretched crystals" quartz veins with a thickness of 0.5 to 15 centimeters (Fig. 11).

*Type 2:* a primary composite quartz-ankerite vein with a maximum thickness of 1.5 centimeters is crosscut perpendicularly by two sets of secondary antitaxial or in some cases also "stretched crystals" quartz veins, which enclose an angle of 70° to 90° with each other, showing a chocolate tablet structure (Fig. 12). The primary composite quartz-ankerite vein is usually parallel to S<sub>3a</sub>, but other orientations are also observed.

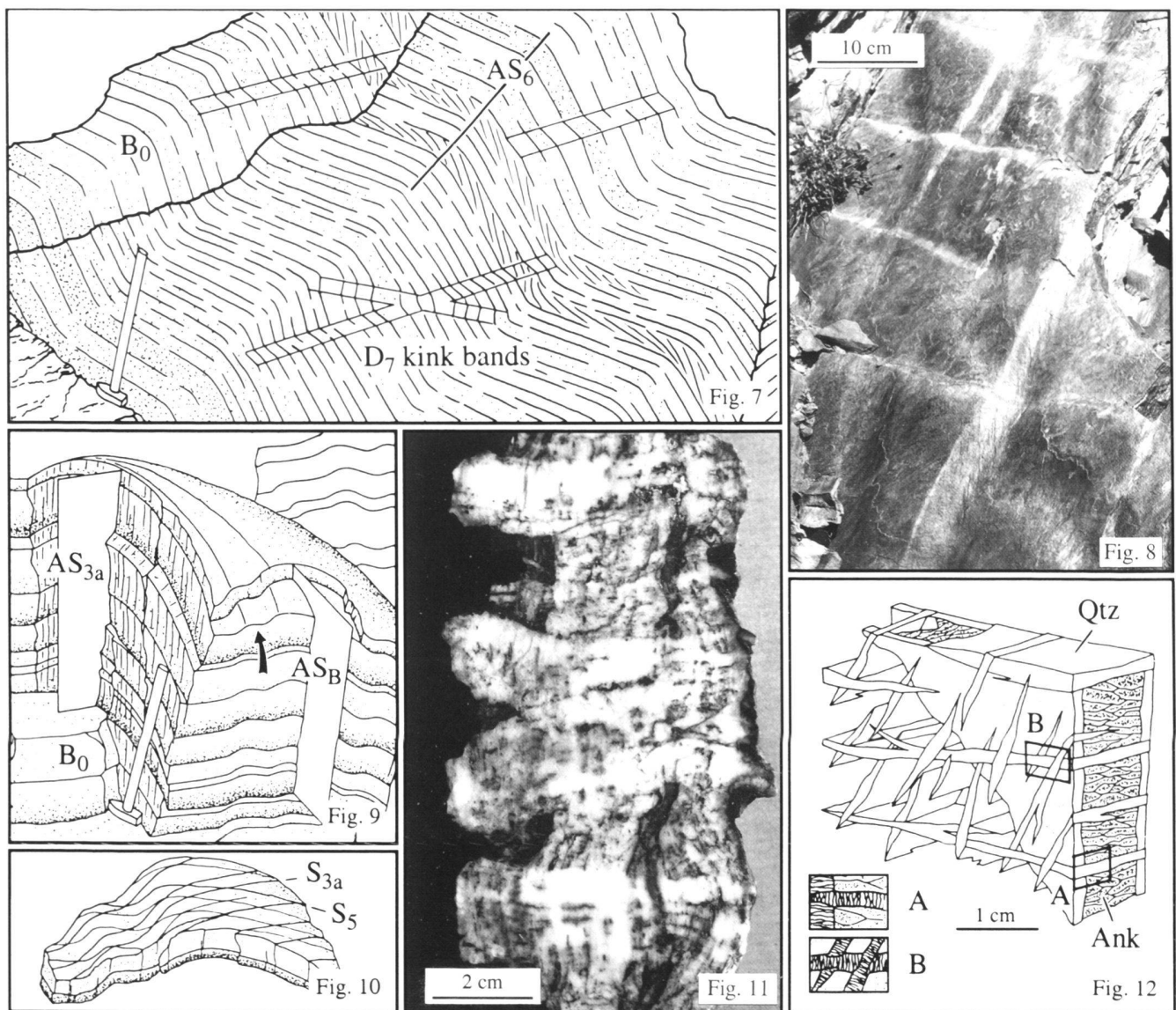


Fig. 7. Open  $F_6$  folds, crosscut by kink bands of the phase  $D_7$  (Phe Fm., hammer for scale: 45 cm, SW is on the left hand side).

Fig. 8.  $F_7$  kink folds (subhorizontal), interfering with  $F_B$  kink folds with steep axes (Phe Fm., NW is on the left hand side).

Fig. 9. Open  $F_{3a}$  fold, overprinted by an open  $F_B$  fold with a nearly perpendicular axial surface, forming a dome-basin (type 1) interference pattern (Phe Fm., hammer for scale: 45 cm, NW is on the left hand side).

Fig. 10. Hand specimen from the open  $F_B$  fold in Fig. 9 (arrow), displaying the schistosity  $S_{3a}$  and  $S_5$ .

Fig. 11. Complex composite quartz-ankerite vein system of type 1. Primary veins are vertical, secondary veins are horizontal (Phe Fm., SW is on the left hand side).

Fig. 12. Complex composite quartz-ankerite vein system of type 2. Inset A) The primary composite quartz-ankerite vein is crosscut by a secondary quartz vein. Inset B) The two sets of secondary quartz veins crosscut each other (Phe Fm., NW is on the left hand side).

### Large-scale structures

In the lower Taktisi valley, a km-scale  $F_{3a}$  anticline-syncline structure with gently NW-plunging fold axes is predominant, which is called the Taktisi Fold in this study (Fig. 13, Plate 1), affecting mainly the Middle Ordovician Thaple Formation and

the Middle Devonian Muth Formation. The related  $S_{3a}$  cleavage appears preferentially in the siltstones of the Thaple Formation. In the anticline that verges toward SW,  $S_{3a}$  dips to NE and in the syncline,  $S_{3a}$  dips to SW. This is interpreted in that  $S_{3a}$  in the syncline was overturned to its present orientation by



Fig. 13. The Taktisi Fold on the northwestern slope of the Taktisi valley (view towards NW). The anticline verges to SW. The valley to the right hand side is the uppermost Spiti valley, SW is on the left hand side. 1)  $D_{3b}$  thrust faults with a top-to-the SW shear sense. 2) NE-verging folds. 3) Normal faults with a top-to-the SW shear sense that were reactivated with a shear sense top-to-the NE. 4) Thrust fault with a top-to-the NE shear sense. 5) High-angle normal faults. The black layer corresponds to a series of beds of white to pink massive quartz sandstone in the Thaple Formation. The wavy line (6) marks an angular discordance between the Karsha Formation and the Thaple Formation. (Karsha Fm.: Lower Cambrian, Thaple Fm.: Middle Ordovician, Muth Fm.: Middle Devonian, Lipak Fm.: Lower Carboniferous)

Tab. 5. Deformational phases and stages of metamorphic crystallization occurring in section 2, presented in their sequential order. Geometry and orientations of structures, foliations and mineral assemblages are shown for the Precambrian to Lower Cambrian Phe Formation. For the Lower Ordovician Hanuman Tibba Intrusion, the geometry of the structures is shown. Minerals in bold are related to the respective stage of metamorphic crystallization and/or foliation. Axial surfaces and schistositities related to the coaxial phases  $D_{3a}$ ,  $D_6$  and  $D_7$  are distributed along a NE-SW-trending axis. This demonstrates that  $D_7$  was overprinted by  $D_8$ , that  $D_6$  was overprinted by  $D_7$  and by  $D_8$  and that  $D_{3a}$  was affected by all three subsequent phases. In contrast to section 1, overprinting by  $D_6$  and  $D_7$  was not only local, but pervasive.

Phase	Phe Formation			Hanuman Tibba Intrusion
	Geometry	Foliation	Mineral assembl.	Geometry
$D_2$		Cleavage $S_2$	Qtz, pl, Kfs, <b>wm, chl</b>	
$D_{3a}$ $M_3$		Slaty cleavage $S_{3a}$	Qtz, pl, Kfs, <b>wm, chl, gr, +- bt</b>	
$D_{3b}$		Shear bands $SB_{3b}$ top - to - the SW	Qtz, pl, Kfs, <b>wm, chl, gr, +- bt</b>	
$D_6$		Crenulation cleavage $S_6$	Qtz, pl, Kfs, wm, chl, gr	
$D_7$		Crenulation cleavage $S_{7a}$	Qtz, pl, Kfs, wm, chl, gr	
$D_8$			Qtz, pl, Kfs, wm, chl, gr	
$D_B$			Qtz, pl, Kfs, wm, chl, gr	

Orientation of structural elements, projected on the lower hemisphere of the Schmidt equal area stereonet

○ Fold axis  
 • Axial surface  
 □ Schistosity



D<sub>5</sub>. SW of the Taktsi Fold, a large-scale F<sub>3a</sub> anticline is revealed by mapping out of the small-scale parasitic folds in the Phe Formation with an axial surface approximately dipping to WSW (Plate 1). Parasitic meter- to ten meter-scale F<sub>3a</sub> folds show all signs of D<sub>5</sub> reorientation as described above, indicating that this fold was overturned to its present orientation by D<sub>5</sub> fold reorientation. A set of SW-directed D<sub>3b</sub> thrust faults with a dip angle of 60–70° is observed in the normal limb of the Taktsi Fold anticline (1 on Fig. 13). These faults are suggested to be reoriented to their present steep orientation by D<sub>5</sub> as well.

The Taktsi Fold is affected by several structures with an unclear position in the sequence of phases. On the normal limb of the anticline, several NE-verging folds are observed (2 on Fig. 13). The syncline is crosscut by SW-dipping normal faults with displacements of several hundred meters (3 on Fig. 13). Small-scale shear criteria, however, indicate that these normal faults were subsequently reactivated in the reverse sense, forming thrust faults with a direction of transport top-to-the NE, similar to the single thrust fault, that crosscuts the syncline in its southwesternmost part (4 on Fig. 13). The Taktsi fold is also crosscut by high-angle normal faults with fault planes dipping to E and W (5 on Fig. 13).

### Metamorphism

In the low-Al metapelites of the Phe Formation, S<sub>3</sub> is marked by reoriented detrital white mica and by fine-grained white mica that is a product of recrystallization of the original detrital pelitic fraction. Chlorite is observed as intergrowths with white mica. The metamorphic conditions in section 1 are thus within the lower chlorite zone for low-Al metapelites, corresponding to lower greenschist facies. As S<sub>3</sub> is the main schistosity, this stage of metamorphic crystallization is assigned to D<sub>3</sub> and termed M<sub>3</sub>. However, chlorite is not directly related to the formation of S<sub>3</sub> and therefore it cannot be excluded that an earlier stage of metamorphic crystallization within chlorite zone conditions existed, that was most probably related to S<sub>2</sub> and F<sub>2</sub>.

### Section 2: Northeastern upper Chandra valley

#### Deformation in the metasediments

In the northeastern upper Chandra Valley seven deformational phases (D<sub>2</sub>, D<sub>3a</sub>, D<sub>3b</sub>, D<sub>6</sub>, D<sub>7</sub>, D<sub>8</sub> and D<sub>B</sub>) are observed (Table 5). D<sub>2</sub>, D<sub>3a</sub>, D<sub>6</sub>, and D<sub>7</sub> display axial surface cleavages, which are deformed by the respective subsequent phases. Together with microscopic and/or macroscopic interference patterns, this allows the sequence of deformation to be unequivocally established. The structures are best documented in the Phe Formation slates and phyllites (Fig. 14).

The dominant structural element in the Phe Formation slates is the slaty cleavage S<sub>3a</sub> that is marked by white mica, chlorite and graphite and in the southwestern part of the section also by biotite. S<sub>3a</sub> is related to open to isoclinal, asymmet-

ric, SW-verging F<sub>3a</sub> folds that are generally observed on a small scale (Fig. 15). Large-scale F<sub>3a</sub> folds are rarely observed. D<sub>3a</sub> is predated by older structures. Occasionally, a S<sub>2</sub> cleavage occurs that is marked by white mica and chlorite. S<sub>2</sub> is mainly observed along or inside thin quartz layers that are affected by asymmetric boudinage displaying a shear sense top-to-the NE (Fig. 16). Both S<sub>2</sub> and the boudinaged quartz layers are subsequently deformed by F<sub>3a</sub> folds. Locally, S<sub>3a</sub> is overprinted by C'-type shear bands SB<sub>3b</sub>, showing a shear sense top-to-the SW. Asymmetric boudinage of competent metamarl layers is observed with the same shear sense.

Throughout the northern upper Chandra valley, the sedimentary bedding, S<sub>2</sub>, the main cleavage S<sub>3a</sub> and the SB<sub>3b</sub> shear bands were subsequently overprinted by three coaxial deformational phases D<sub>6</sub>, D<sub>7</sub> and D<sub>8</sub> that all form open to close, mostly angular polyharmonic folds. F<sub>6</sub> folds are generally observed on a decimeter- to meter-scale, but they occur also on a kilometer-scale, verging towards SW. They are characterized by moderately to steeply inclined, SW-dipping axial surfaces and by a strong crenulation cleavage S<sub>6</sub> parallel to the axial surface that overprints the main cleavage S<sub>3a</sub>.

The subsequent F<sub>7</sub> folds are also observed on a decimeter- to meter-scale, verging towards NE (Fig. 17). Their axial surfaces are subhorizontal or dip gently to NE. On their inverted fold limbs, F<sub>7</sub> folds reorientate the axial surfaces of F<sub>6</sub> folds from a moderately to steeply SW-dipping orientation to a gently SW-dipping or gently NE-dipping orientation (Fig. 18). F<sub>7</sub> is associated with a strong crenulation cleavage S<sub>7</sub> parallel to the axial surface, overprinting S<sub>3a</sub> and S<sub>6</sub> (Figs. 15, 18).

The F<sub>8</sub> folds are generally observed on a 10- to 100 meter-scale and locally even up to a kilometer-scale. They display a subhorizontal to gently SW-dipping axial surface and a vergence towards NE. On inverted limbs of F<sub>8</sub> folds, the axial surfaces of F<sub>6</sub> and F<sub>7</sub> are generally reoriented to a moderately to steeply inclined NE-dipping orientation. F<sub>8</sub> folds do not display a crenulation cleavage. Rare D<sub>B</sub> folds are observed in section 2, corresponding to D<sub>B1</sub> in section 1.

#### Metamorphism in the metasediments

Two stages of metamorphic crystallization are documented in the Phe Formation slates and phyllites of section 2. The first stage M<sub>2</sub>, related to D<sub>2</sub>, is expressed by chlorite and white mica on relics of S<sub>2</sub>, indicating chlorite zone conditions for low-Al metapelites. This corresponds to greenschist facies conditions. The main metamorphism M<sub>3</sub>, however, took place during D<sub>3</sub>. Generally, graphite, chlorite and white mica are related to S<sub>3a</sub>. White mica displays an increasing grain size from NE to SW and additional biotite is observed in the southwesternmost part of the section. Thus, the metamorphic conditions of M<sub>3</sub> increase from NE to SW from upper chlorite zone to biotite zone conditions, corresponding to greenschist- to upper greenschist facies conditions. Mineral growth related to the crenulation cleavages S<sub>6</sub> and S<sub>7</sub> is not observed, S<sub>6</sub> and S<sub>7</sub> only reoriented the minerals on S<sub>3a</sub>. Contact metamorphism along the

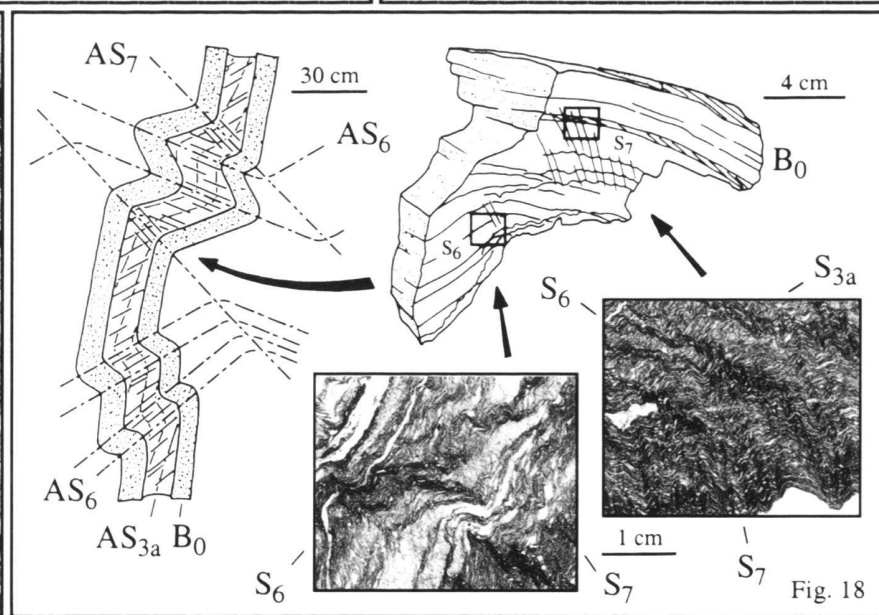
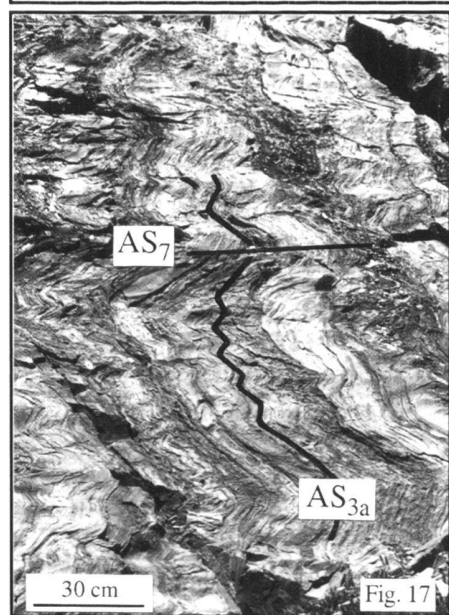
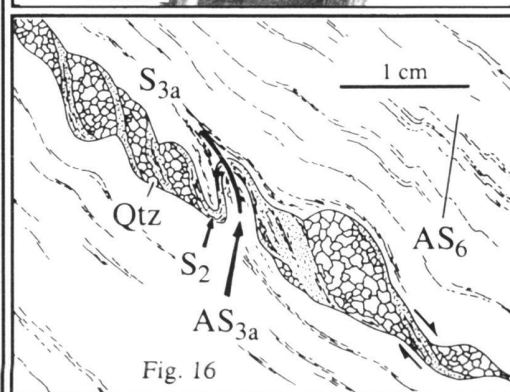
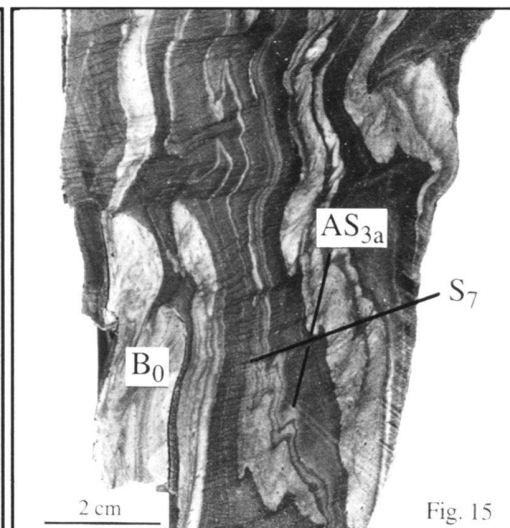
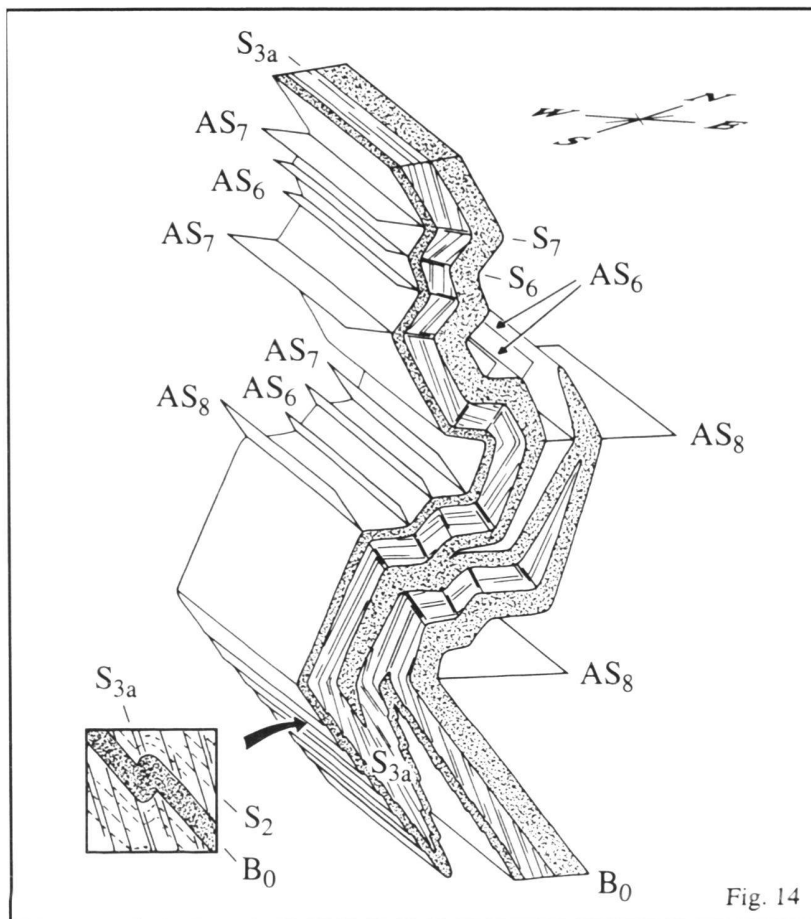


Fig. 14. Block diagram, summarizing the style of the main phases of deformation and their relationships in section 2, observed in the Phe Fm. (not to scale, for abbreviations see Table 3).

Fig. 15.  $F_{3a}$  folds, affecting the sedimentary bedding  $B_0$ . Both  $B_0$  and  $F_{3a}$  are overprinted by the  $S_7$  crenulation cleavage (Phe Fm. slate, polished hand specimen, SW is on the left hand side).

Fig. 16. Asymmetric boudinage of quartz layers, containing  $S_2$ . The boudinaged quartz layers and  $S_2$  are subsequently affected by  $F_{3a}$  folds.  $S_{3a}$  is overprinted by  $F_6$  crenulations (Phe Fm., drawing from a thin section, SW is on the left hand side).

Fig. 17.  $F_7$  folds, overprinting an isoclinal  $F_{3a}$  fold (Phe Fm., SW is on the left hand side).

Fig. 18. Interference between  $D_{3a}$ ,  $D_6$  and  $D_7$  on the inverted limb of a  $F_8$  fold. The main cleavage  $S_{3a}$  is overprinted by the crenulation cleavage  $S_6$ , and both  $S_{3a}$  and  $S_6$  are overprinted by the crenulation cleavage  $S_7$  (Phe Fm. slate, SW is on the left hand side, insets: photomicrographs).

Tab. 6. Deformational phases and stages of metamorphic crystallization occurring in section 3, presented in their sequential order. Geometry and orientations of structures, foliations and mineral assemblages are shown for the Precambrian to Lower Cambrian Phe Formation. For the Lower Ordovician Hanuman Tibba Intrusion, the geometry of the structures is shown. Minerals in bold are related to the respective stage of metamorphic crystallization and/or foliation. Axial surfaces and schistosity related to the phases D<sub>2</sub>, D<sub>3a</sub> and D<sub>6</sub> are distributed along a NE-SW-trending axis. This demonstrates that D<sub>6</sub> was overprinted by D<sub>7</sub>, that D<sub>3a</sub> was overprinted by D<sub>6</sub> and by D<sub>7</sub> and that D<sub>2</sub> was affected by all three subsequent phases. D<sub>3a</sub>, D<sub>6</sub> and D<sub>7</sub> are coaxial phases.

Phase	Phe Formation			Hanuman Tibba Intrusion
	Geometry	Foliation	Mineral assembl.	Geometry
D <sub>1</sub> M <sub>1</sub>		Continuous cleavage/schistosity S <sub>1</sub>	Qtz, pl, <b>bt</b> , <b>wm</b> , <b>grt</b>	
D <sub>2</sub> M <sub>2</sub>		Continuous cleavage/schistosity S <sub>2</sub>	Qtz, pl, <b>bt</b> , <b>wm</b> , <b>gr</b> , <b>grt</b>	
D <sub>3a</sub> M <sub>3</sub>		Crenulation cleavage S <sub>3a</sub>	Qtz, pl, <b>bt</b> , <b>wm</b> , <b>grt</b>	
D <sub>3b</sub>				
D <sub>6</sub>		Crenulation cleavage S <sub>6</sub>	Qtz, pl, <b>bt</b> , <b>wm</b>	
D <sub>7</sub>			Qtz, pl, <b>bt</b> , <b>wm</b>	
D <sub>B</sub>			Qtz, pl, <b>bt</b> , <b>wm</b>	

Orientation of structural elements, projected on the lower hemisphere of the Schmidt equal area stereonet

- Fold axis
- ▲ Axial surface
- Schistosity
- + Lineation
- Shear zone

contact with the Hanuman Tibba intrusion is locally revealed by a biotite hornfels rim.

#### Deformation in the Hanuman Tibba intrusion

Two structural elements are observed in the orthogneiss: a schistosity S<sub>2</sub>, marked by biotite and white mica and systematic parallel joints and shear zones crosscutting S<sub>2</sub>. Often, the joints are sealed with quartz and/or tourmaline. Both joints and shear zones are generally parallel to S<sub>3a</sub> in the metasediments. They are locally deformed by phases postdating D<sub>3a</sub>.

#### Section 3: Southwestern upper Chandra valley

##### Deformation in the metasediments

In the southwestern upper Chandra valley section, seven phases of deformation (D<sub>1</sub>, D<sub>2</sub>, D<sub>3a</sub>, D<sub>3b</sub>, D<sub>6</sub>, D<sub>7</sub> and D<sub>B</sub>) are ob-

served (Table 6). For all phases, the sequence is clearly indicated by microscopic and/or macroscopic interference patterns, which are best documented in the phyllites, two-mica schists and biotite schists of the Phe Formation (Fig. 19).

The dominant structural element in the Phe Formation phyllites and schists is a continuous cleavage or a continuous schistosity S<sub>2</sub>, depending on the grain size. S<sub>2</sub> locally appears as a crenulation cleavage superposed on the oldest observable cleavage S<sub>1</sub> (Fig. 21). S<sub>1</sub> and S<sub>2</sub> are both marked by biotite and white mica, occasionally also by graphite flakes. S<sub>2</sub> is related to the isoclinal, asymmetric D<sub>2</sub> folding of the sedimentary bedding, that is observed generally on a centimeter- to meter-scale (Figs. 22, 23). A strong, consistently E-W-oriented mineral stretching lineation L<sub>2</sub> is observed, marked by biotite in the metapelites and by actinolite in the metamarl layers. Field analyses of the relationships between the sedimentary bedding and S<sub>2</sub> as well as of small-scale F<sub>2</sub> parasitic folds reveal a kilo-

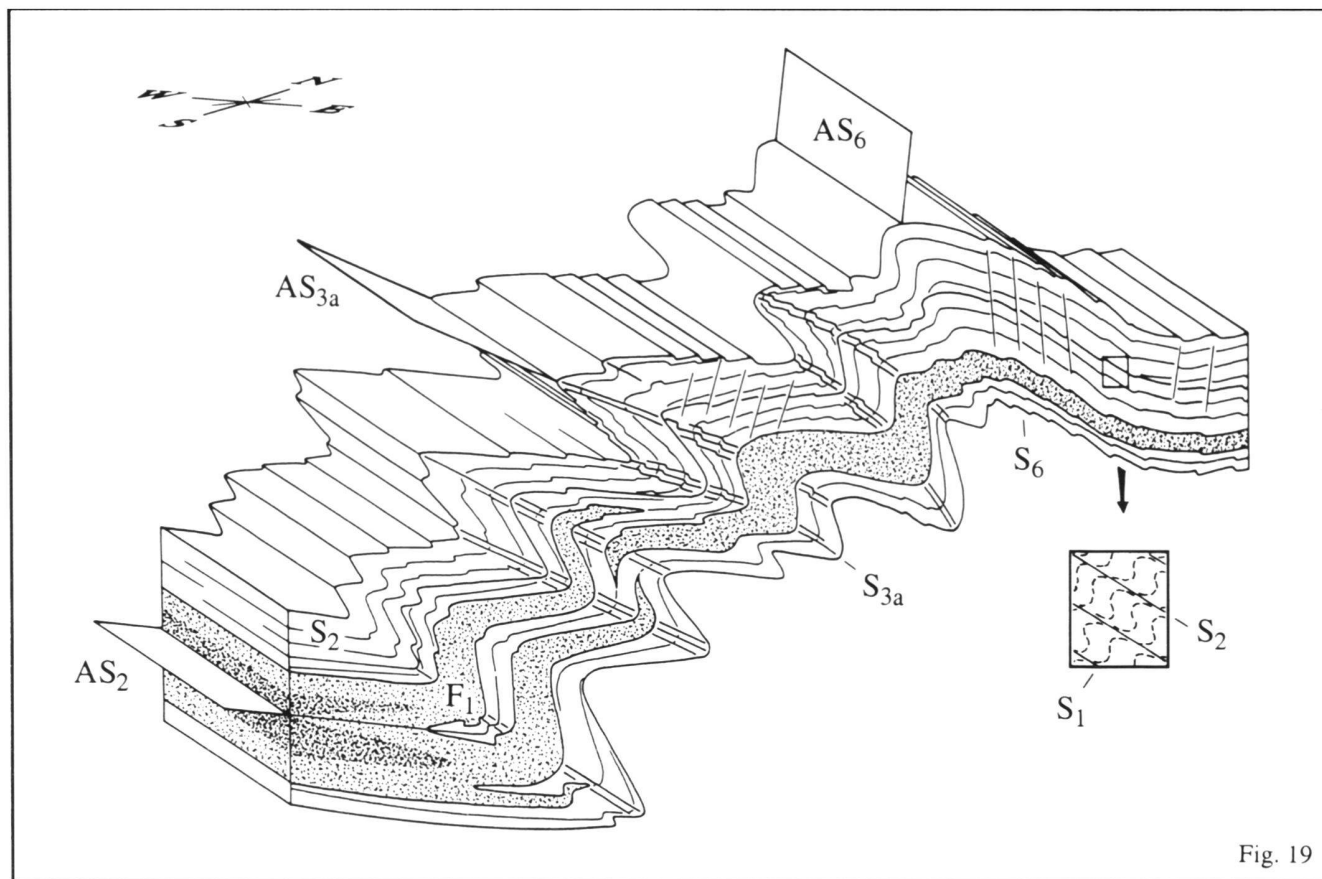


Fig. 19

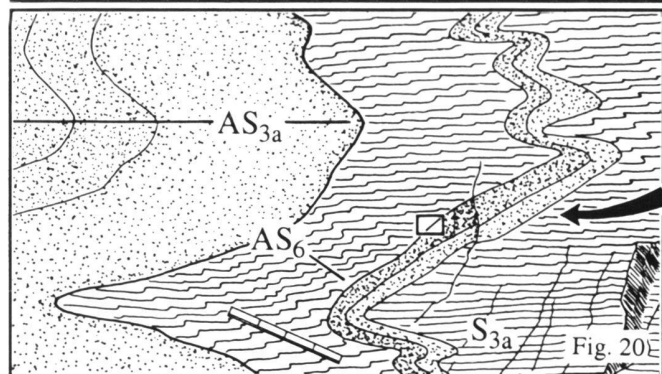


Fig. 20

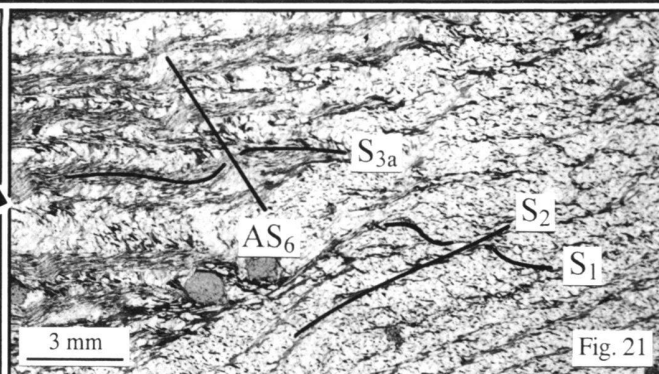


Fig. 21

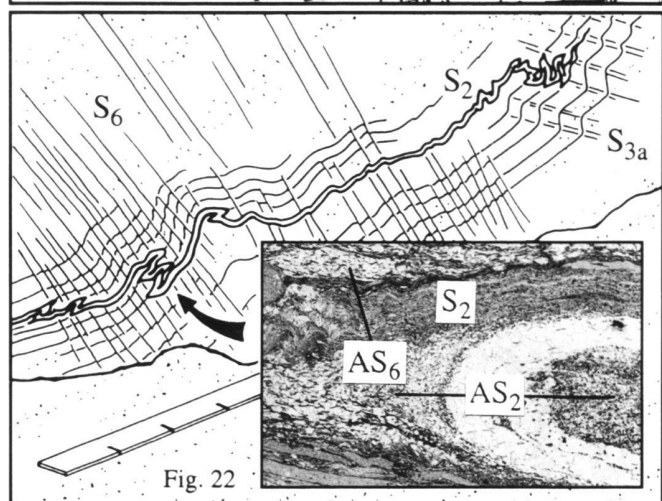


Fig. 22

Fig. 19. Block diagram, summarizing the style of the main phases of deformation and their relationships in section 3, observed in the Phe Fm. (not to scale, for abbreviations see Table 3).

Fig. 20.  $F_{3a}$  folds, affecting the sedimentary bedding. The crenulation cleavage  $S_{3a}$  is overprinted by  $F_6$  crenulations (Phe Fm., measuring rod for scale: 20 cm, SW is on the left hand side).

Fig. 21. Detail of Fig. 20 (frame), showing three schistosity:  $S_1$  and  $S_2$  are documented in the competent bed on the right hand side and the crenulation cleavage  $S_{3a}$  is well developed in the incompetent bed on the left hand side.  $S_{3a}$  is crenulated by  $D_6$  (garnet-bearing two-mica schist, photomicrograph).

Fig. 22. Thin quartz layer, affected by  $F_2$  folds. The  $F_2$  folds and  $S_2$  are overprinted by  $F_{3a}$  folds and by  $F_6$  crenulations (Phe Fm., chlorite-bearing two-mica schist, measuring rod for scale: 20 cm, SW is on the left hand side, inset: photomicrograph).



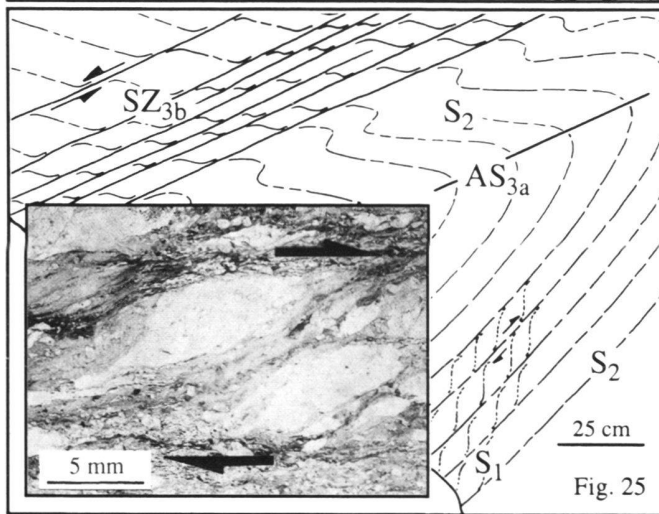
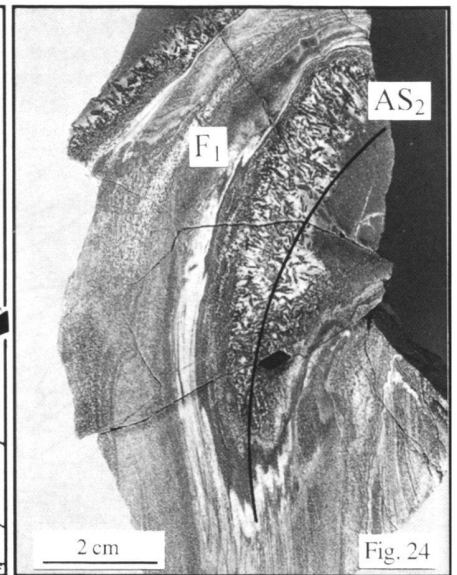
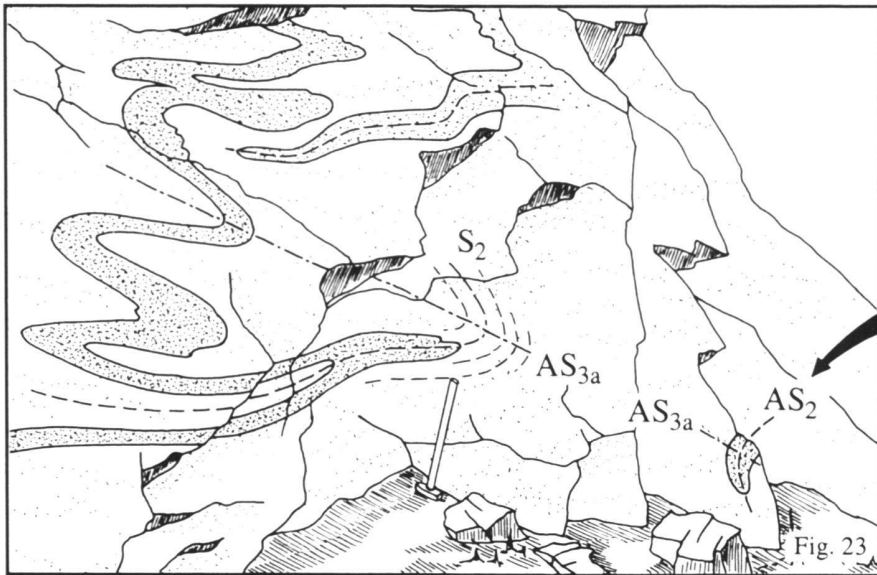


Fig. 23.  $F_2$  folds, overprinting the sedimentary bedding. The  $F_2$  folds and  $S_2$  are affected by  $D_{3a}$  (Phe Fm., Hammer for scale: 45 cm, SW is on the left hand side).

Fig. 24. Detail of Fig. 23 (arrow), showing a  $F_2$  fold that overprints a metamorphic layer in metapelite. The small fold, which displays a wrong vergence with respect to the  $F_2$  fold is interpreted as a  $F_1$  fold. The  $F_2$  fold is overprinted by an open  $F_{3a}$  fold (garnet- and hornblende-bearing biotite schist, polished hand specimen).

Fig. 25.  $S_1$  is overprinted by C-type shear bands with a shear sense top-to-the NE, representing  $S_2$ .  $S_1$  and  $S_2$  are affected by a  $F_{3a}$  fold that is crosscut by a ductile shear zone  $SZ_{3b}$  with a shear sense top-to-the SW (Hanuman Tibba orthogneiss, inset: photomicrograph, SW is on the left hand side).

meter-scale  $F_2$  fold in the southwestern upper Chandra valley termed the Shigri Fold in this study (Plate 1). The existence of  $D_1$  is documented by  $S_1$  only, with the exception of one outcrop, where a small isoclinal  $F_1$  fold is revealed by its incorrect vergence on a  $F_2$  fold (Fig. 24).

The sedimentary bedding,  $S_1$  and  $S_2$  are affected by the close to isoclinal asymmetric polyharmonic  $F_{3a}$  folds on a decimeter- to hundred-meters-scale (Fig. 20).  $F_{3a}$  is the dominant folding in this section with a consistent vergence towards SW. In mica-rich layers,  $S_2$  is occasionally overprinted by a crenulation cleavage  $S_{3a}$ , marked by biotite and white mica (Fig. 20).

The subsequent deformation  $D_6$  is observed as  $F_6$  folds or crenulations, verging towards NE or SW and overprinting the sedimentary bedding,  $S_2$  and/or  $S_{3a}$  (Figs 20, 21, 22). Their axes are coaxial with  $FA_{3a}$  and their axial surfaces are always mod-

erately to steeply inclined. Often, a strong  $S_6$  crenulation cleavage is associated (Fig. 22).

Where  $S_6$  dips steeply towards NE, it is locally deformed by open  $F_7$  folds with a subhorizontal axial surface. No cleavage is associated with  $F_7$ .  $D_7$  may account on a large scale for the relatively wide range of orientations of  $S_6$  and  $F_6$  axial surfaces (Table 6). Rare  $D_B$  folds are observed that correspond in style to  $D_{B1}$  in section 1, displaying steep axes and variable vergences and orientations of axial surfaces.

#### Metamorphism in the metasediments

Three stages of metamorphic crystallization are observed in the Phe Formation phyllites and schists. Stage  $M_1$  is related to  $D_1$ , stage  $M_2$  is related to  $D_2$  and stage  $M_3$  is related to  $D_{3a}$ . Biotite and white mica are observed on  $S_1$ , on the main schistosi-

Tab. 7. Deformational phases and stages of metamorphic crystallization occurring in section 4, presented in their sequential order. Geometry and orientations of structures, foliations and mineral assemblages are shown for the Precambrian to Lower Cambrian Phe Formation. For the Hanuman Tibba Intrusion, the geometry of the structures is shown and D<sub>2</sub>-orientations in the Sara Umga valley are indicated. Minerals in bold are related to the respective stage of metamorphic crystallization and/or foliation.

The axial surfaces of F<sub>A</sub> folds are orientated along an E-W-trending axis. This indicates that they were affected by a later deformational phase with N-S-trending fold axes, probably phase D<sub>C</sub> that occurs in section 5 on a outcrop scale.

Phase	Phe Formation			Hanuman Tibba Intrusion	Orientation of structural elements, projected on the lower hemisphere of the Schmidt equal area stereonet
	Geometry	Foliation	Mineral assembl.	Geometry	
D <sub>1</sub> M <sub>1a</sub> M <sub>1b</sub>		Schistosity S <sub>1</sub>	Qtz, pl, <b>bt</b> , <b>wm</b> , <b>grt</b> , <b>sil</b> , ky, +- st, +- Kfs		
D <sub>2</sub> M <sub>2</sub>		Crenulation cleavage S <sub>2</sub> (cleavage domains)	Qtz, pl, <b>bt</b> , <b>wm</b> , <b>grt</b> , <b>ky</b> , +- st		
D <sub>3</sub> M <sub>3</sub>		Very rare schistosity/ crenulation cleavage S <sub>3</sub>	Qtz, pl, <b>bt</b> , <b>wm</b> , <b>ky</b> , <b>grt</b>		
D <sub>5</sub> M <sub>5</sub>		Shear bands SB <sub>5</sub>	Qtz, pl, <b>bt</b> , <b>wm</b> , <b>grt</b> , <b>sil</b>		
D <sub>6</sub>			Qtz, pl, <b>bt</b> , <b>wm</b> , <b>grt</b>		
D <sub>7</sub>		Shear bands SB <sub>7</sub>	Qtz, pl, <b>bt</b> , <b>wm</b> , <b>grt</b>		
D <sub>A</sub>			Qtz, pl, <b>bt</b> , <b>wm</b> , <b>grt</b>		

ty S<sub>2</sub> and on S<sub>3a</sub> and are therefore related to all three stages. Garnet is on one hand wrapped around by S<sub>2</sub> in an augen-like texture, documenting its existence prior to S<sub>2</sub> but on the other hand, it also overgrows S<sub>1</sub>, establishing that it crystallized post-D<sub>1</sub> and pre-or syn- D<sub>2</sub>. As a consequence, garnet growth is considered to be related to both stages of metamorphic crystallization M<sub>1</sub> and M<sub>2</sub>, indicating that both of them reached garnet zone conditions that correspond to upper greenschist facies conditions or lower epidote amphibolite facies conditions. By contrast, no garnet growth related to S<sub>3a</sub> is observed. However, garnets do not show any signs of resorption. This may indicate that the M<sub>3</sub> metamorphic conditions were also within or very close to the stability of garnet. Mineral growth parallel to the crenulation cleavage S<sub>6</sub> is not observed.

#### Deformation in the Hanuman Tibba intrusion

As in section 2, generally two structural elements are observed in the orthogneiss: a schistosity S<sub>2</sub>, marked by biotite and white mica and systematic parallel joints and small-scale shear zones crosscutting S<sub>2</sub>. These shear zones are parallel to S<sub>3a</sub> in the metasediments. In addition, large-scale ductile shear zones SZ<sub>3b</sub> with a width of up to one meter are observed (Fig. 25) that crosscut the joints and small-scale shear zones with a small angle. These shear zones are characterized by C- and C'-type shear bands SB<sub>3b</sub>, superimposed on S<sub>2</sub>. Their shear sense is top-to-the SW. Both S<sub>2</sub> and SB<sub>3b</sub> are locally overprinted by D<sub>6</sub> and D<sub>7</sub> crenulations. A F<sub>3a</sub> fold in a microgranite layer near a SZ<sub>3b</sub> shear zone (Fig. 25) affects two schistositities that are con-

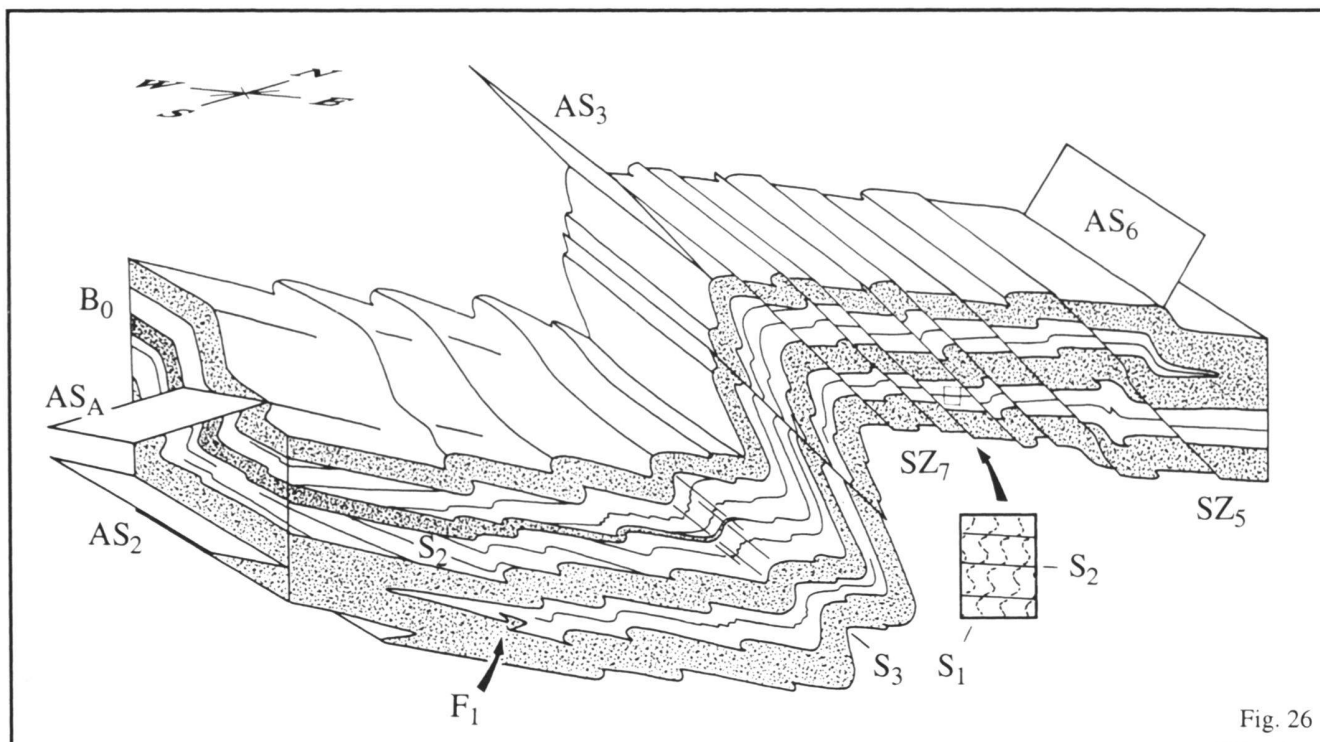


Fig. 26



Fig. 27

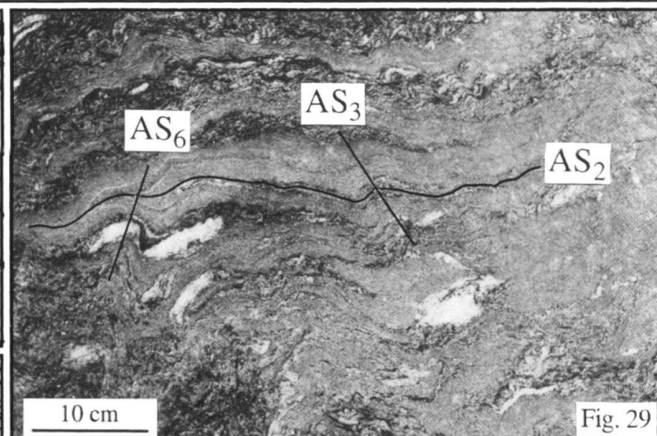


Fig. 29

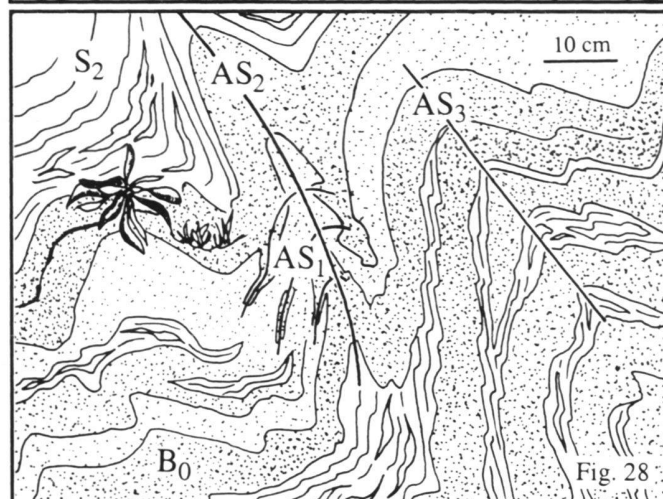


Fig. 28

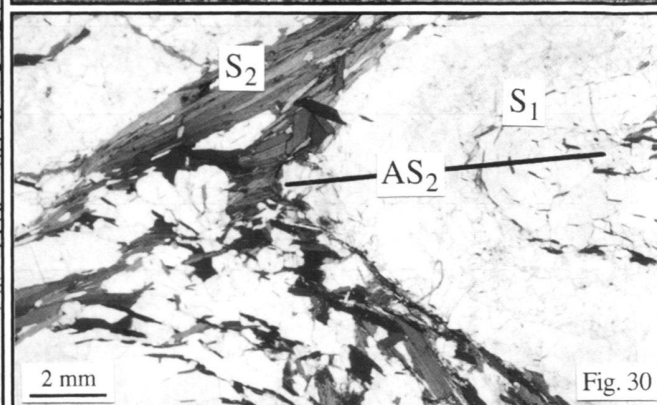


Fig. 30

Fig. 26. Block diagram, summarizing the style of the most important phases of deformation and their relationships in section 4, observed in the Phe Fm. (not to scale, for abbreviations see Table 3).

Fig. 27. Crenulation cleavage  $S_2$ , overprinting  $S_1$ .  $S_1$  is preserved in the microlithons (Phe Fm., two-mica gneiss, photomicrograph).

Fig. 28.  $F_1$  folds and  $F_2$  folds, displaying a mushroom (type 2) interference pattern.  $F_1$  and  $F_2$  were subsequently affected by  $F_3$  folds (Phe Fm., SW is on the left hand side).

Fig. 29.  $F_2$  folds are overprinted by  $F_3$  folds and  $F_6$  folds, displaying a convergent-divergent (type 3) interference pattern (Phe Fm., SW is on the left hand side).

Fig. 30.  $F_2$  fold, affecting  $S_1$  (Phe Fm., two-mica gneiss, photomicrograph).

sidered to be  $S_1$  and  $S_2$ .  $S_1$  is overprinted by C-type shear bands with a shear sense top-to-the NE, representing  $S_2$ . The contact with the Phe Formation metasediments is locally folded by  $F_2$  folds that display an axial surface schistosity  $S_2$  on both sides of the contact, and by  $F_3$  folds.

#### *Section 4: Tos- and Sara Umga valleys*

##### *Deformation in the metasediments*

In the Tos valley section, seven phases of deformation ( $D_1$ ,  $D_2$ ,  $D_3$ ,  $D_5$ ,  $D_6$ ,  $D_7$ ,  $D_A$ ) are observed (Table 7). For all phases the sequence is indicated by microscopic and/or macroscopic interference patterns which are best documented in the paragneiss of the Phe Formation (Fig. 26).

The dominant structural element is a spaced schistosity  $S_2$ , marked by biotite, white mica and kyanite.  $S_2$  represents cleavage domains, overprinting the oldest recognizable schistosity  $S_1$  that is marked by biotite and white mica (Fig. 27).  $S_1$  also occurs in quartz lenses and as relic inclusions in garnet. It is related to an isoclinal  $F_1$  folding that is only observed on a small scale (Fig. 28).

$S_2$  is related to the isoclinal  $F_2$  folding with strongly varying fold axes that is observed on a centimeter- to hundred meter-scale. In the Phe Formation paragneiss, mainly centimeter- to meter-scale  $F_2$  folds are observed, macroscopically affecting the sedimentary bedding and/or quartz layers (Fig. 29) and microscopically affecting  $S_1$  (Fig. 30). In the metamarl layers,  $S_2$  is revealed by hornblende growing parallel to the  $AS_2$  axial surface in  $F_2$  fold hinges. Numerous repetitions of the carbonaceous graphitic quartzite bed are observed in the Tos valley (Plate 1). Alternating relationships between  $S_2$  and the sedimentary bedding and alternating local vergences of parasitic  $F_2$  folds on repeated beds indicate that large-scale isoclinal  $F_2$  folding is responsible for these repetitions (Fig. 31).  $L_2$  mineral stretching lineations, marked by biotite, kyanite and tourmaline in the metapelites and by hornblende in the carbonaceous graphitic quartzites are all E-W oriented. The related shear sense top-to-the E is best documented by asymmetrically boudinaged dikes (Figs. 32, 33).

The sedimentary bedding,  $S_1$  and  $S_2$  are affected by open to close, rarely also isoclinal, centimeter- to kilometer-scale  $F_3$  folds. Their asymmetric fold geometry indicates a vergence towards SW (Figs 34, 35). Locally, in  $F_3$  fold hinges of mica-rich layers, a  $S_3$  schistosity or crenulation cleavage occurs (Fig. 36). However, a penetrative schistosity  $S_3$  is not observed. Convergent-divergent (type 3) interference patterns between  $F_2$  and  $F_3$  folds are a common feature in this section (Fig. 29). Field analyses of small-scale parasitic fold systems reveal a kilometer-scale  $F_3$  fold in the central Tos valley, termed the Sharm Fold in this study (Plate 1).

$S_2$ ,  $F_2$ - and  $F_3$  folds are crosscut by innumerable, ductile, moderately inclined, NE-dipping  $SB_5$  shear bands (Fig. 37) that are distributed throughout the middle Tos valley. These shear bands are always discrete and marked by biotite and sil-

limanite. Often, they are observed to crosscut kyanite on  $S_2$  (Fig. 38). The average orientation of the  $L_5$  stretching lineation on the shear bands, defined by biotite and sillimanite, plunges to the ENE. Shear criteria on  $SB_5$  indicate a hanging wall down-to-the ENE shear sense. The shear bands are rarely longer than some decimeters and wider than some millimeters. Often, they are concentrated locally and combined into huge shear zones of some hundred meters in length and several meters in width. Generally, the  $SB_5$  shear bands are folded by the subsequent deformation  $D_6$  (Figs. 37, 39).

The open  $F_6$  folding overprints macroscopically all structural elements related to  $D_1$ ,  $D_2$ ,  $D_3$  and  $D_5$ .  $F_6$  folds are observed on a centimeter- to ten meters-scale. Their fold axes are coaxial with the axes of  $F_3$  folds and their vergence is towards NE. Locally,  $F_6$  generates a crenulation on  $S_2$ . Convergent-divergent (type 3) interference patterns between  $F_2$  folds and  $F_6$  folds are a common feature in the northern part of the Tos Valley (Fig. 29).

Locally, the  $F_6$  folds are crosscut by the moderately inclined  $SB_7$  shear bands that dip to the NE. These shear bands are marked by biotite and white mica. Clear lineations are not observed. Local shear criteria, however, suggest a hanging wall-down-to the NE shear sense. The  $SB_7$  shear bands are some decimeters long and some millimeters wide. Like  $SB_5$  shear bands, they are often concentrated locally and combined into huge shear zones of some hundred meters in length and several meters in width. Occasionally, they are observed in direct vicinity of  $SB_5$  shear bands (Fig. 37).

$D_1$ ,  $D_2$ ,  $D_3$ ,  $D_5$  and  $D_7$ - structures are affected by the open to close  $F_A$  folding on a centimeter- to hundred meters-scale. Although its axial surfaces vary between moderately W-dipping orientations and shallowly E-dipping orientations, the  $F_A$  fold geometry indicates clearly a vergence towards E. Crenulations of  $S_2$ , caused by  $F_A$  folds, are often observed. Mushroom (type 2) interference patterns between  $F_3$  folds and  $F_A$  folds are a common feature in the southern part of the Tos valley (Fig. 40). The  $F_A$  axial surfaces are rotated around a N-S-trending axis (Table 7). This indicates deformation by a subsequent phase displaying large-scale, open folds with upright, N-S-trending axial surfaces.

##### *Metamorphism and migmatization in the metasediments*

Microtextural analyses reveal five stages of metamorphic crystallization in the metapelitic Phe Formation rocks, the conditions of which were all within the upper amphibolite facies:  $M_{1a}$  and  $M_{1b}$ ,  $M_2$ ,  $M_3$  and  $M_5$  (Table 7). In addition, a contact metamorphism along the contact with the Hanuman Tibba intrusion is well preserved in this section.

##### *Regional metamorphism*

$D_1$  is associated with two stages of metamorphic crystallization  $M_{1a}$  and  $M_{1b}$ . The first stage of metamorphic crystallization  $M_{1a}$  is represented by relics of kyanite in the center of aggregates of fibrolitic sillimanite that were originally oriented par-



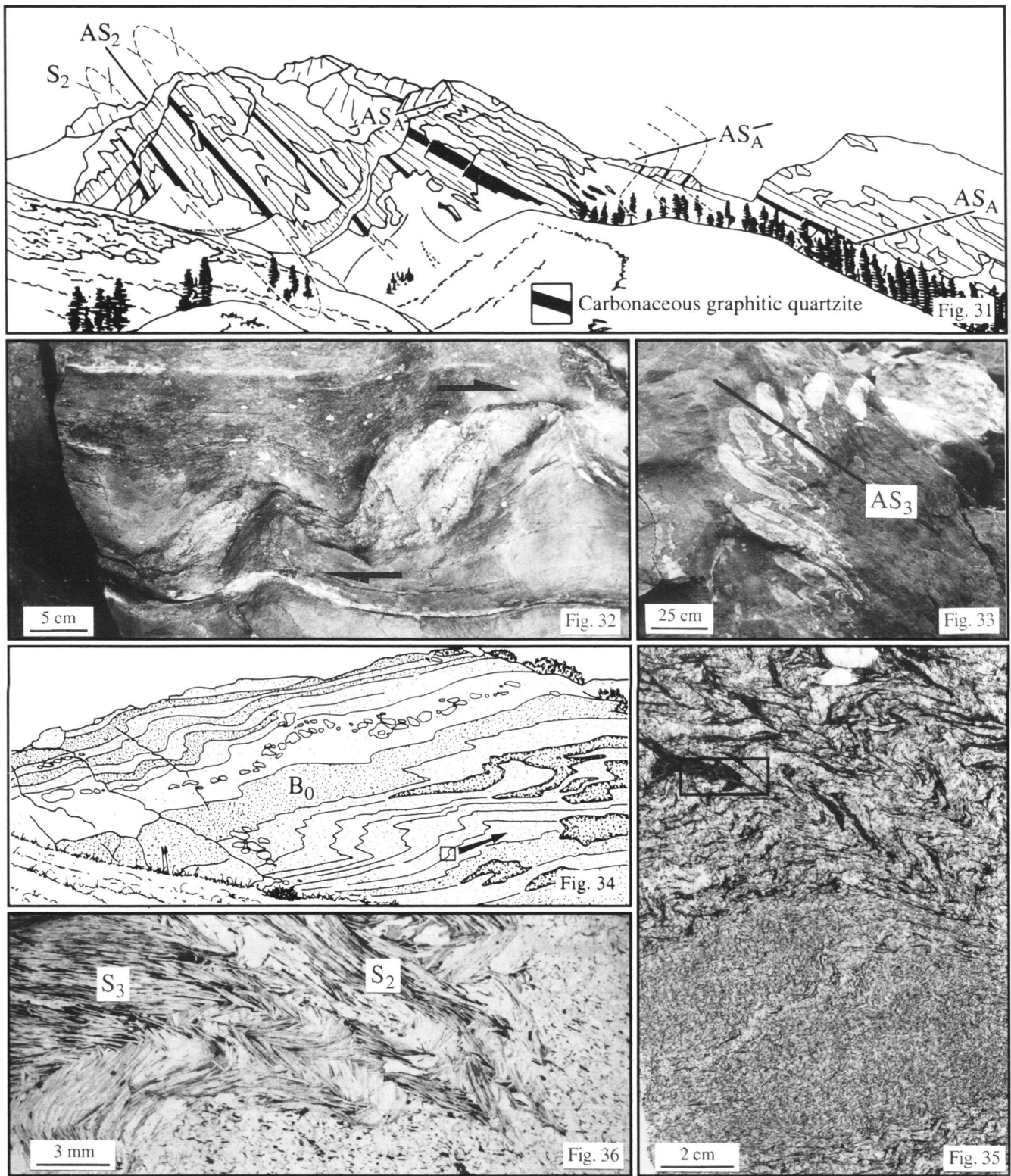


Fig. 31. View of the western slope of the lower Tos valley, NE of the village Tos. Numerous repetitions of a carbonaceous graphitic quartzite layer in the Phe Fm. are the result of  $F_2$  folding. The isoclinal  $F_2$  folds were subsequently overprinted by  $F_A$  folds.

Fig. 32. Pegmatite dike in the Phe Fm., sheared during  $D_2$ . The actual shear sense is top-to-the E (W is on the left hand side).

Fig. 33. Pegmatite dike, sheared during  $D_2$  and folded by a  $F_3$  fold. The actual shear sense is top-to-the E (Phe Fm., W is on the left hand side).

Fig. 34.  $F_3$  folds, affecting the sedimentary bedding  $B_0$  (Phe Fm., ski sticks for scale: 1.3 m, SW is on the left hand side).

Fig. 35. Detail of Fig. 34 (arrow), showing  $F_3$  folds that overprint  $S_2$  in a two-mica gneiss.  $F_3$  folds are well developed in the mica-rich, competent layer (polished hand specimen).

Fig. 36. Detail of Fig. 35 (frame), showing a  $S_3$  schistosity that developed in a mica-rich layer (photomicrograph).

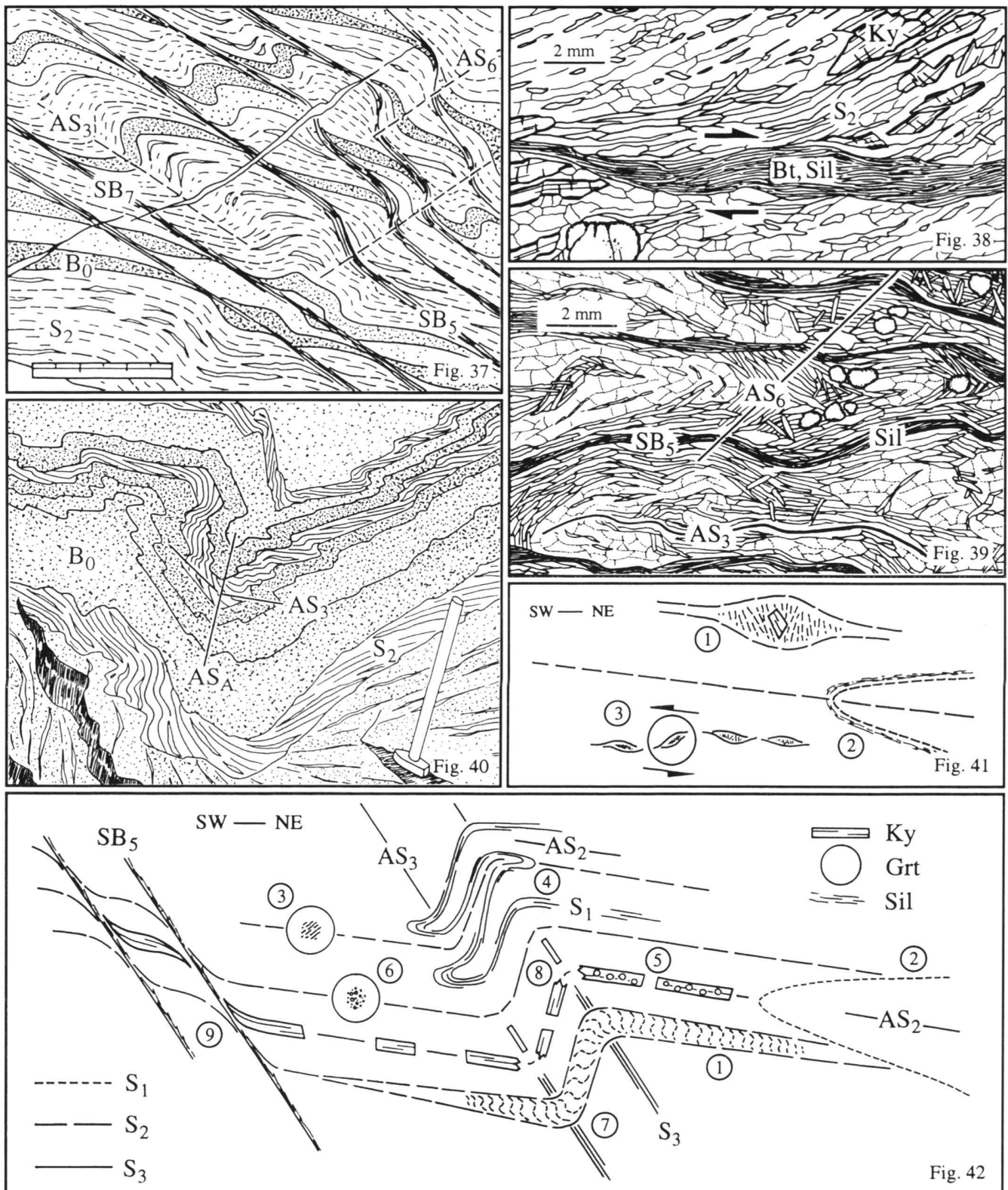


Fig. 37. SB<sub>5</sub> shear bands that are deformed by F<sub>6</sub> folds and SB<sub>7</sub> shear bands that crosscut F<sub>6</sub> folds (Phe Fm. gneiss, measuring rod for scale: 15 cm, SW is on the left hand side). Note that, as in the presented example, SB<sub>5</sub> and SB<sub>7</sub> shear bands are occasionally oriented parallel to AS<sub>3</sub>.

Fig. 38. SB<sub>5</sub> shear band with sillimanite and biotite, crosscutting kyanite on the schistosity S<sub>2</sub> (Phe Fm., kyanite-, sillimanite- and garnet-bearing two-mica gneiss, drawing after thin section, SW is on the left hand side).

Fig. 39. SB<sub>5</sub> shear bands with sillimanite and biotite that are deformed by F<sub>6</sub> folds (Phe Fm., kyanite- and sillimanite-bearing two-mica gneiss, drawing after thin section, SW is on the left hand side).

Fig. 40. Mushroom (type 2) interference pattern between F<sub>3</sub> folds and F<sub>A</sub> folds (Phe Fm., hammer for scale: 45 cm, W is on the left hand side).

Fig. 41. Microtextural relationships in fine-grained sillimanite- and garnet-bearing biotite schist (not to scale), legend: see Fig. 42.

Fig. 42. Microtextural relationships in coarse-grained garnet-, sillimanite- and kyanite-bearing two-mica gneiss (not to scale).

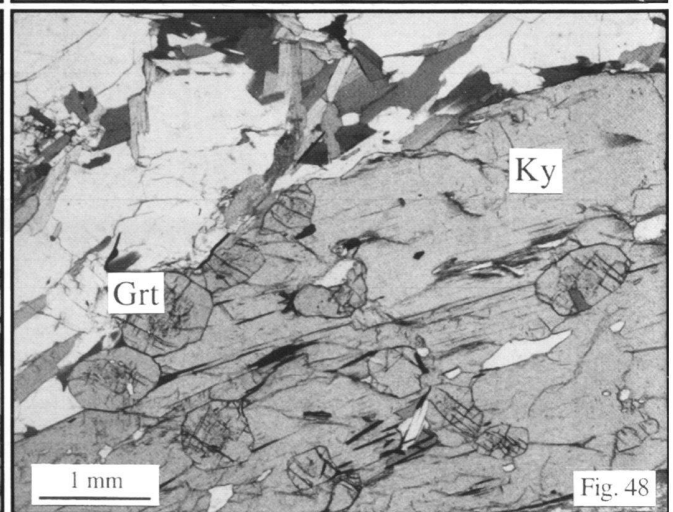
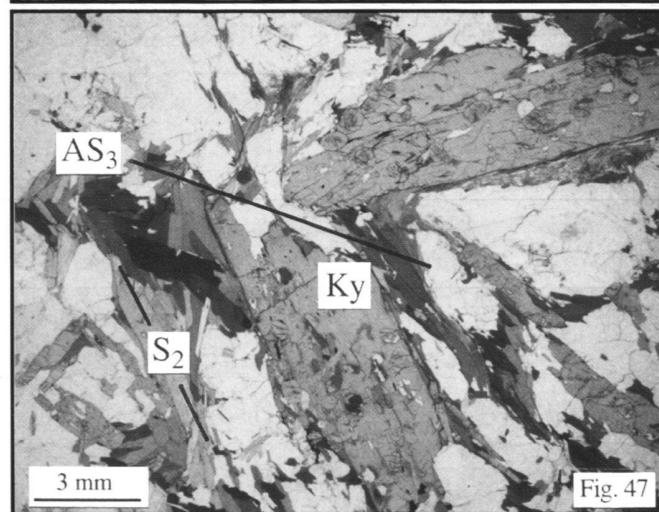
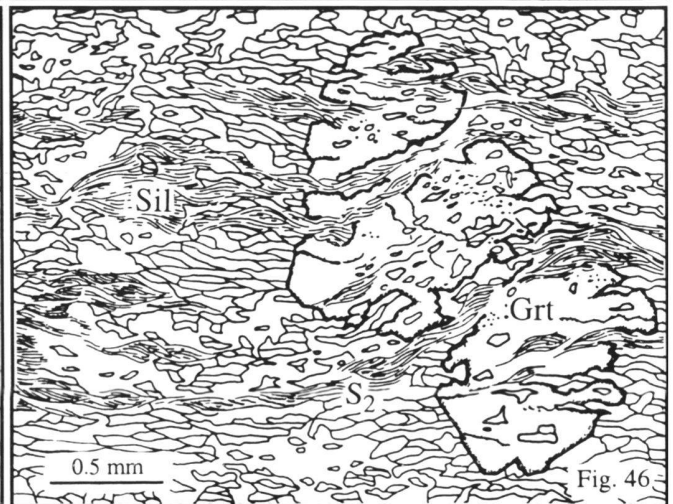
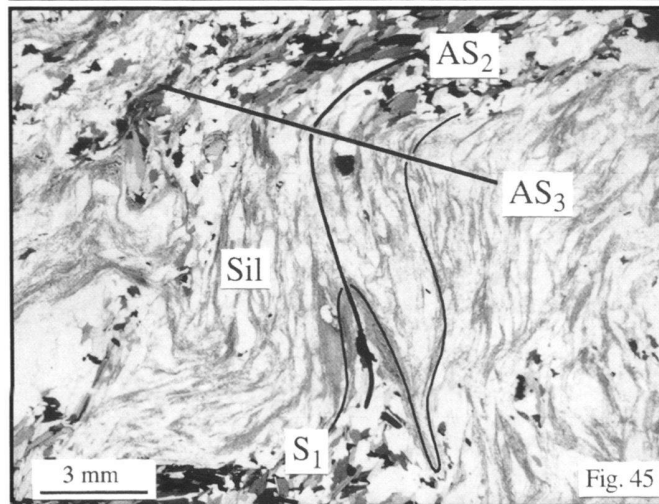
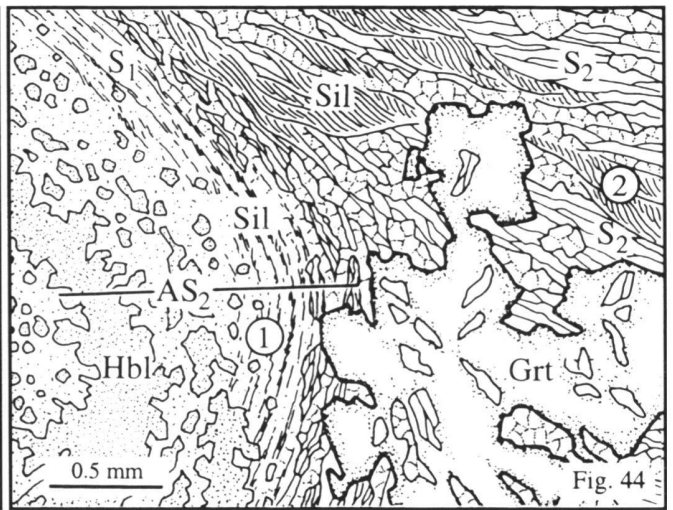
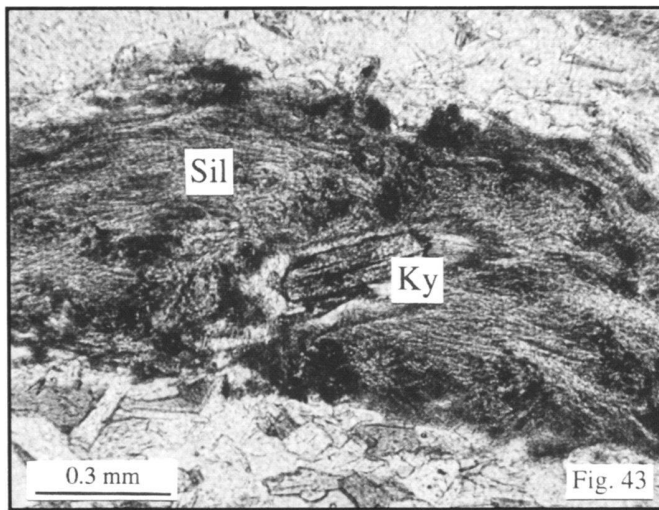


Fig. 43. Relic of kyanite, surrounded by aggregates of fibrolitic sillimanite. (Phe Fm., fine-grained sillimanite- and garnet-bearing biotite schist, photomicrograph).

Fig. 44. (1) Fibrolitic sillimanite, oriented parallel to  $S_1$ , overprinted by a  $F_2$  fold. (2) Fibrolitic sillimanite, reoriented parallel to and wrapped around by  $S_2$  (Phe Fm., fine-grained sillimanite- and garnet-bearing biotite schist with a metamarl layer, drawing after thin section).

Fig. 45. Sillimanite on  $S_1$  is folded by  $F_2$  folds and by  $F_3$  folds, forming a convergent-divergent (type 3) interference pattern (Phe Fm., sillimanite- and garnet-bearing two-mica schist, photomicrograph).

Fig. 46. Fibrolitic sillimanite on  $S_1$ , reoriented parallel to and wrapped around by  $S_2$  and included in a  $D_2$ -synkinematic garnet poikiloblast (Phe Fm., fine-grained sillimanite- and garnet-bearing biotite schist, drawing after thin section).

Fig. 47. Kyanite on  $S_2$ , broken by  $F_3$  folding. The kyanite contains small garnet inclusions (Phe Fm., garnet-, sillimanite- and kyanite-bearing two-mica gneiss, photomicrograph).

Fig. 48. Detail of Fig. 47, showing garnet inclusions in kyanite (photomicrograph).



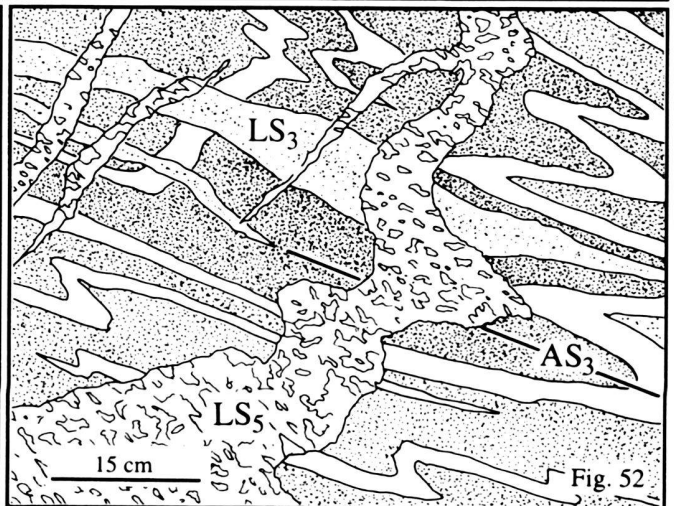
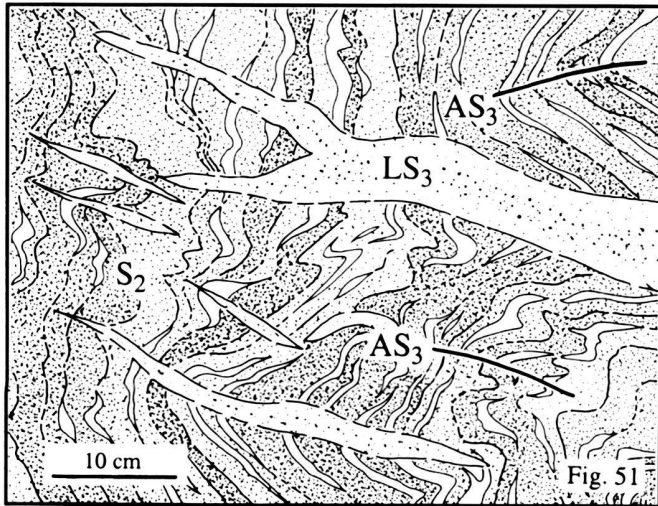
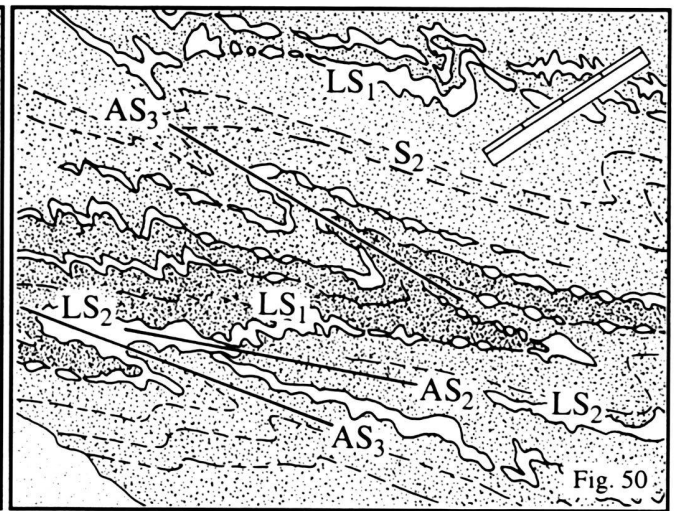
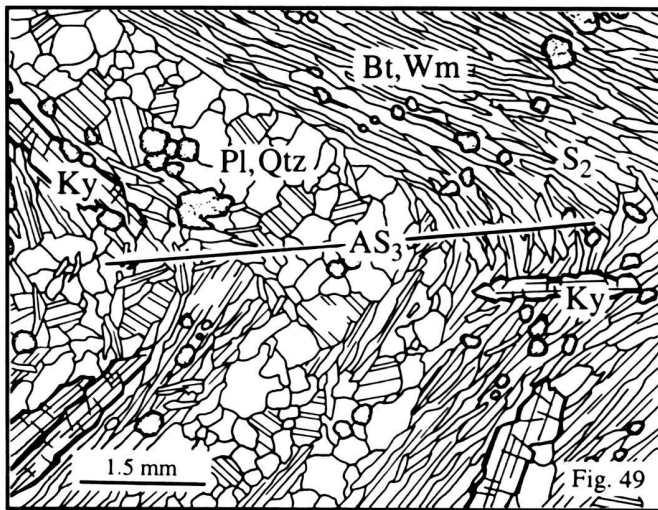


Fig. 49.  $S_2$  schistosity, folded by a  $F_3$  fold. Kyanite occurs on  $S_2$  and parallel to the axial surface of  $F_3$  (Phe Fm., garnet- and kyanite-bearing two-mica gneiss, drawing after thin section).

Fig. 50.  $F_2$  fold, affecting a leucosome that formed during  $D_1/M_1$  ( $LS_1$ ). Leucosomes oriented parallel to  $AS_2$  ( $LS_2$ ) are interpreted to be related to  $D_2/M_2$ . Both  $LS_1$  and  $LS_2$  leucosomes were subsequently deformed by  $F_3$  folds (Phe Fm., measuring rod for scale: 20 cm. SW is on the left hand side).

Fig. 51.  $F_3$  folds affecting the schistosity  $S_2$  that is crosscut by  $D_3/M_3$  leucosomes ( $LS_3$ ) oriented parallel to the axial surface of  $F_3$ . (Phe Fm., SW is on the left hand side)

Fig. 52.  $F_3$  folds and  $LS_3$  leucosomes are crosscut by coarse-grained dikes with an irregular shape that are interpreted to be  $LS_5$  leucosomes (Phe Fm., SW is on the left hand side).

allel to  $S_1$  (1 on Fig. 41 and Fig. 43).  $M_{1a}$  is therefore interpreted to be related to an early stage of  $D_1$  that reached kyanite zone conditions for metapelitic rocks.

The second stage of metamorphic crystallization  $M_{1b}$  is characterized by the mineral assemblage occurring on  $S_1$ . Generally,  $S_1$  is either marked by biotite and white mica in microlithons (1 on Fig. 42 and Fig. 27), along or inside quartz lenses (2 on Fig. 42 and Fig. 30) and in garnet poikiloblasts (3 on Fig. 42) or by fibrolitic sillimanite (2 on Fig. 41 and Fig. 44, 4 on Fig. 42 and Fig. 45). Frequently, this originally  $S_1$ -parallel sillimanite was reoriented parallel to  $S_2$  and/or wrapped around by  $S_2$  (1 on Fig. 41 and Fig. 44). Locally,  $S_2$ -reoriented  $S_1$  sillimanite is also included in  $D_2$ -synkinematic garnet poik-

iloblasts (3 on Fig. 41 and Fig. 46). K-feldspar frequently occurs in samples in which  $S_1$  is preserved. Kyanite crystals oriented parallel to  $S_2$  display small inclusions of garnet that are interpreted to be part of the  $M_1$  mineral assemblage (5 on Fig. 42 and Figs. 47, 48). The mineral assemblage biotite + white mica + sillimanite  $\pm$  garnet  $\pm$  K-feldspar indicates sillimanite zone conditions for  $M_{1b}$ , corresponding to the upper amphibolite facies.

The third stage of metamorphic crystallization  $M_2$  is related to  $S_2$ . Generally,  $S_2$  is marked by biotite and white mica that occur in cleavage domains, separating quartz- and plagioclase-rich microlithons (1 on Fig. 42 and Fig. 27), which are the product of metamorphic segregation during  $D_2/M_2$ . In addition,



kyanite crystals several centimeters long grew parallel to  $S_2$  (5 on Fig. 42 and Figs 47, 49), marking the stretching lineation  $L_2$ . Garnet poikiloblasts including relics of  $S_1$  and  $S_2$  display syntectonic growth with respect to  $D_2$  (3 on Fig. 41 and Fig. 46). Staurolite occurs as small, strongly resorbed relics on  $S_2$  and it is also observed as inclusions in  $D_2$ -syntectonic garnet. It is thus not clear, if staurolite crystallized during  $M_2$ , during  $M_1$ , or during both  $M_2$  and  $M_1$ . The  $M_2$  mineral assemblage plagioclase + quartz + biotite + white mica + garnet + kyanite  $\pm$  staurolite indicates metamorphic conditions within the kyanite zone for  $M_2$  (= amphibolite facies).

During the fourth stage  $M_3$ , minor mineral growth is documented. Biotite and white mica on  $S_2$  were crenulated during  $D_3$ . They were perfectly annealed, and no curved mica is observed (Fig. 36). The same recrystallization may be responsible for inclusion-free rims which are observed around many garnet poikiloblasts (6 on Fig. 42). Locally, biotite and white mica formed a schistosity  $S_3$  (7 on Fig. 42 and Fig. 36) and in a few cases, small kyanite crystals grew parallel to the axial surface of  $F_3$  folds (8 on Fig. 42 and Fig. 49). Broken kyanites on  $S_2$  are a common feature in  $F_3$  fold hinges (8 on Fig. 42 and Fig. 47). Although less mineral growth is documented during  $M_3$  than during  $M_2$ , the associated mineral assemblage reveals kyanite zone conditions for  $M_3$  as well.

The fifth stage of metamorphic crystallization  $M_5$  is restricted to the  $SB_5$  shear bands that are characterized by the crystallization of sillimanite and biotite (9 on Fig. 42 and Fig. 38), indicating sillimanite zone conditions for  $M_5$  (= amphibolite facies). The deformational phases  $D_6$  and  $D_A$  are not associated with any crystallization of minerals parallel to the axial surface of the  $F_6$  and  $F_A$  folds. Biotite and white mica on  $S_2$ , that were crenulated during  $D_6$  and  $D_A$ , were perfectly annealed and no curved mica is observed. In most cases, garnet remained stable during  $D_6$  and  $D_A$ . This indicates that  $D_6$  and  $D_A$  occurred at least under biotite to garnet zone conditions, corresponding to the upper greenschist or epidote-amphibolite facies. The  $SB_7$  shear bands are marked by biotite and white mica, indicating biotite zone conditions for low-Al metapelites, corresponding to greenschist facies conditions.

#### *Migmatite formation*

Migmatization occurred in the mica-rich Phe Formation beds only. Our observations suggest four phases of migmatite formation that are related to  $D_1$ ,  $D_2$ ,  $D_3$  and  $D_5$ . The respective leucosomes  $LS_1$ ,  $LS_2$ ,  $LS_3$  and  $LS_5$  consist of quartz, plagioclase and rare K-feldspar.

Numerous outcrops displaying interferences between  $F_2$  folds and  $F_3$  folds show two types of leucosomes: leucosomes oriented parallel to  $S_2$  that were folded by  $F_3$ , crosscutting the  $F_2$  fold hinges parallel to the axial surfaces  $AS_2$ , and leucosome bands that were folded by  $F_2$  and  $F_3$  (Fig. 50). The leucosomes that were affected by  $F_2$  folds ( $LS_1$ ) are interpreted to be related to the metamorphism  $M_1$  (a/b not distinguishable). The leucosomes that crosscut the  $F_2$  folds ( $LS_2$ ) are suggested to have formed contemporaneously with  $D_2/M_2$ .  $F_3$  fold

hinges are locally crosscut by a series of leucosomes, that are oriented parallel to the axial surface  $AS_3$ . These leucosomes ( $LS_3$ ) are interpreted to be the result of  $D_3$  and  $M_3$ . (Fig. 51). The leucosomes  $LS_1$ ,  $LS_2$  and  $LS_3$  generally represent in-situ melting of the metapelites, as melt migration is not observed.  $F_2$  and  $F_3$  folds are crosscut by leucosomes forming dikes with an irregular shape (Fig. 52) that are interpreted to represent migrated melts ( $LS_5$ ). These melts always crosscut  $LS_3$  leucosomes, indicating that they are not migrated  $LS_3$  melts and, as a consequence, they formed after  $D_3/M_3$ , most probably during  $M_5$ .

#### *Contact metamorphism*

The fine-grained texture of the sillimanite- and garnet-bearing biotite schist, that occurs near the contact of the Phe Formation with the Hanuman Tibba intrusion only, is interpreted to represent the record of a hornfels texture due to contact metamorphism of previously unmetamorphosed pelitic sediments during intrusion of the Hanuman Tibba intrusion. In addition andalusite that is characterized by chistolite crosses crystallized in the direct vicinity of the contact with the intrusion, indicating high temperature-low pressure conditions that fit well with contact metamorphism. The intrusion of the Hanuman Tibba intrusion is therefore predating the first regional metamorphism  $M_1$ . Andalusite was subsequently overgrown by white mica and quartz that formed pseudomorphs.

#### *Deformation and migmatization in the Hanuman Tibba intrusion*

In the orthogneiss,  $S_2$  is the dominant structural element. In general, the imprint of  $S_2$  is strong along the contact with the Phe Formation metasediments and decreases towards the center of the intrusion.  $F_2$  folds are observed to affect magmatic layering near the contact and  $F_3$  folds overprint both magmatic layering and  $S_2$ . On  $F_3$  normal limbs, K-feldspar augen show a shear sense top-to-the E on  $S_2$ . C'-type shear bands overprinting  $S_2$  indicate a shear sense hanging wall down-to-the NE. Therefore, they may be related to  $D_5$  or  $D_7$ . In the Sara Umga valley,  $S_2$  dips generally either to the W or to the E (Table 7) indicating deformation by a late stage phase displaying large-scale open folds with upright, N-S-trending axial surfaces.

Migmatization is well documented in the orthogneiss by leucosomes consisting of quartz, plagioclase and K-feldspar. The most common feature in these rocks are leucosomes parallel to  $S_2$  that formed during  $M_2$  and leucosomes crosscutting  $F_3$  fold hinges parallel to their axial surface  $AS_3$  that are interpreted to be related to  $M_3$ .

#### *Section 5: Parvati- and Brahamganga valleys*

This section deals with the lowest part of the High Himalayan Crystalline and the uppermost part of the Lesser Himalayan Sequence, exposed in the Larji-Kullu-Rampur tectonic window.

Tab. 8. Deformational phases and stages of metamorphic crystallization occurring in section 5, presented in their sequential order. Geometry and orientations of structures, foliations and mineral assemblages are shown for the Precambrian to Lower Cambrian Phe Formation in the High Himalayan Crystalline. For the Lesser Himalayan Sequence, the geometry of the structures is shown. Minerals in bold are related to the respective stage of metamorphic crystallization and/or foliation.

Phase	High Him. Crystalline, Phe Formation			Phase	Lesser Himalayan Sequence	Orientation of structural elements, projected on the lower hemisphere of the Schmidt equal area stereonet
	Geometry	Foliation	Mineral assembl.		Geometry	
				D <sub>I</sub>	?	<p>○ Fold axis ▲ Axial surface □ Schistosity + Lineation ◆ Shear bands S2b</p>
D <sub>2</sub> M <sub>2</sub>		Cleavage domains S <sub>2</sub>	Qtz, pl, <b>wm</b> , <b>bt</b> , ky, grt	D <sub>II</sub> M <sub>II</sub> ?	?	
D <sub>3</sub>			Qtz, pl, wm, bt, ky, grt	D <sub>III</sub>		
D <sub>4</sub> M <sub>4</sub>		C- and C'-type shear bands SB <sub>4</sub>	<b>Qtz</b> , pl, <b>wm</b> , <b>chl</b> , <b>bt</b>	D <sub>4</sub> M <sub>4</sub>		
D <sub>6</sub>			Qtz, pl,wm, bt, chl	D <sub>6</sub>		
D <sub>A</sub>			Qtz, pl,wm, bt, chl	D <sub>A</sub>		
D <sub>C</sub>			Qtz, pl,wm, bt, chl	D <sub>C</sub>		

## Deformation

At the base of the High Himalayan Crystalline six phases of deformation (D<sub>2</sub>, D<sub>3</sub>, D<sub>4</sub>, D<sub>6</sub>, D<sub>A</sub> and D<sub>C</sub>) are observed (Table 8). In the Lesser Himalayan Sequence, the structures predating D<sub>3</sub> cannot be correlated directly with the structures in the High Himalayan Crystalline. They are therefore labeled with Roman numbers (D<sub>I</sub>, D<sub>II</sub>, D<sub>III</sub>). Fig. 53 shows a schematic structural and petrographic profile through the uppermost Lesser Himalayan Sequence and through the base of the High Himalayan Crystalline.

### The base of the High Himalayan Crystalline

The dominant structural elements at the base of the High Himalayan Crystalline are C- and C'-type shear bands SB<sub>4</sub> on a centimeter- to decimeter-scale, overprinting S<sub>2</sub>. L<sub>4</sub> lineations on these shear bands are oriented NE-SW and the shear bands indicate a hanging wall-to-the SW displacement. Locally, several superposed generations of SB<sub>4</sub> shear bands are observed. The

frequency and intensity of SB<sub>4</sub> is strongest at the base of the High Himalayan Crystalline and decreases upward. Near the base of the High Himalayan Crystalline, D<sub>4</sub> shear zones up to a hundred meters thick occur that are dominated by C-type shear bands (1 on Fig. 53). With increasing distance from the base of the High Himalayan Crystalline, C'-type shear bands predominate (2 on Fig. 53, Fig. 54), the most distant ones occurring as far as 2500 m above the base of the High Himalayan Crystalline. C- and C'-type shear bands are characterized by the crystallization of chlorite, biotite and quartz. In large-scale shear zones near the base of the High Himalayan Crystalline, biotite disappears in favour of chlorite. Chlorite and biotite are also observed on S<sub>2</sub> between the SB<sub>4</sub> shear bands, indicating reactivation of S<sub>2</sub> during D<sub>4</sub> shearing. Leucosomes and D<sub>2</sub> microlithons were deformed to thin quartz-feldspar ribbons during D<sub>4</sub>.

Structures predating the SB<sub>4</sub> shear bands include relics of F<sub>2</sub>- and F<sub>3</sub> folds (3 on Fig. 53). D<sub>4</sub> is postdated by F<sub>6</sub>-, F<sub>A</sub>- and F<sub>C</sub> folds (4 on Fig. 53; Fig. 55). D<sub>C</sub> is observed in section 5 only. It displays subvertical, NNW-SSE-trending axial surfaces and

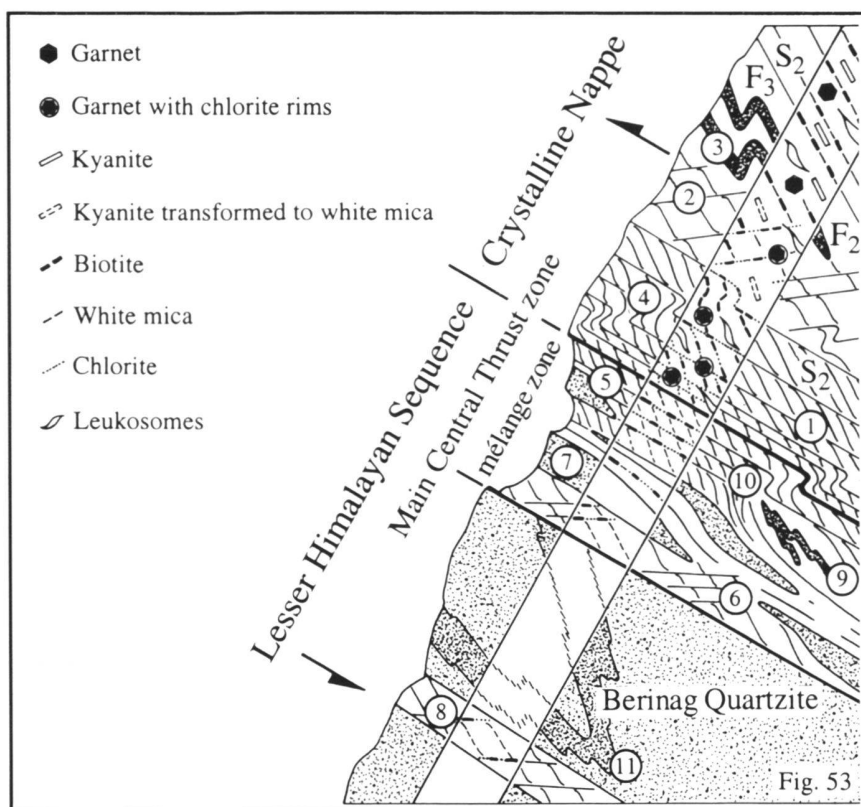


Fig. 53. Schematic section through the uppermost Lesser Himalayan Sequence and the base of the High Himalayan Crystalline (Crystalline Nappe), showing the main structures and the main mineral assemblages (not to scale, explanations to the numbers see text).

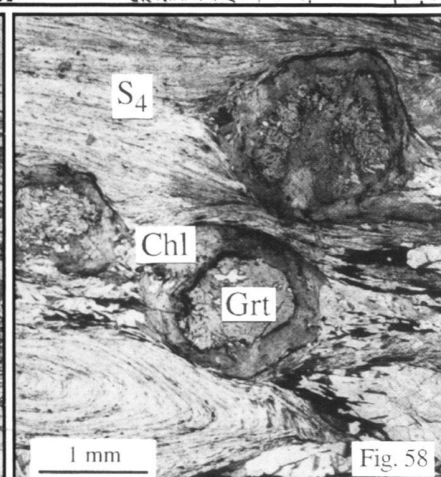
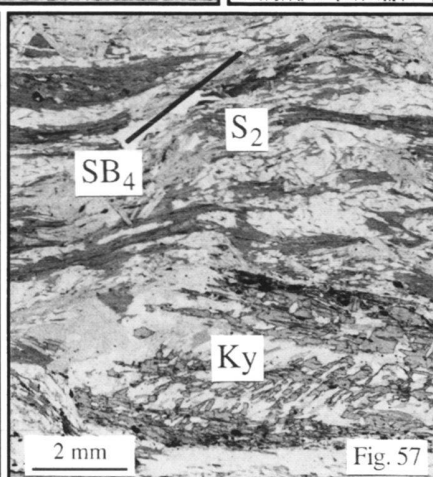
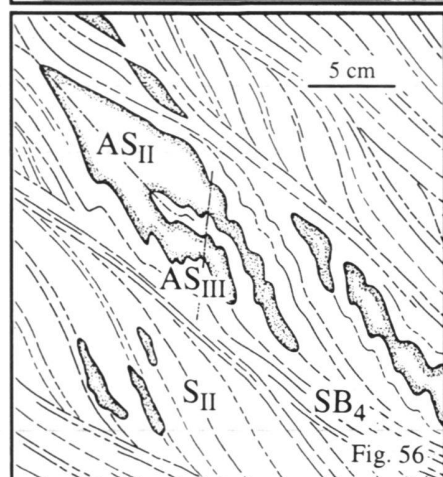
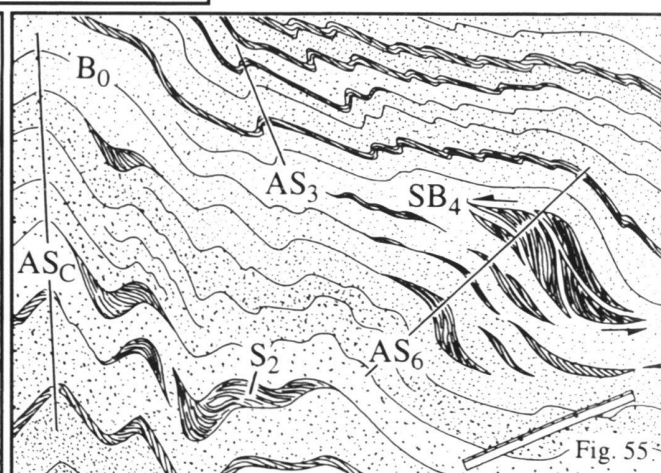
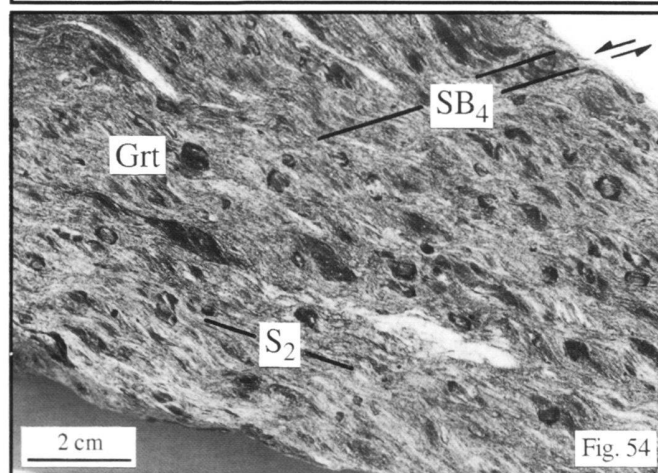
Fig. 54. C'-type SB<sub>4</sub> shear bands with a shear sense top-to-the SW, affecting S<sub>2</sub>. The shear bands and S<sub>2</sub> are dominated by chlorite, and garnet rims are transformed to chlorite (Phe Fm., polished hand specimen, SW is on the left hand side).

Fig. 55. F<sub>6</sub> folds and F<sub>C</sub> folds, affecting the sedimentary bedding B<sub>0</sub>, S<sub>2</sub> and SB<sub>4</sub> C'-type shear bands (Phe Fm., measuring rod for scale: 15 cm, SW is on the left hand side).

Fig. 56. Convergent-divergent (type 3) interference pattern between a F<sub>II</sub> fold and F<sub>III</sub> folds that are preserved as relics in quartz layers between SB<sub>4</sub> shear bands (calcschist of the Lesser Himalayan Sequence, SW is on the left hand side).

Fig. 57. Kyanite on S<sub>2</sub>, partly transformed to white mica. S<sub>2</sub> is overprinted by SB<sub>4</sub> shear bands (Phe Fm., photomicrograph).

Fig. 58. Garnets that are transformed to chlorite on their rims. SB<sub>4</sub> shear bands predominate, forming a S<sub>4</sub> schistosity (Phe Fm., photomicrograph).



subhorizontal fold axes. If a vergence is observed, it is towards SW.  $F_C$  folds clearly affected  $F_3$  folds, but no interference patterns with  $F_A$ - and  $F_6$  folds are observed.

#### *The uppermost Lesser Himalayan Sequence*

The deformation in the Lesser Himalayan Sequence is concentrated in the calcschists and phyllites of the 400-700 meters thick *mélange* zone directly below the base of the High Himalayan Crystalline and in layers of phyllites within the massive Berinag Quartzite. Generally, a continuous main cleavage  $S_{II}$ , marked by white mica, chlorite and rare biotite is observed.  $S_{II}$  is overprinted by C- and C'-type shear bands  $SB_4$ , defined by white mica, chlorite and biotite (5, 6 on Fig. 53).  $L_4$  Stretching lineations and  $SB_4$  shear bands indicate a hanging wall-to-the SW displacement. The C-type shear bands partly form the main schistosity  $S_4$ , restricting  $S_{II}$  to relic micafishes. Meter- to hundred meters-scale isolated lenses of Berinag Quartzite occur inside the *mélange* zone, which are interpreted to indicate tectonic disruption of the quartzite due to SW-directed  $D_4$  thrusting. In phyllite layers within the massive Berinag Quartzite, C- and C'-type shear bands occur at distances up to 2000 meters below the top of the Lesser Himalayan Sequence (8 on Fig. 53).

Relics of two generations of folds predating  $SB_4/S_4$  are observed in mica-rich calcschists:  $F_{II}$ , related to  $S_{II}$  and  $F_{III}$  that deformed  $S_{II}$  (9 on Fig. 53, Fig. 56). Locally, relics of a cleavage  $S_I$  occur. The  $SB_4$  shear bands were subsequently affected by  $F_6$ ,  $F_A$  and  $F_C$  folds (10 on Fig. 53).

In the massive Berinag Quartzite, a schistosity occurs locally, marked by graphite, white mica and fuchsite and related to isoclinal polyharmonic folds (11 on Fig. 53) of unknown vergence. It most probably corresponds to  $S_{II}$  in the calcschists and phyllites. In lenses containing thick layers of fuchsite, this schistosity is affected by two crenulations with styles and orientations corresponding to  $F_{III}$  and  $F_A$ .

### Metamorphism

#### *The base of the High Himalayan Crystalline*

At the base of the High Himalayan Crystalline, the  $M_2/M_3$  mineral assemblage is identical to the  $M_2/M_3$  assemblage in section 4. It consists of biotite, white mica, plagioclase, quartz, garnet and kyanite, indicating kyanite zone conditions. Leucosomes that cannot be assigned to a distinct phase are widespread.

$SB_4$  shear bands and parts of  $S_2$  are characterized by the mineral assemblage chlorite + biotite + quartz, overprinting the  $M_2/M_3$  mineral assemblage. In domains with strong  $D_4$  overprint, kyanite is transformed to white mica and quartz (Fig. 57) and garnet displays coronas of chlorite (Fig. 58). Thus, the metamorphic conditions of  $M_4$  are within greenschist facies and retrograde with respect to  $M_2$  and  $M_3$ . Biotite and white mica in  $F_A$ - and  $F_C$  crenulations are completely annealed. This indicates that greenschist facies conditions outlasted  $M_4$  at the base of the High Himalayan Crystalline.

#### *The uppermost Lesser Himalayan Sequence*

In the calcschists and phyllites, the schistosity  $S_{II}$  and the shear bands  $SB_4$  are defined by the mineral assemblage white mica + chlorite + biotite, indicating greenschist facies conditions. The only constraint for the metamorphic conditions in the Berinag Quartzite is a ductile isoclinal folding, probably related to  $S_{II}$ , that requires at least greenschist facies conditions.

## 6. Correlation of deformational phases and regional metamorphism over the sections 1 to 5

### *Basis of correlation*

Each deformational phase is observed in one or more sections, represented by specific structures. These structures may vary from section to section. Within the pelitic Phe Formation metasediments, the regional variations depend on the pre-existing geometry (e.g. the style and orientation of earlier folds), the intensity of deformation and the associated metamorphic conditions. For some phases, the structures vary in geometry only (e.g. different styles of folding for  $D_{3(a)}$  in the sections 1 to 4). For other phases, different types of structures are observed in different sections (e.g. conjugated kink bands for  $D_7$  in section 1, folds in section 2 and ductile shearing in section 4) or even in one section (e.g. folds and conjugated kink bands for  $D_7$  in section 1).

In spite of these differences, it is possible to establish an overall sequence of tectonic phases valid for the transect as a whole. Each structure is assigned to a certain phase of deformation in the light of a combination of characteristics that constitute the basis of our correlation: (1) the general geometry (e.g. vergences of folds), (2) specific orientations of related geometric elements (e.g. fold axis, axial surface), (3) schistosity and/or mineral stretching lineations, (4) the number and type of phases by which a structure is affected or which it superposes in interference patterns and (5) directions of shortening and/or stretching that can be determined approximately from field observations.

In the Tethyan Himalaya and in the High Himalayan Crystalline, the most consistent deformational phase is the folding  $D_3$  ( $D_{3a}$  in the sections 1 to 3) that occurs in all sections (Table 9). It deforms all earlier phases and the associated structures are affected by all subsequent phases.  $D_3$  is therefore used as a reference for the correlation. The phases  $D_1$  and  $D_2$ , predating  $D_3$ , generally interfere with each other and with  $D_3$  and, consequently, they are clearly distinguishable from each other and from  $D_3$ . The phases postdating  $D_3$  are often represented by different structures in the individual sections. In the sections 1 to 4,  $D_3$  is postdated by  $D_5$ ,  $D_6$ ,  $D_7$  and  $D_8$ , the sequence of which is indicated by interference patterns in each individual section. In section 5,  $D_3$  is overprinted by  $D_4$  and  $D_6$ . The phases  $D_I$ ,  $D_{II}$  and  $D_{III}$  in the Lesser Himalayan Sequence are not incorporated into this correlation, because their relationships to the phases observed in the Tethyan Himalaya and in the High Himalayan Crystalline are not known. The phases  $D_A$ ,



Tab. 9. Compilation of the sequence of deformational phases and of the stages of metamorphic crystallization over the whole transect. The orientations of the structures are similar to Tables 4 to 8. The sequence of deformation established by Steck et al. (1993a, b), Epard et al. (1995) and Vannay and Steci (1995) are shown for comparison. X = observed phase without number.

Phase	Section 5	Phase	Section 5	Section 4	Section 3	Section 2	Section 1	Steck et al., 1993a,b	Epard et al. 1995	Vannay & Steck, 1995
	LHS		Phe Formation and Hanuman Tibba Intrusion				Phe, Thaple, Muth, Lipak			
D <sub>I</sub>	?	D <sub>I</sub>				?				
		M <sub>I</sub>		a) Amphib. facies, kyanite zone b) Amphib. facies, sillimanite zone	Epidote amphibolite facies, garnet zone				D <sub>1a</sub>	
D <sub>II</sub>	?	D <sub>2</sub>				?		D <sub>Ta1</sub>	D <sub>1b</sub>	D <sub>I</sub>
M <sub>II</sub> ?	Greensch. facies	M <sub>2</sub>	Amphib. facies, kyanite zone	Amphib. facies, kyanite zone	Epidote amphib. facies, garnet zone	Greensch. facies, chlorite zone				
D <sub>III</sub>		D <sub>3</sub>			a)			D <sub>Ta2</sub> D <sub>2</sub>	D <sub>2a</sub>	D <sub>2A</sub> D <sub>2B</sub>
					b)					
		M <sub>3</sub>	Amphib. facies, kyanite zone	Amphib. facies, kyanite zone	Greensch. facies, biotite zone	Greensch. facies, chlorite/biotite zone	Greensch. facies, chlorite zone			
D <sub>4</sub>		D <sub>4</sub>							D <sub>2b</sub>	
M <sub>4</sub>	Greensch. facies	M <sub>4</sub>	Greensch. facies							
		D <sub>5</sub>						D <sub>5</sub> ?	X	D <sub>3</sub> ?
		M <sub>5</sub>		Amphib. facies, sillimanite zone			Greensch. facies, chlorite zone			
D <sub>6</sub>		D <sub>6</sub>							D <sub>4</sub>	D <sub>4</sub>
		D <sub>7</sub>						D <sub>5</sub> ?	X	D <sub>3</sub> ?
		D <sub>8</sub>								
D <sub>A</sub>		D <sub>A</sub>								
		D <sub>B</sub>								
D <sub>C</sub>		D <sub>C</sub>								

D<sub>B</sub> and D<sub>C</sub> occurred late in the sequence of phases. A clear overprinting sequence with the phases D<sub>1</sub> to D<sub>8</sub> does not exist in all cases and their sequence among each other also remains unclear. As all stages of regional metamorphic crystallization are related to structures, the metamorphic evolution can be correlated with the tectonic evolution throughout all sections. Phases or sequences of phases reported by studies from adjacent areas are also integrated in our compilation (Steck et al. 1993; Epard et al. 1995; Vannay & Steck 1995; Table 9).

#### *Phase D<sub>1</sub>-M<sub>1a,b</sub>: Early independent tectonic event*

The oldest documented structural and metamorphic record is restricted to the sections 3 and 4 in the High Himalayan Crystalline. It is documented by the S<sub>1</sub> schistosity, by rare isoclinal F<sub>1</sub> folds and by the M<sub>1</sub> mineral assemblages. The preservation of D<sub>1</sub> structures and M<sub>1</sub> mineral assemblages in spite of a strong overprint by ductile F<sub>2</sub>- and F<sub>3</sub> folding and by the high-grade M<sub>2</sub>/M<sub>3</sub> metamorphisms indicates that D<sub>1</sub> represents an important tectonic event. However, neither shear criteria nor clear fold vergences are documented for D<sub>1</sub> and therefore, the deformational conditions are poorly constrained. The metamorphic evolution by contrast is documented by the stages of metamorphic crystallization M<sub>1</sub> in section 3 and M<sub>1a/b</sub> in section 4 that are locally well preserved. In section 3, M<sub>1</sub> reached garnet zone conditions for metapelites. In section 4, M<sub>1a</sub> reached kyanite zone conditions and M<sub>1b</sub> is characterized by the presence of sillimanite and most probably also K-feldspar, indicating a change in metamorphic conditions to the sillimanite zone. As the subsequent main metamorphism M<sub>2</sub> was prograde, reaching only kyanite zone conditions in section 4, M<sub>1a</sub>-M<sub>1b</sub> are considered to represent an independent metamorphic cycle that cannot be part of M<sub>2</sub>. Consequently, D<sub>1</sub>/M<sub>1</sub> are suggested to represent an independent tectonometamorphic event including considerable crustal thickening.

#### *Phase D<sub>2</sub>-M<sub>2</sub>: (N)E-verging Shikar Beh Nappe*

In the southwestern part of the transect, in the sections 3, 4 and 5, the deformation D<sub>2</sub> is documented by the schistosity S<sub>2</sub> and by the related isoclinal relic folds F<sub>2</sub>. S<sub>2</sub> is the main schistosity in this part of the transect (Fig. 59). The related main metamorphism M<sub>2</sub> reached garnet zone conditions for metapelites in section 3 and increased to kyanite zone conditions in the sections 4 and 5. Neither a tectonic nor a metamorphic discontinuity has been detected between the M<sub>2</sub> mineral zones in the sections 3 and 4, indicating that M<sub>2</sub> was a prograde Barrovian-type metamorphism. S<sub>2</sub> is associated with a strong W-E-trending L<sub>2</sub> mineral stretching lineation. Shear sense criteria parallel to L<sub>2</sub> indicate a direction of transport to the E. The F<sub>2</sub> folds are isoclinal and do not display a preferred orientation of their axes, however, S<sub>2</sub> dips mostly to NE or SW (Tables 6, 7). Coupled with strong linear fabrics, this points to sheath folding as the principal mechanism of deformation. Thus, the southwestern part of the transect is interpreted to

represent the thinned, strongly sheared, basal part of a (north) eastwards transported nappe that is correlated with the NE-verging Shikar Beh Nappe described first by Steck et al. (1993a, b) and by Vannay & Steck (1995) west of the studied area.

In the studied area, L<sub>2</sub> stretching lineations and shear sense criteria related to the Shikar Beh Nappe indicate a transport towards E. However, AS<sub>2</sub> axial surfaces mostly dipping to NE or SW, as well as the large-scale distribution pattern of the D<sub>2</sub> deformation and the distribution of the M<sub>2</sub> mineral zones (Fig. 59) rather point to a direction of transport towards NE than towards E. This is supported by consistently SW-NE-oriented L<sub>2</sub> stretching lineations in the Kullu valley and Darcha areas W and NW of the studied transect (Epard et al. 1995; Vannay & Steck 1995) and by the NE-verging F<sub>2</sub> Tandri syncline in western Lahul that has NW-SE-trending fold axes (Steck et al. 1993a, b; Vannay 1993; Vannay & Steck 1995; for locations see Fig. 2). These data indicate a direction of transport towards NE and shortening in a NE-SW direction during D<sub>2</sub>. It is therefore suggested that the L<sub>2</sub> lineations were reoriented passively to their present W-E orientation by dextral strike-slip shearing that occurred during the later deformational phase D<sub>5</sub> (see also section "D<sub>5</sub>-M<sub>5</sub>").

The intensity of the imprint of D<sub>2</sub> structures decreases abruptly towards the northeastern part of the transect at the boundary between section 3 and section 2, south of Batal in eastern Lahul (Fig. 59). In section 3, S<sub>2</sub> is the main schistosity, whereas in section 2 only relics of S<sub>2</sub> occur. In section 1, S<sub>2</sub> is not even clearly identified as of a tectonic origin. Fig. 59 shows a similar distribution pattern for the metamorphic mineral assemblages: M<sub>2</sub> decreases abruptly from garnet zone conditions in section 3 to chlorite zone conditions in section 2. This feature may be interpreted in two ways: (1) It may represent a sudden decrease of the metamorphic degree beyond the front of the (north) eastwards transported Shikar Beh Nappe. This assumption requires the presence of a thrust zone at the base of the nappe. (2) It may reflect a constriction of the M<sub>2</sub> isograds due to extensional normal faulting. Small-scale weak top-to-the NE shearing in section 2 could be compatible with both features, representing either reverse faulting at shallow depth in the foreland NE of the nappe front, related to nappe thrusting, or normal shearing, related to extension. However, neither a large-scale thrust zone occurs nor is widespread normal faulting documented at this time in the sequence of phases.

#### *Phase D<sub>3</sub>-M<sub>3</sub>: SW-verging Main Fold Zone*

Throughout the Tethyan Himalaya and the High Himalayan Crystalline, D<sub>3</sub> is characterized by SW-verging F<sub>3</sub> folds (F<sub>3a</sub> in the sections 1-3) of different styles and scales, termed the Main Fold Zone in this study, indicating that these domains underwent a common structural evolution during D<sub>3</sub>. A common evolution during D<sub>3</sub> is also indicated by the related metamorphism M<sub>3</sub>, the grade of which increases continuously from NE to SW from the lower chlorite zone for metapelites in section 1

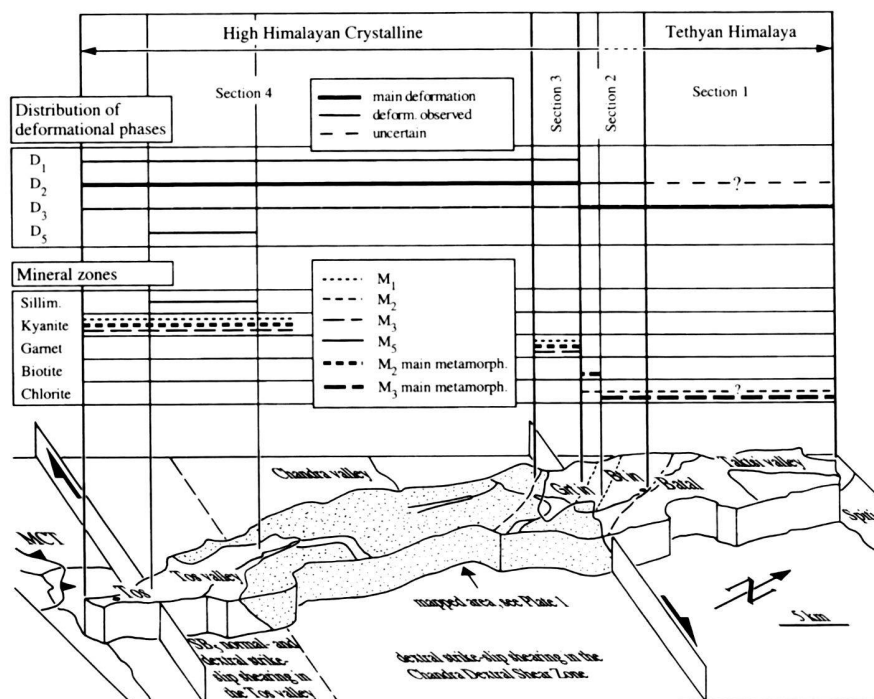


Fig. 59. Distribution of structures and mineral assemblages related to  $D_1$ ,  $D_2$ ,  $D_3$  and  $D_4$  on traverse I (see Fig. 2 and Plate 1). Stippled: Hanuman Tibba intrusion. Note that the  $M_2$  metamorphic conditions decrease from garnet zone conditions to chlorite zone conditions at the limit between section 3 and section 2. In the sections 3 and 4,  $M_2$  and  $D_2$  are the main metamorphism and deformation, respectively, whereas in the sections 1 and 2,  $M_3$  and  $D_3$  are the main metamorphism and deformation. The transition from the Tethyan Himalaya to the High Himalayan Crystalline is gradual as no tectonic discontinuity disrupts the  $M_3$  mineral zones that show gradually increasing metamorphic conditions from NE to SW. SB<sub>3</sub> normal- and dextral strike-slip shearing in the Tso valley passes over into dextral strike-slip shearing in the Chandra Dextral Shear Zone toward NE.

to the kyanite zone in the sections 4 and 5 (Fig. 59). In the sections 1 and 2,  $D_3$  and  $M_3$  are the main deformational and metamorphic phases that strongly overprint the weakly imprinted  $D_2$  structures and  $M_2$  metamorphism, respectively. By contrast, in the sections 3, 4 and 5, although the  $F_3$  folds deform all structures related to the NE-verging  $D_2$  Shikar Beh Nappe, the main schistosity  $S_2$  and the main  $M_2$  mineral assemblage are only occasionally overprinted by  $S_3$  and by an  $M_3$  mineral assemblage, respectively. In these sections, the metamorphic grade of  $M_3$  ranges within the same conditions as  $M_2$  (Fig. 59) and therefore,  $M_3$  is interpreted as a continuation of  $M_2$ .

The occurrence of biotite- garnet- and kyanite zone crystalline rocks in the sections 2-5, that form the High Himalayan Crystalline, depends on the distribution of  $M_2$  and  $M_3$  mineral assemblages. The garnet- and kyanite zones in the sections 3-5 are mainly the result of  $M_2$ ,  $M_3$  being of subordinate importance, whereas the biotite zone in section 2 is the result of  $M_3$  (Fig. 59). The Tethyan Himalaya is restricted to the  $M_3$  lower chlorite zone rocks in section 1. The  $M_3$  upper chlorite zone rocks in section 2 are considered to represent the transition between the Tethyan Himalaya and the High Himalayan Crystalline (Fig. 59).

Striking differences are observed between the SW-verging  $F_3$  folds in section 4 of the studied transect and corresponding structures to the W. In section 4,  $F_3$  folds are generally open to close, displaying short, steeply inclined overturned limbs, long, moderately inclined normal limbs and moderately inclined axial surfaces. Large-scale  $F_3$  folds are rare. Only one close, km-scale  $F_3$  fold with a moderately inclined axial surface, the

Sharm Fold, is documented. W of the studied area, the  $F_3$  folds are generally more tight and display more inclined or even recumbent axial surfaces. Thöni (1977) described the large-scale, tight, recumbent Phojal-Kallath Fold in the Kullu valley area and Epard et al. (1995) documented the isoclinal, recumbent Sagor Pass Fold in that area (for locations, see Fig. 2).  $S_3$  axial surface schistositities are rarely observed in the sections 3 and 4. By contrast, Epard et al. (1995) and Vannay & Steck (1995) reported strong  $S_3$  axial surface schistositities W of the sections 3 and 4 in the Kullu valley-Rohtang La area and in the lower Chandra valley. This indicates that  $D_3$  deformation in the studied area was less intensive than to the W.

NW and NE of the studied area, along the Hemis-Tandi transect and along the Tso Morari-Spiti transect, Steck et al. (1993a, b) and Steck et al. (1998) described SW-verging nappe structures termed the Nyimaling-Tsarap Nappe and the Mata Nappe, respectively, the lateral relationships of which are unclear. These north Himalayan nappes are delimited by a series of frontal thrust faults, the most important ones being the Baralacha La Thrust and the Parang La Thrust, respectively (Fig. 1). According to Steck et al. (1993a, b), the Baralacha La Thrust transforms towards SE into the Chandra Flexure Zone, that corresponds to the northeastern part of the Main Fold Zone. Thus, the northeastern part of the Main Fold Zone replaces frontal thrusts of the north Himalayan nappes. Minor SW-directed thrusting is indicated by rare  $SZ_{3b}$  shear zones with a shear sense top-to-the SW that occur together with  $F_{3a}$  folds in the sections 1, 2, and 3. Consequently, in this area,  $D_3$  is interpreted to represent the southwesternmost deformation

related to the SW-verging stacking of the north Himalayan nappe system, developed below and in front of the Nyimaling-Tsarap- and Mata Nappes.

Although  $F_3$  folds in section 5 are clearly crosscut by later  $D_4$  structures, the transition from  $D_3$  to  $D_4$  is considered to be gradual. According to Epard et al. (1995), two schistositys are observed in the Phojal-Kallath Fold. This is interpreted as the progressive deformation of a  $F_3$  fold during early  $D_4$  Crystalline Nappe formation. Consequently, over the whole transect,  $D_3$  represents a phase of southwestwards progressing deformation between late thrusting of the north Himalayan nappes (early  $F_3$  folding in the northeastern part of the Main Fold Zone) and early Crystalline Nappe formation (late  $F_3$  folding in the southwestern part of the Main Fold Zone).

*Phase  $D_4$ - $M_4$ : SW-directed thrusting of the Crystalline Nappe along the Main Central Thrust zone*

$D_4$  is observed only in section 5, in the tectonostratigraphically deepest parts of the Phe Formation metapelites of the High Himalayan Crystalline and in the underlying calcschists, phyllites and quartzites of the Lesser Himalayan Sequence. It is characterized by a NE-plunging  $L_4$  stretching lineation and by C- and C'-type  $SB_4$  shear bands, indicating top-to-the SW thrusting.  $D_4$  thrusting affects a zone with an average thickness of 4 to 5 kms, termed the Main Central Thrust zone (MCT zone). The occurrence of  $D_4$  structures at the base of the High Himalayan Crystalline and in the underlying Lesser Himalayan Sequence indicates that the High Himalayan Crystalline was thrust over the Lesser Himalayan Sequence during  $D_4$  thrusting. Most of the thrusting along the MCT zone occurred in a zone of tectonic mélange in the uppermost Lesser Himalayan Sequence and at the very base of the High Himalayan Crystalline, where the highest concentrations of shear bands are observed.

$D_4$  thrusting along the MCT zone occurred under  $M_4$  greenschist facies conditions at the base of the High Himalayan Crystalline as well as in the uppermost Lesser Himalayan Sequence. As a consequence, from the Lesser Himalayan Sequence through the base of the High Himalayan Crystalline upward to the center of the High Himalayan Crystalline, the metamorphic conditions increase from the greenschist facies to the amphibolite facies. This feature is referred to as an inverted metamorphic field gradient. On the basis of this observation, Frank et al. (1973) defined the overthrust high-grade High Himalayan Crystalline slab as the Crystalline Nappe. It is, however, important to note that the metamorphic conditions prior to  $D_4$  thrusting were different in the Phe Formation rocks of the High Himalayan Crystalline and in the Lesser Himalayan Sequence sediments. The High Himalayan Crystalline rocks reached amphibolite facies peak conditions during  $M_2$  and  $M_3$  and retrogressed to greenschist facies conditions during  $M_4$ , whereas the rocks in the Lesser Himalayan Sequence reached their greenschist facies peak conditions during  $D_4$  thrusting.

The early stage of formation of the Crystalline Nappe, most probably prior to MCT thrusting or during early MCT thrusting, is considered as coincident with the latest and southwesternmost  $F_3$  folding, the transition between these two phases being gradual (see previous section above). During the main stage of thrusting of the Crystalline Nappe along the MCT zone, however, no major folding is documented in the studied area. The SW-verging folds of the  $D_3$  Main Fold Zone were then transported passively toward SW. Therefore, during the main stage of  $D_4$  thrusting, the Crystalline Nappe is suggested to represent a thrust sheet rather than a fold nappe.

*Phase  $D_5$ - $M_5$ : NE-directed extensional normal shearing associated with dextral strike-slip motion*

$D_5$  occurs in the sections 1 and 4, represented by different structures. In section 1, the axial surfaces of close to tight  $F_{3a}$  folds as well as  $S_{3a}$  that dipped originally towards NE, were overturned to their present WSW dip by  $D_5$ . Contemporaneously,  $F_{3a}$  fold axes were rotated about  $20^\circ$  to  $40^\circ$  from a gently NW plunging position to a gently NNW plunging position and the intersections between  $B_0$  and  $S_{3a}$  were wrapped around the  $D_5$ -reoriented  $FA_{3a}$  fold axes. This reorientation of pre-existing structures suggests large-scale  $D_5$  NE-directed normal movement combined with dextral strike-slip motion, that did not produce a well defined shear zone, but caused widely distributed rotation of previous structures.

NW of the studied area in Zaskar, normal- and dextral strike-slip shearing is related to the Zaskar Shear Zone (Searle 1986; Searle et al. 1988; Herren 1987; Kündig 1989; Searle & Rex 1990; Gapais et al. 1992; Searle et al. 1992; Patel et al. 1993 and Dèzes et al. in press) that juxtaposed high-grade metamorphic rocks of the High Himalayan Crystalline against low-grade metamorphic rocks of the Tethyan Himalaya. According to Patel et al. (1993) and Dèzes et al. (in press), the Zaskar Shear Zone represents a SW-directed large-scale thrust fault at the front of the SW-verging north Himalayan nappe system (the Zaskar Nappes of Bassoulet et al., 1980 and the Nyimaling-Tsarap Nappe of Steck et al., 1993a, b) that was reactivated in the opposite sense as an extensional normal fault. In the studied area, such large-scale SW-verging thrust faults at the base of the north Himalayan nappes were replaced by the SW-verging folds of the Main Fold Zone. Consequently, no zone of tectonic weakness occurs that could work as a shear plane during  $D_5$ . This helps to explain why, in the studied area, normal- and dextral strike-slip motion is not restricted to a well defined shear zone and, consequently, why the transition between the Tethyan Himalaya and the High Himalayan Crystalline is gradual (Fig. 59). As a consequence, the Tethyan Himalaya and the High Himalayan Crystalline are defined by the metamorphic grade rather than by tectonic arguments in the studied area (see section  $D_3$ - $M_3$  above).

Structures related to normal and dextral strike-slip movement are not restricted to the Tethyan Himalaya-High Himalayan Crystalline transition as reported generally from the



NW Himalaya, but extended deep into the High Himalayan Crystalline. In section 4, innumerable small-scale, ductile, NE-dipping SB<sub>5</sub> shear bands crosscut the D<sub>2</sub> and D<sub>3</sub> structures. L<sub>5</sub> stretching lineations and related shear senses indicate movement of the hanging wall down-to-the ENE. This oblique movement sense within the NE-dipping shear bands is interpreted to represent NE-directed normal shearing combined with a dextral strike-slip component. L<sub>5</sub> is marked by biotite and sillimanite, indicating a change of the metamorphic conditions within the amphibolite facies from the kyanite zone during M<sub>2</sub> and M<sub>3</sub> to the sillimanite zone during M<sub>5</sub>. In addition, a series of late-stage leucosomes, that crosscut all previous structures, are interpreted to have formed during M<sub>5</sub>. Related to normal shearing, the transition from the stability of kyanite to the stability of sillimanite and the formation of melt may indicate decompression during extension of the middle part of the Crystalline Nappe.

L<sub>2</sub> stretching lineations are consistently oriented W-E in the studied area and related shear sense criteria indicate a transport of the D<sub>2</sub> Shikar Beh Nappe towards E. The large-scale distribution of the D<sub>2</sub> structures and of the M<sub>2</sub> mineral zones in the studied transect (Fig. 59), however, as well as SW-NE-trending L<sub>2</sub> stretching lineations and NE-verging F<sub>2</sub> folds in higher crustal levels W and NW of the studied area (Epard et al., 1995; Vannay & Steck, 1995) suggest a transport of the Shikar Beh Nappe towards NE (see section D<sub>2</sub>-M<sub>2</sub> above). In the lower Chandra valley in western Lahul, Epard et al. (1995) and Vannay and Steck (1995) reported a continuous clockwise rotation of L<sub>2</sub> stretching lineations from an original SW-NE-striking orientation to a W-E-striking orientation. The NW-SE-oriented FA<sub>2</sub> fold axes of the F<sub>2</sub> Tandri Syncline, however, were not reoriented. This feature was interpreted by these authors to be the result of dextral strike-slip movement that was concentrated into a NW-SE-oriented shear zone about 20 kms wide, trending from the Tandri area over Rohtang La, termed the Chandra Dextral Shear Zone (for locations, see Fig. 2). Consequently, it is suggested that in the studied area, the L<sub>2</sub> stretching lineations were also rotated passively to their present W-E-striking orientation by dextral strike-slip movement. E-dipping S<sub>2</sub> schistosity in section 4 may indicate that part of the F<sub>2</sub> sheath folds were also rotated from an originally SW-NE-trending orientation to a W-E-trending orientation.

In section 4, this rotation is considered to be the result of dextral strike-slip shearing on SB<sub>5</sub> shear bands (Fig. 59). North of the Tos valley area, L<sub>2</sub> is also W-E oriented, but no SB<sub>5</sub> shear bands are observed. It is therefore suggested that L<sub>2</sub> rotation was caused by dextral strike-slip shearing in the continuation of the Chandra Dextral Shear Zone toward SE, the Chandra Dextral Shear Zone being therefore part of phase D<sub>5</sub>.

#### *Phase D<sub>6</sub>: NE-verging folding*

In the sections 1 to 3, D<sub>6</sub> occurs as mostly open F<sub>6</sub> folds and crenulations with vergences towards SW and NE, whereas in

the sections 4 and 5, F<sub>6</sub> folds verge toward NE only. The axial surfaces of F<sub>6</sub> folds dip moderately to steeply towards SW in the sections 1 to 3. In the sections 4 and 5, they dip shallowly to moderately towards SW. D<sub>6</sub> is therefore suggested to form open, upright to steeply inclined, NE-verging macrofolds, the scale of which is in the range of some hundred meters to a kilometer, as it is indicated by a kilometer-scale F<sub>6</sub> fold in section 2. In all sections, the metamorphic conditions associated with D<sub>6</sub> are retrograde with respect to M<sub>3</sub>. W, NW and NE of the studied area, similar folds were reported by Steck et al. (1993a, b), Epard et al. (1995), Vannay & Steck (1995) and Steck et al. (1998).

#### *Phases D<sub>7</sub>-D<sub>8</sub>: SW-NE-directed extension*

Phase D<sub>7</sub> is observed in the sections 1, 2 and 4. In section 4, discrete NE-dipping SB<sub>7</sub> shear bands crosscut F<sub>6</sub> folds. SB<sub>7</sub> shear bands display a shear sense hanging wall down-to-the NE, indicating NE-directed normal shearing and, as a consequence, vertical shortening. In section 2, F<sub>7</sub> folds with gently NE-dipping axial surfaces overprint F<sub>6</sub> folds, also indicating vertical shortening. The development of such folds requires pre-existing steeply inclined to vertical planar geometric elements. In section 2, this requirement was met by the folding F<sub>6</sub> that folded the sedimentary bedding B<sub>0</sub> and S<sub>2</sub> to a steeply NE-dipping position. In section 1, the most prominent D<sub>7</sub> structures are conjugate kink bands with bisectors of the small angle slightly dipping to NE, that locally overprint F<sub>6</sub> folds, also indicating vertical shortening. As all D<sub>7</sub> structures indicate vertical shortening, it is suggested that they were all related to extension in a SW-NE direction as indicated by SB<sub>7</sub> shear bands in section 4. The metamorphic conditions associated to D<sub>7</sub> are retrograde with respect to M<sub>3</sub> in all sections.

In section 2, F<sub>7</sub> folds are overprinted by F<sub>8</sub> folds with gently SW-dipping axial surfaces, that also indicate vertical shortening. Although D<sub>7</sub> and D<sub>8</sub> show clear overprinting relationships, they are regarded as one tectonic phase, the orientations of their axial surfaces being nearly parallel.

#### *Late stage phases*

DA, DB and DC are assigned to the end of the sequence of phases. The sequence among these late stage phases remains unclear.

#### *Phase DA: E-verging folding*

DA is observed in sections 4 and 5. It is characterized by E-verging folds observed on all scales. The FA axial surfaces dip either moderately to the W or shallowly to the E. This is interpreted to indicate subsequent reorientation by a large-scale folding with nearly upright, N-S-trending axial surfaces. This folding may eventually correspond to phase DC, observed on an outcrop scale in section 5.

#### Phase D<sub>B</sub>: NW-SE-directed shortening

F<sub>B</sub> folds occur in the sections 1 to 3. Their subvertical, SW-NE-trending axial surfaces indicate NW-SE-directed shortening parallel to the mountain chain. Guntli (1993) reports large-scale upright folds with subvertical, SSW-NNE to SW-NE-trending axial surfaces from the Kishtwar region in SE Kashmir that could correspond to F<sub>B</sub> folds. As F<sub>B</sub> folds mostly occur in section 1, where D<sub>5</sub> dextral strike-slip movement operated, it could alternatively be interpreted as the result of shortening parallel to pre-existing structural elements such as the sedimentary bedding, the S<sub>3a</sub> cleavage and the AS<sub>3a</sub> axial surfaces during their rotation by D<sub>5</sub> dextral strike-slip movement.

#### Phase D<sub>C</sub>: WSW-ENE-directed shortening

F<sub>C</sub> folds are observed in section 5 only, in the Crystalline Nappe as well as in the Lesser Himalayan Sequence. Their subvertical, NNW-SSE-trending axial surfaces indicate shortening in a WSW-ENE direction. On a large scale, D<sub>C</sub> could account for the arrangement of F<sub>A</sub> axial surfaces around subhorizontal, N-S trending fold axes in the sections 4 and 5. Interference patterns on outcrop scale, however, are not observed.

Thöni (1973) described the large-scale upright Shali Dolomite Anticline in the Lesser Himalayan Sequence south of Bajaura with a NNW-SSE-trending fold axis (for location, see Fig. 2). We consider this fold as a large-scale equivalent of F<sub>C</sub>. The axis of a late stage dome exposed in the Larji-Kullu-Rampur tectonic window trends from NNW to SSE, parallel to the axis of F<sub>C</sub> folds. Consequently, this dome may also be the result of large-scale F<sub>C</sub> folding.

#### Phases D<sub>I</sub>, D<sub>II</sub> and D<sub>III</sub> in the Lesser Himalayan Sequence

In the calcschists and phyllites exposed in the Larji-Kullu-Rampur tectonic window, the schistosity S<sub>I</sub> and S<sub>II</sub> and the foldings F<sub>II</sub> and F<sub>III</sub> are observed, which predate D<sub>4</sub> thrusting along the Main Central Thrust zone. In the Berinag Quartzite, a folding that may correspond to F<sub>II</sub> occurred prior to D<sub>4</sub> thrusting. The sequence of the three phases D<sub>I</sub>, D<sub>II</sub> and D<sub>III</sub> resembles the sequence of the phases D<sub>1</sub>, D<sub>2</sub> and D<sub>3</sub> in the Crystalline Nappe. However, as the Lesser Himalayan Sequence was situated several hundred kilometers SW of the High Himalayan Crystalline prior to MCT thrusting (for review see Brookfield 1993), it is proposed that these structures either belong to a independent tectonic evolution in the Lesser Himalayan Sequence or represent early, more ductile phases related to thrusting along the MCT zone that predated D<sub>4</sub>.

## 7. The tectonometamorphic evolution

### *Tectonic evolution*

The tectonic evolution of the studied transect is subdivided into four periods. The oldest period A is recorded only as relics and it cannot clearly be related to the Tertiary Hi-

malayan orogeny (D<sub>1</sub>). The periods B and C are documented in detail (Fig. 60). They represent the main processes involved in Tertiary mountain building in the studied area (D<sub>2</sub> to D<sub>8</sub>). Period D includes late stage phases (D<sub>A</sub>, D<sub>B</sub> and D<sub>C</sub>).

### Period A) Early Himalayan crustal thickening (D<sub>1</sub>)

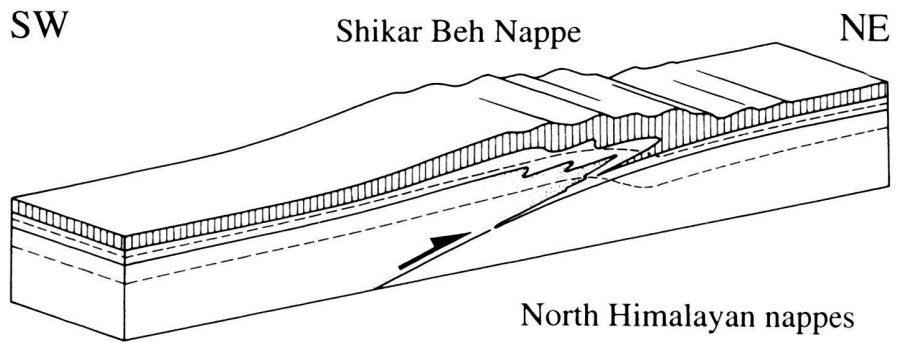
D<sub>1</sub> is documented by relic isoclinal folds associated with a prograde metamorphism that reached sillimanite zone peak conditions. As the subsequent main metamorphism M<sub>2</sub> was also prograde, reaching only kyanite zone peak conditions, D<sub>1</sub> is considered as an independent tectonometamorphic event. It is older than the Eohimalayan NE-verging D<sub>2</sub> Shikar Beh Nappe, that has until now been considered to be the oldest established structure in the NW Himalaya, and younger than the 495 ± 16 Ma old Hanuman Tibba intrusion (Rb/Sr whole rock isochron, Frank et al. 1977). The upper age constraint is documented by D<sub>2</sub> structures overprinting D<sub>1</sub> structures and the lower age constraint is documented by a contact metamorphism in the Phe Formation rocks due to the Hanuman Tibba intrusion, that predates the first regional metamorphism M<sub>1</sub>. As a consequence, D<sub>1</sub> can be interpreted either as an early Himalayan or as a pre-Himalayan tectonometamorphic event. In the sedimentary record of the NW Himalaya, exposure to erosion and continental clastic sedimentation is documented in several time intervals from the Precambrian to the Mesozoic (e.g. Gaetani & Garzanti 1991) and has been interpreted by several authors as a record of pre-Himalayan orogeny (e.g. Pande & Saxena 1968; Saxena 1973; Bhargava 1980; Jain et al. 1980; Saxena 1980; Garzanti et al. 1986; Gaetani & Garzanti 1991; Fuchs 1992 and Valdiya 1995). However, as no components displaying high-grade metamorphism and/or an additional phase of deformation have been found in these clastic sediments, that could document a pre-Himalayan high-grade metamorphism and/or deformation, we prefer to consider D<sub>1</sub> as an early Himalayan tectonometamorphic event. Upper amphibolite facies metamorphic conditions indicate considerable crustal thickening that may be the result of nappe formation, as suggested by isoclinal folding.

Figure caption for p. 36–37

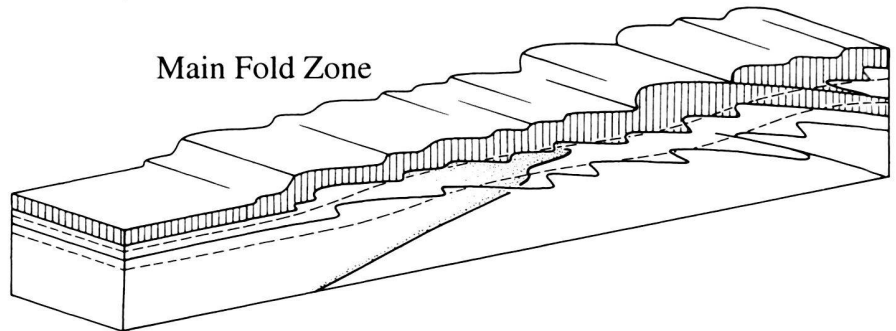
Fig. 60. Model for the tectonic evolution of the NW Himalaya along the Spiti-eastern Lahul-Parvati valley transect, illustrating the tectonometamorphic periods B and C. On the left hand side, the tectonic evolution of the studied traverse is represented. The three folded lines and the hatched layer are drawn to clarify the geometry of each phase; they represent all planar structural elements, that are affected by the respective deformation, they do not, however, represent interference patterns between different phases. The drawings represent intermediate stages of the respective phases. The broken lines represent the 300°C and the 600°C isogrades. (1) and (2) are subunits of the Crystalline Nappe. On the right hand side, the tectonic evolution of the orogen is represented on a crustal scale. (MCT = Main Central Thrust, MBT = Main Boundary Thrust, ITSZ = Indus-Tsangpo Suture Zone, TH = Tethyan Himalaya, HHC = High Himalayan Crystalline, LHS = Lesser Himalayan Sequence)

Period B

Phase D<sub>2</sub>

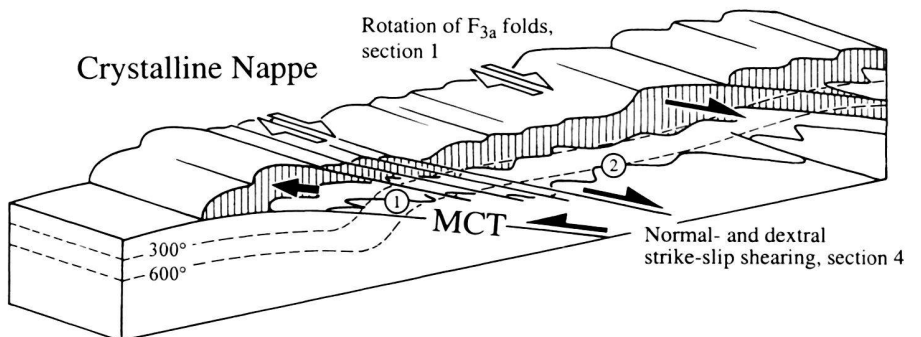


Phase D<sub>3</sub>

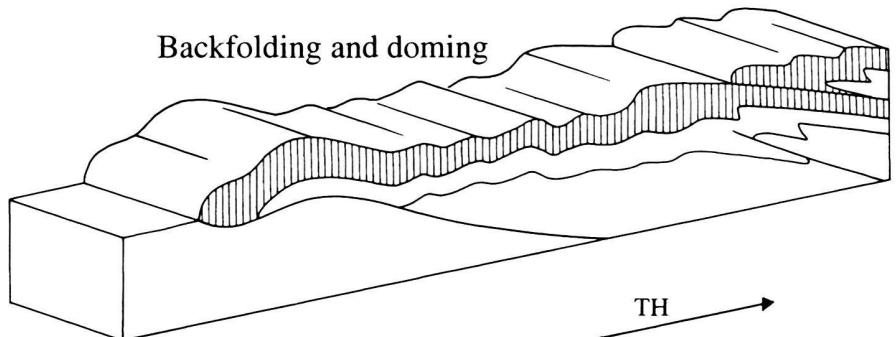


Period C

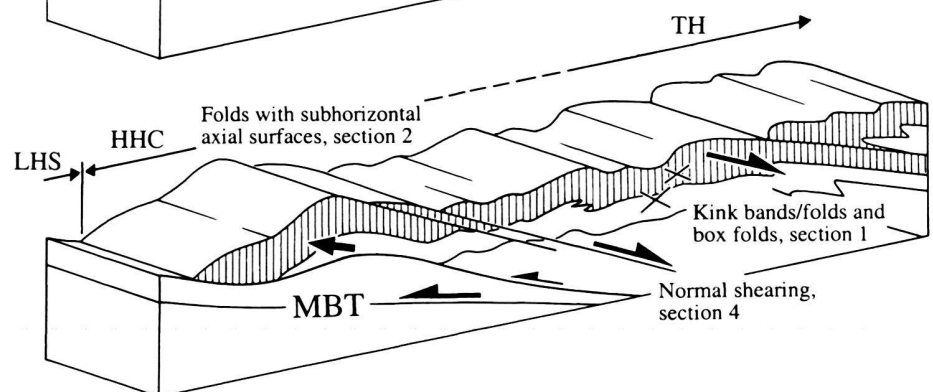
Phases D<sub>4</sub> - D<sub>5</sub>

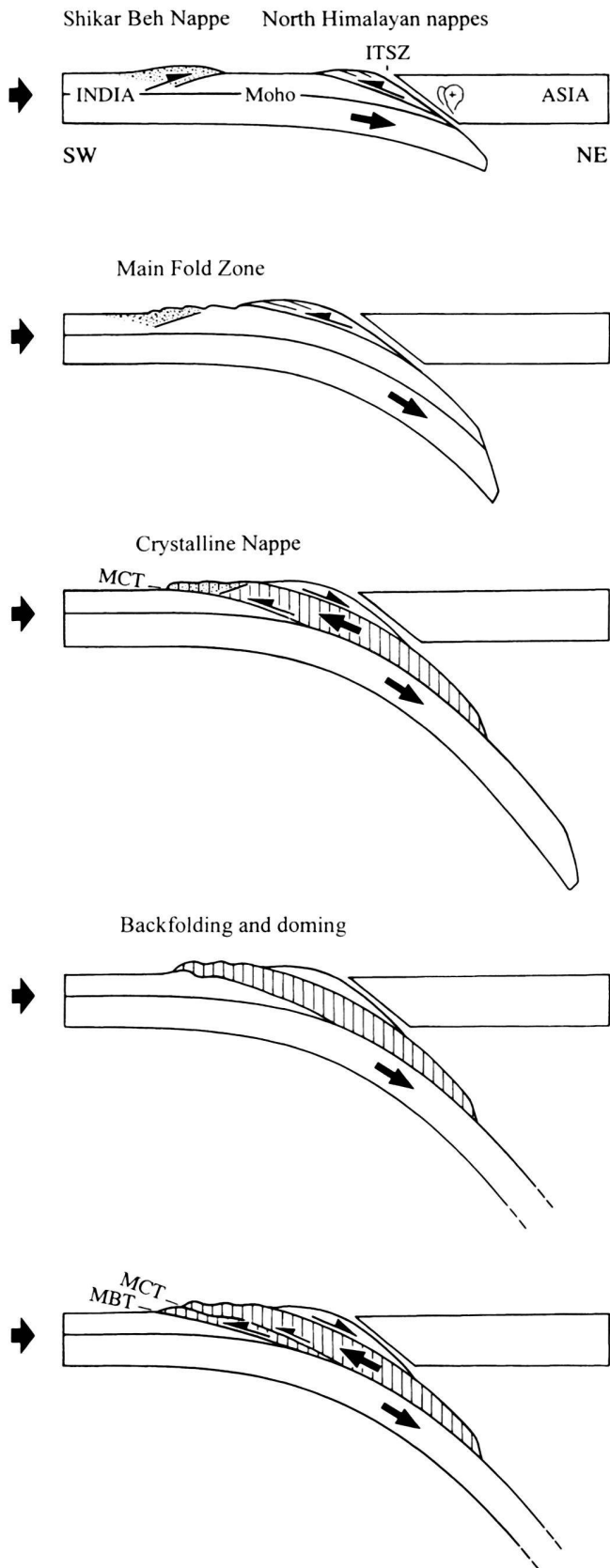


Phase D<sub>6</sub>



Phase D<sub>7</sub> (+D<sub>8</sub>)





### Period B, phase D<sub>2</sub>

Initiation of the NE-verging Shikar Beh Nappe within the Indian crust SW of the subduction zone and contemporaneous initiation of the SW-verging north Himalayan nappes from the north-eastern edge of the Indian crust. The Indian continent was subducted at the base of the north Himalayan nappes.

### Phase D<sub>3</sub>

Ongoing subduction of the Indian continent at the base of the north Himalayan nappes. The front of the north Himalayan nappes reached the area NE of the front of the Shikar Beh Nappe. Initiation of the SW-verging Main Fold Zone SW of the north Himalayan nappe system. D<sub>3</sub> is a southwestward progressing transitional phase between late thrusting of the north Himalayan nappes and early formation of the Crystalline Nappe.

### Period C, phases D<sub>4</sub> - D<sub>5</sub>

Formation of the Main Central Thrust (MCT) and SW-directed extrusion of the Crystalline Nappe between the Lesser Himalayan Sequence and the north Himalayan nappe system. This is the result of contemporaneous SW-directed thrusting along the Main Central Thrust and concurrent NE-directed normal movement in the center of the Crystalline Nappe and below the north Himalayan nappes. The zone of subduction has stepped from the base of the north Himalayan nappes to the Main Central Thrust.

### Phase D<sub>6</sub>

Thrusting along the Main Central thrust slowed down or stopped. The ongoing continental convergence caused large-scale upright to slightly NE-verging domes and backfolds.

### Phase D<sub>7</sub> (+D<sub>8</sub>)

Extrusion of the Crystalline Nappe continues most probably due to late stage thrusting along the Main Central Thrust and/or formation of the Main Boundary Thrust (MBT) and concurrent normal movement in the center of the Crystalline Nappe and below the north Himalayan nappe system. Formation of the Main Boundary Thrust caused extrusion of the Lesser Himalayan Sequence together with the Crystalline Nappe.



Period B) Continental collision and incipient subduction of the Indian continental crust (D<sub>2</sub>, D<sub>3</sub>)

Continental collision and incipient subduction of the Indian continental crust included D<sub>2</sub> NE-verging nappe stacking as well as D<sub>3</sub> SW-verging nappe stacking (Fig. 60). The earliest deformational and metamorphic event in the studied area that is incontestably related to the Tertiary Himalayan orogeny is represented by the NE-directed D<sub>2</sub> formation of the Shikar Beh Nappe. D<sub>2</sub> caused the main metamorphism M<sub>2</sub> in the High Himalayan Crystalline. Although this phase is of great importance for both the deformational and the metamorphic evolution, it has only been reported from the NW Himalaya until now (Steck et al. 1993a, b; Epard & Steck 1995; Vannay & Steck 1995) and, as a consequence, it is regarded as a local feature.

The SW-verging north Himalayan nappe system was thrust toward the front of the NE-verging Shikar Beh Nappe. At the front of the north Himalayan nappes, the first folds of the D<sub>3</sub> Main Fold Zone formed, replacing frontal thrust faults during late stage nappe thrusting. D<sub>3</sub> folding then propagated towards SW, where it overprinted the Shikar Beh Nappe structures. Late stage D<sub>3</sub> folding coincided with early folding related to D<sub>4</sub> SW-directed thrusting of the Crystalline Nappe along the Main Central Thrust. D<sub>3</sub> folding within the Main Fold Zone therefore progressed from late stage north Himalayan nappe thrusting into early formation of the Crystalline Nappe.

According to Steck et al. (1993a, b) and Steck et al. (1998), the north Himalayan nappes were thrust from the northern edge of the subducted Indian continent towards SW, corresponding to a first record of crustal thickening related to continental collision and incipient subduction. It is suggested that stacking of the Shikar Beh Nappe started at the same time within the Indian continent far SW of the subduction zone. Models for the motion between India and Asia (McKenzie & Sclater 1971; Molnar & Tapponnier 1975; Pierce 1978; Patriat & Achache 1984; Scotese et al. 1988; Dewey et al. 1989) show a rapid decrease in the plate motion rate of India between 54 Ma and 35 Ma. The collision between India and Asia and the onset of NE- and SW-directed nappe formation is therefore suggested to have occurred at the beginning of this time interval. This is confirmed by the sedimentary record (Garzanti et al. 1987; Garzanti et al. 1996), which constrains the collision at 55–50 Ma. It is, however, not clear if the initiation of stacking of the north Himalayan nappe system predated or postdated the onset of formation of the Shikar Beh Nappe. Field data only show that its latest folding, represented by the Main Fold Zone, was still active after the formation of the Shikar Beh Nappe.

Period C) Extrusion of the previously subducted crust and dextral strike-slip shearing (D<sub>4</sub>, D<sub>5</sub>, D<sub>6</sub> and D<sub>7</sub>/D<sub>8</sub>)

Subsequently, the SW-verging Crystalline Nappe, comprising the D<sub>3</sub> Main Fold Zone and relics of the D<sub>2</sub> Shikar Beh Nappe, was formed (Fig. 60). Formation of the Crystalline Nappe was

the result of opposite movements at the base of the High Himalayan Crystalline and in higher crustal levels, represented by different structural and metamorphic evolutions. The base of the High Himalayan Crystalline, corresponding to the base of the Crystalline Nappe, was affected by SW-directed D<sub>4</sub> thrusting along the Main Central Thrust zone (MCT zone). The central part of the High Himalayan Crystalline and the transition between the Tethyan Himalaya and the High Himalayan Crystalline, beneath the base of the north Himalayan nappes, by contrast, underwent D<sub>5</sub> normal shearing and dextral strike-slip motion. After reaching metamorphic kyanite zone peak conditions during M<sub>2</sub> and M<sub>3</sub>, the base of the High Himalayan Crystalline was retrogressively overprinted by greenschist facies conditions M<sub>4</sub>, whereas the central part was overprinted by M<sub>5</sub> sillimanite zone conditions. The contemporaneity of D<sub>4</sub>/M<sub>4</sub> and D<sub>5</sub>/M<sub>5</sub> is documented by the sequence of deformational and metamorphic phases. (1) Both D<sub>4</sub>- and D<sub>5</sub> structures crosscut F<sub>3</sub> folds and were overprinted by F<sub>6</sub> folds. (2) M<sub>4</sub> and M<sub>5</sub> mark the beginning of the post-M<sub>2</sub>/M<sub>3</sub> metamorphic evolution at the base of the nappe as well as in its central part.

Both movements, D<sub>4</sub> thrusting along the MCT zone as well as D<sub>5</sub> normal- and dextral strike-slip shearing caused orogen-scale structures. The Main Central Thrust can be followed all along the Himalayan chain and D<sub>5</sub> is interpreted to be part of a large-scale system of normal and/or dextral strike-slip shear zones that were reported from many sectors of the Himalayan orogen (e.g. Burg et al. 1984; Brun et al. 1985; Burchfiel & Royden 1985; Searle 1986; Searle et al. 1988; Herren 1987; Pêcher & Scaillet 1989; Pêcher 1991; Pêcher et al. 1991; Gapais et al. 1992; Burchfiel et al. 1982; Metcalfe 1993), referred to as the North Himalayan Shear Zone (Pêcher et al. 1991) or the South Tibetan Detachment System (Burchfiel et al. 1992).

Thrusting at the base of the Crystalline Nappe along the MCT zone and simultaneous normal shearing in its central parts and at the base of the overlying north Himalayan nappes indicate that the Crystalline Nappe extruded between the Lesser Himalayan Sequence and the north Himalayan Nappe system during continental convergence. The Crystalline Nappe represents a high-grade crustal slab that was previously subducted under the north Himalayan nappes. As a consequence, at the transition between period B and period C, the zone of subduction stepped from the base of the north Himalayan nappes, represented by frontal thrusts such as the Baralacha La Thrust or by the northeasternmost folds of the Main Fold Zone, to the base of the Crystalline Nappe, represented by the MCT zone (Fig. 60). Physical modeling of the subduction of continental lithosphere by Chemenda et al. (1995) showed that normal faulting can operate simultaneously with overthrusting. Rapid exhumation of a subducted crustal sheet after the formation of a frontal thrust fault (equivalent of the MCT zone) due to the buoyancy force provokes a normal sense motion along the upper surface of the rising sheet, corresponding to normal extensional shearing in the High Himalayan Crystalline and in the Tethyan Himalaya-High Himalayan Cryst-

talline transition. This model could not, however, account for the dextral strike-slip shearing. According to Pêcher (1991) and Pêcher et al. (1991), this movement indicates an eastward displacement of Tibet relative to India.

As D<sub>5</sub> normal movement occurred in the Tethyan Himalaya-High Himalayan Crystalline transition and inside the High Himalayan Crystalline, the upper boundary of the Crystalline Nappe is not clearly delimited. As a consequence, it is suggested that the Crystalline Nappe consists of two subunits (1 and 2 in Fig. 60), displaying a gradual transition between each other and toward the overlying low-grade rocks at the front of the north Himalayan nappes.

D<sub>4</sub>/D<sub>5</sub> extrusion of the Crystalline Nappe was postdated by the large-scale open, upright to NE-verging folding F<sub>6</sub>. This may indicate that thrusting along the MCT zone slowed down and that, as a consequence, thrusting could no longer accommodate all the crustal convergence, which resulted in doming and backfolds. F<sub>6</sub> folds were subsequently affected by another phase of normal extensional movement D<sub>7</sub> (+D<sub>8</sub>) in the central parts of the Crystalline Nappe and in the Tethyan Himalaya-High Himalayan Crystalline transition. It is suggested that this normal extensional movement operated simultaneously with a new period of thrusting along the MCT zone or that it started when the Main Boundary Thrust developed SW of the MCT zone. D<sub>7</sub> (+D<sub>8</sub>) may therefore represent ongoing extrusion of crustal material during continental convergence that operated similar to extrusion during D<sub>4</sub>/D<sub>5</sub>.

Contemporaneity of Miocene extension and shortening in the central Himalayan orogen was first suggested by Burchfiel et al. (1992) and Hodges et al. (1992), based on structural and age constraints. Hodges et al. (1993) proposed a model driven by gravitational compensation for extension along the South Tibetan Detachment System in the Mount Everest area in south Tibet. For the Central Annapurna Range, Hodges et al. (1996) improved this model, suggesting multistage extrusion of high-grade metamorphic rocks between thrusting at the MCT and normal movement at the South Tibetan Detachment System on the basis of structural observations and U/Pb age determinations. As these models are gravity-driven, the South Tibetan Detachment System is proposed to meet the MCT below the Tethyan Himalaya and consequently, the extruded slab displays the shape of a prism. Thus, both the mechanism and the geometry of these models differ considerably from the model proposed above.

The concurrence of thrusting along the MCT zone and extensional shearing is also confirmed by age constraints. Rb/Sr biotite cooling ages decrease from  $21 \pm 1$  Ma at the front of the Crystalline Nappe near the MCT zone to  $16 \pm 2$  Ma in the center of the Nappe (Frank et al. 1977). The 21 Ma age is interpreted as a maximum age for the exhumation of the Crystalline Nappe by thrusting along the MCT zone. Along the Zaskar Shear Zone, normal faulting occurred between 22 and 19.8 Ma (U/Pb,  $^{40}\text{Ar}/^{39}\text{Ar}$ , Dèzes et al. *subm.*) and in central Nepal, Pêcher et al. (1991) constrained the dextral strike-slip shearing along the South Tibetan Detachment System be-

tween 25 and 15 Ma., both periods coinciding with thrusting along the MCT zone.

#### Period D) Late stage phases (D<sub>A</sub>, D<sub>B</sub>, and D<sub>C</sub>)

The E-verging folds of D<sub>A</sub> point to E-W shortening, D<sub>B</sub> and D<sub>C</sub> reveal more an open folding in a NW-SE- and a WSW-ENE direction, respectively. These phases may account for late large-scale doming, exposed in the Kishtwar and Larji-Kullu-Rampur tectonic windows.

#### Metamorphic evolution

The tectonic evolution from period A to period C is related to two metamorphic cycles. Cycle 1 includes the metamorphism M<sub>1</sub>, related to the early deformation D<sub>1</sub> (period A) in the High Himalayan Crystalline. In section 3, M<sub>1</sub> reached garnet zone conditions and in section 4, M<sub>1a</sub> kyanite zone conditions and subsequent M<sub>1b</sub> sillimanite zone conditions are documented, indicating a prograde M<sub>1</sub> evolution from the garnet zone over the kyanite zone to the sillimanite zone.

Cycle 2 includes the stages of metamorphic crystallization M<sub>2</sub> to M<sub>5</sub> that are related to the deformational phases D<sub>2</sub> to D<sub>5</sub> (periods B and C). The evolution of cycle 2 is best documented in sections 3 and 4. In these sections, neither a tectonic nor a metamorphic discontinuity has been observed between the M<sub>2</sub> mineral zones. Consequently, M<sub>2</sub> is considered to represent a prograde Barrovian-type metamorphic evolution. Cycle 2 started with M<sub>2</sub> garnet zone conditions recorded in section 3, related to the formation of the NE-verging D<sub>2</sub> Shikar Beh Nappe. In section 4, the main metamorphism M<sub>2</sub> reached kyanite zone conditions. M<sub>3</sub>, associated to the subsequent formation of the SW-verging D<sub>3</sub> Main Fold Zone, is considered as a continuation of M<sub>2</sub> within kyanite zone conditions. This is also confirmed by observations from the neighbouring Kullu valley-Rohtang La area (Epard et al. 1995). Posterior to M<sub>3</sub>, the kyanite zone rocks underwent retrograde M<sub>4</sub> greenschist facies metamorphism at the base of the Crystalline Nappe, whereas in the central part of the nappe, they were overprinted by M<sub>5</sub> sillimanite zone conditions.

#### 8. Conclusions

The structural record in the Tethyan Himalaya, the High Himalayan Crystalline and the Lesser Himalayan Sequence permits a reconstruction of the tectonic evolution of the High Himalayan Range along the Spiti valley-eastern Lahul-Parvati valley traverse in Himachal Pradesh. The tectonic evolution is the consequence of eight phases of deformation D<sub>1</sub> to D<sub>8</sub>, acting perpendicular to the axis of the mountain chain and of three late stage phases D<sub>A</sub>, D<sub>B</sub> and D<sub>C</sub>, two of them acting more or less parallel to the axis of the mountain chain. In the High Himalayan Crystalline, the metamorphic evolution is exceptionally well documented by five stages of metamorphic crystallization that can be correlated with the tectonic evolution.

The oldest phase D<sub>1</sub> is documented as relics in the High Himalayan Crystalline. Its deformational conditions are poorly known, but the metamorphic conditions are well documented by a prograde metamorphism reaching peak conditions within the sillimanite zone. This indicates that D<sub>1</sub> was an important tectonometamorphic event including considerable crustal thickening. The structural, metamorphic and sedimentary record suggest that D<sub>1</sub> most probably occurred during an early stage of continental collision. D<sub>1</sub> predated the D<sub>2</sub> stacking of the Shikar Beh Nappe, that has until now been considered to be the oldest established structure in the NW Himalaya.

The oldest structure that is incontestably related to continental collision is the NE-verging D<sub>2</sub> Shikar Beh Nappe. Stacking of the Shikar Beh Nappe is interpreted to have initiated during incipient continental collision and early subduction of the Indian below the Asian continent far SW of the subduction zone, within the Indian continental crust. The Shikar Beh Nappe is considered to be a local feature in the NW Himalaya. However, it caused the main deformation and main metamorphism in the High Himalayan Crystalline, reaching kyanite zone peak conditions.

The common evolution of the High Himalayan Crystalline and the Tethyan Himalaya began with the SW-verging folds of the D<sub>3</sub> Main Fold Zone. The first F<sub>3</sub> folds developed below the front of the SW-verging north Himalayan nappes in the Tethyan Himalaya. In this area, D<sub>3</sub> and the associated lower greenschist facies metamorphism M<sub>3</sub> are the main deformation and metamorphism, respectively. Folding within the Main Fold Zone subsequently propagated toward SW into the High Himalayan Crystalline, where M<sub>3</sub> represents a continuation of M<sub>2</sub> kyanite zone conditions. Late D<sub>3</sub> folding coincided with early folding related to SW-directed D<sub>4</sub> thrusting of the Crystalline Nappe along the Main Central Thrust zone. The Main Fold Zone therefore represents a transitional phase of southward progressing deformation, from late stacking of the north Himalayan nappes that were thrust from the northern edge of the subducted Indian continent toward SW, to early SW-directed thrusting of the Crystalline Nappe.

During D<sub>4</sub>, the Crystalline Nappe, comprising the Main Fold Zone and relics of the Shikar Beh Nappe, was thrust toward southwest over the Lesser Himalayan Sequence along the 4 to 5 km-thick Main Central Thrust zone (MCT zone). During D<sub>4</sub> shearing, the whole MCT zone, including the base of the Crystalline Nappe and the uppermost Lesser Himalayan Sequence, was affected by a greenschist facies metamorphism M<sub>4</sub>. This metamorphism was prograde in the Lesser Himalayan Sequence and retrogressively overprinted the kyanite zone M<sub>2</sub>- and M<sub>3</sub> mineral assemblages at the base of the Crystalline Nappe. Contemporaneously, the central part of the Crystalline Nappe and the Tethyan Himalaya-High Hi-

malayan Crystalline transition beneath the north Himalayan nappe stack were affected by widespread NE-directed D<sub>5</sub> normal extensional shearing and concurrent dextral strike-slip motion. D<sub>5</sub> was accompanied by a change in metamorphic conditions to the sillimanite zone in the central part of the Crystalline Nappe. Thrusting at the base of the Crystalline Nappe and simultaneous normal movement in higher crustal levels are interpreted to indicate that the Crystalline Nappe was extruded between the Lesser Himalayan Sequence at the base and the north Himalayan Nappe system at the top, representing a high-grade metamorphic crustal slab, that was previously subducted under the north Himalayan nappes. Therefore, at the outset of thrusting along the MCT zone, the subduction zone stepped from the base of the north Himalayan nappes to the base of the Crystalline Nappe.

Extrusion of the Crystalline Nappe was followed by the phase D<sub>6</sub>, characterized by large-scale, open, upright to steeply inclined, NE-verging folds. This may indicate that thrusting at the MCT zone slowed down and that, as a consequence, thrusting could no longer accommodate all the crustal convergence, which resulted in backfolds and domes. D<sub>6</sub> folds were subsequently overprinted by another series of extensional structures D<sub>7</sub> (+D<sub>8</sub>) that may have operated simultaneously with a new period of thrusting along the MCT zone or that may have started when the Main Boundary Thrust developed SW of the MCT zone, representing a mechanism similar to nappe extrusion during D<sub>4</sub>/D<sub>5</sub>.

The late stage evolution was common in the Tethys Himalaya, in the High Himalayan Crystalline and in the Lesser Himalayan Sequence. It is represented by the phases D<sub>A</sub> and D<sub>B</sub> that indicate shortening parallel to the axis of the mountain chain and by D<sub>C</sub> that is interpreted to account for the formation of large-scale domes, an example of which is exposed in the Larji-Kullu-Rampur tectonic window.

#### Acknowledgments:

The study was financed by the University of Lausanne. Financial support for the field work was received from the Swiss National Science Foundation (FNRS grant 20-38917.93). Publication of the study was possible due to the generous financial support of the Dr. Joachim de Giacomo Foundation of the Swiss Academy of Natural Sciences. We thank Johannes Hunziker, Andreas Widler, David Rüttsche, Riccardo Casoli, Olivia Schweingruber, Sabrina Pastorelli, Annachira Bartolini and the Horseman Prehm Singh Negi with his helpers Juni Lal, Nathu and Gladbas for their scientific and infrastructural support during the 11 month of field work in the summers of 1993, 1994 and 1995. We are also grateful to Georges Mascle, Jean-Luc Epard and Jean-Claude Vannay for help and fruitful discussions and suggestions during writing of this paper. We greatly appreciate the help and linguistic revision of Neil Mancktelow, B. Clark Burchfiel and Johannes Hunziker, as well as critical comments of Mike Searle on an earlier version of the manuscript. Last but not least, we thank Raymond Ansermoz and Laurent Nicod for preparation of innumerable thin sections.

## REFERENCES

- BASSOULET, J.P., COLCHEN, M., JUTEAU, T., MARCOUX, J. & MASCLE, G. 1980: L'édifice des nappes du Zaskar (Ladakh-Himalaya). *C. R. Acad. Sc. Paris* 290 D, 389–392.
- BESSE, J., COURTILLOD, V., POZZI, J.P. & ZHOU, Y.X. 1984: Paleomagnetic estimates of Cenozoic convergence in the Himalayan Thrusts and Tsangbo suture. *Nature* 311, 621–626.
- BHARGAVA, O.N. 1980: Pre-Tertiary Orogenies in the Himalaya: A Review of various evidences. *Geol. Rundsch.* 69, 811–823.
- BHAT, M.I. & Le Fort, P. 1992: Sm-Nd age and petrogenesis of Rampur metavolcanic rocks, NW Himalayas: Late Archean relics in the Himalayan belt. *Precambrian Res.* 56, 191–210.
- BROOKFIELD, M.E. 1993: The Himalayan passive margin from Precambrian to Cretaceous times. *Sed. Geol.* 84, 1–35.
- BRUN, J.P., BURG, J.P. & MING, C.G. 1985: Strain trajectories above the Main Central Thrust (Himalaya) in southern Tibet. *Nature* 313, 388–390.
- BUCHER, K. & FREY, M. 1994: *Petrogenesis of Metamorphic Rocks*. Springer-Verlag Berlin, Heidelberg, New York, 318 pp.
- BURCHFIEL, B.C. & ROYDEN, L.H. 1985: North-south extension within the convergent Himalayan region. *Geology* 13, 679–682.
- BURCHFIEL, B.C., ZHILIANG, C., HODGES, K.V., YUPING, L., ROYDEN, L.H., CHANGRONG, D. & JIENE, X. 1992: The South Tibetan Detachment System, Himalayan Orogen: Extension contemporaneous with and parallel to shortening in a collisional mountain belt. *Spec. Pap. Geol. Soc. Am.* 269, 1–41.
- BURG, J.P., BRUNEL, M., GAPAIS, D., CHEN, G.N. & LIU, G.H. 1984: Deformation of leucogranites of the crystalline Main Central Sheet in southern Tibet (China). *J. Struct. Geol.* 6, 535–542.
- CHEMENDA, A.I., MATTAUER, M., MALAVIEILLE, J. & BOKUN, A.N. 1995: A mechanism for syn-collisional rock exhumation and associated normal faulting: Results from physical modeling. *Earth Planet. Sci. Lett.* 132, 225–232.
- DEWEY, J.F., CANDE, S. & PITMAN III W.C. 1989: Tectonic evolution of the India/Eurasia Collision Zone. *Eclogae geol. Helv.* 82, 717–734.
- DÉZES, P., VANNAY, J.C., STECK, A., BUSSY, F. & COSCA, M. in press: Synorogenic extension; quantitative constraints on the age and throw of the Zaskar Shear Zone (NW Himalaya). *Geol. Soc. Am. Bull.*
- EPARD, J.L., STECK, A., VANNAY, J.C. & HUNZIKER, J. 1985: Tertiary Himalayan structures and metamorphism in the Kulu Valley (Mandi-Khoksar transect of the Western Himalaya) – Shikar Beh Nappe and Crystalline Nappe. *Schweiz. Mineral. Petrogr. Mitt.* 75, 59–84.
- FRANK, W., HOINKES, G., MILLER, C., PURTSCHALLER, F., RICHTER, W. & THONI, M. 1973: Relations between Metamorphism and Orogeny in a Typical Section of the Indian Himalayas. *Tscherm. Min. Petr. Mitt.* 20, 303–332.
- FRANK, W., THONI, M. & PURTSCHALLER, F. 1977: Geology and petrography of Kulu-South Lahul area. *Colloq. int. C.N.R.S.* 268/2, 147–172.
- FRANK, W., BAUD, A., HONEGGER, K. & TROMMSDORFF, V. 1987: Comparative studies on profiles across the northwest Himalayas. In: SCHAEER, J.P. & RODGERS, J.: *The Anatomy of Mountain Ranges*. (Ed. by SCHAEER, J.P. & RODGERS, J.) Princeton University Press, Princeton, New Jersey, 261–275.
- FRANK, W., GASEMANN, B., GUNTLLI, P. & MILLER, C. 1995: Geological Map of the Kishtwar-Chamba-Kulu Region (NW Himalayas, India). *Jb. Geol. B.-A.* 138/2, 299–308.
- FUCHS, G. 1987: The Geology of southern Zaskar (Ladakh) – Evidence for the autochthony of the Tethys Zone of the Himalaya. *Jb. Geol. B.-A.* 130/4, 465–491.
- FUCHS, G. 1992: Pre-Alpine and Alpine Orogenic Phases in the Himalaya. In: A.K. Sinha (Ed): *Himalayan Orogen and Global Tectonics. The International Lithosphere Programme Publ.* 197, A.A. Balkema, Rotterdam, 19–34.
- GAETANI, M. & GARZANTI, E. 1991: Multicyclic History of the Northern India Continental margin (Northwestern India). *Bull. Amer. Assoc. Petroleum Geol.* 75 /9, 1427–1446.
- GAETANI, M., NICORA, A., PREMOLI-SILVA, E., FOIS, E., GARZANTI, E. & TINTORI, A. 1983: Upper Cretaceous and Paleocene in Zaskar range (NW Himalaya). *Rivista. Ital. Paleont. Stratigr.* 89/1, 81–118.
- GAETANI, M., GARZANTI, E. & TINTORI, A. 1990: Permo-Carboniferous stratigraphy in SE-Zaskar and NW-Lahul (NW Himalaya, India). *Eclogae geol. Helv.* 83/1, 143–161.
- GANSSER, A. 1964: *Geology of the Himalayas*. John Wiley & Sons, London, 289 pp.
- GAPAIS, D., PÉCHER, A., GILBERT, E. & BALLÈVRE, M. 1992: Synconvergence spreading of the higher Himalaya crystalline in Ladakh. *Tectonics* 11, 1045–1056.
- GARZANTI, E., CASNEDI, R. & JADOUL, F. 1986: Sedimentary evidence of a Cambro-Ordovician orogenic event in the Northwestern Himalaya. *Sed. Geol.* 48, 237–265.
- GARZANTI, E., BAUD, A. & MASCLE, G. 1987: Sedimentary record of the northward flight of India and its collision with Eurasia (Ladakh Himalaya, India). *Geodynamica Acta* 1, 297–312.
- GARZANTI, E., CRITELLI, S. & INGERSOLL, R.V. 1996: Paleogeographic and paleotectonic evolution of the Himalayan Range as reflected by detrital modes of Tertiary sandstones and modern sands (Indus transect, India and Pakistan). *Geol. Soc. Am. Bull.* 108/6, 631–642.
- GUNTLLI, P. 1993: *Geologie und Tektonik des Higher und Lesser Himalaya im Gebiet von Kishtwar, SE-Kashmir (NW Indien)*. Dissertation Nr. 10211 der ETH Zürich, 1–198.
- HAYDEN, H.H. 1904: The Geology of Spiti, with parts of Bashar and Rupshu. *Mem. Geol. Surv. India* 36, 1–129.
- HERREN, E. 1987: Northeast-southwest extension within the Higher Himalayas (Ladakh, India). *Geology* 15, 409–413.
- HODGES, K.V., PARRISH, R.R., HOUST, T.B., LUX, D.R., BURCHFIEL, B.C., ROYDEN, L.H. & CHEN, Z. 1992: Simultaneous Miocene extension and shortening in the Himalayan Orogen. *Science* 258, 1466–1469.
- HODGES, K.V., BURCHFIEL, B.C., ROYDEN, L.H., CHEN, Z. & LIU, Y. 1993: The metamorphic signature of contemporaneous extension and shortening in the central Himalayan orogen: data from the Nyalam transect, southern Tibet. *J. Metamorphic Geol.* 11, 721–737.
- HODGES, K.V., PARRISH, R.R. & SEARLE, M.P. 1996: Tectonic evolution of the central Annapurna Range, Nepalese Himalayas. *Tectonics* 15/6, 1264–1291.
- JAIN, A.K., GOEL, R.K. & NAIR, N.G.K. 1980: Implications of pre Mesozoic orogeny in the geological evolution of the Himalaya and Indo-Gangetic plains. *Tectonophysics* 62, 67–86.
- KÜNDIG, R. 1989: Domal structures and High-grade metamorphism in the Higher Himalayan Crystalline, Zaskar region, north-west Himalaya, India. *J. Metamorphic Geol.* 7, 43–55.
- MCKENZIE, D.P. & SCLATER, J.C. 1971: The evolution of the Indian Ocean since the Late Cretaceous. *Geophys. J. r. astron. Soc.* 24, 437–528.
- METCALFE, R.P. 1993: Pressure, temperature and time constraints on metamorphism across the Main Central Thrust Zone and the High Himalayan Slab in the Garhwal Himalaya. In: *Himalayan Tectonics*. (Ed. by TRELOAR, P.J. AND SEARLE M. P). *Geol. Soc. Spec. Publ. London* 74, 485–509.
- MOLNAR, P. & TAPPONNIER, P. 1975: Cenozoic tectonics of Asia: effects of a continental collision. *Science* 189, 419–426.
- PANDE, I.C. & SAXENA, M.N. 1968: Birth and development of the Himalayas. *Publ. Centre Adv. Study Geol., Punjab Univ.* 4, Chandigarh.
- PASSIER, C.W. & TROUW, R.A.J. 1996: *Microtectonics*. Springer-Verlag Berlin, Heidelberg, New York, 289 pp.
- PATEL, R.C., SANDEEP SINGH, ASOKAN, A., MANICKAVASAGAM, R.M. & JAIN, A.K. 1993: Extensional tectonics in the Himalayan orogen, Zaskar, NW India. In: *Himalayan Tectonics*. (Ed. by TRELOAR, P.J. AND SEARLE M. P). *Geol. Soc. Spec. Publ. London* 74, 445–459.
- PATRIAT, P. & ACHACHE, J. 1984: India-Eurasia collision chronology has implications for crustal shortening and driving mechanism of plates. *Nature* 311, 615–621.
- PÉCHER, A. 1991: The contact between the Higher Himalaya Crystallines and the Tibetan sedimentary series: Miocene large-scale dextral shearing. *Tectonics* 10, 587–598.
- PÉCHER, A. & SCAILLET, B. 1989: La structure du Haut-Himalaya au Gharwal (Indes). *Eclogae geol. Helv.* 82, 655–668. PÉCHER, A., BOUCHEZ, I.L. & LEFORT, P. 1991: Miocene dextral shearing between Himalaya and Tibet. *Geology* 19, 683–685.



- PIERCE, J. 1978: The northward motion of India since the Late Cretaceous. *Geophys. J. r. astron. Soc.* 52, 277–311.
- RAMSAY, J.G. & HUBER, M.I. 1987: The techniques of modern structural geology. Volume 1: Strain analysis, volume 2: Folds and fractures. Academic Press, London, 307 pp.
- SAXENA, M.N. 1973: Problems in Himalayan geology. *Geol. Rundsch.* 162, 563–581.
- 1980: Orogenic and epirogenic cycles in the Himalaya. *Himalayan Geology* 10, 191–210.
- SCOTese, C.R., GAHAGAN, L.M. & LARSON, R.L. 1988: Plate tectonic reconstructions of the Cretaceous and Cenozoic ocean basins. *Tectonophysics* 155, 27–48.
- SEARLE, M.P. 1986: Structural evolution and sequence of thrusting in the High Himalayan, Tibetan-Tethys and Indus suture zones of Zaskar and Ladakh, Western Himalaya. *J. Struct. Geol.* 8, 923–936.
- SEARLE, M.P. & REX, A.J. 1989: Thermal model for the Zaskar Himalaya. *J. Metamorphic Geol.* 7, 127–134.
- SEARLE, M.P., COOPER, D.J.W. & REX, A.J. 1988: Collision tectonics of the Ladakh-Zaskar Himalaya. *Philos. Trans. R. Soc. London A* 326, 117–150.
- SEARLE, M.P., WATERS, D.J., REX, D.C. & WILSON, R.N. 1992: Pressure, temperature and time constraints on Himalayan metamorphism from eastern Kashmir and western Zaskar. *J. Geol. Soc. London* 149, 753–773.
- SPEAR, F.S. 1993: Metamorphic Phase Equilibria and Pressure-Temperature-Time Paths. *Min. Soc. Am. Monograph*, Washington, D.C., 799 pp.
- SPRING, L. & CRESPO-BLANC, A. 1992: Nappe tectonics, extension and metamorphic evolution in the Indian Tethys Himalaya. *Tectonics* 11, 978–989.
- SPRING, L., MASSON, H., STUTZ, E., THÉLIN, P., MARCHANT, R. & STECK, A. 1993: Inverse metamorphic zonation in very low-grade Tibetan zone series of SE Zaskar and its tectonic consequences (NW India, Himalaya). *Schweiz. Mineral. Petrogr. Mitt.* 73, 85–95.
- SRIKANTIA, S.V. & BHARGAVA, O.N. 1982: An outline of the structure of the area between the Rohtang pass in Lahaul and the Indus valley in Ladakh. *Geol. Surv. India, Misc. Publ.* 41, 193–204.
- STECK, A., SPRING, L., VANNAY, J.C., MASSON, H., BUCHER, H., STUTZ, E., MARCHANT, R. & TIÉCHE, J.C. 1993a: Geological transect across the northwestern Himalaya in eastern Ladakh and Lahul (a model for the continental collision of India and Asia). *Eclogae geol. Helv.* 86, 219–263.
- STECK, A., SPRING, L., VANNAY, J.C., MASSON, H., BUCHER, H., STUTZ, E., MARCHANT, R. & TIÉCHE, J.C. 1993b: The tectonic evolution of the Northwestern Himalaya in eastern Ladakh and Lahul, India. In: *Himalayan Tectonics*. (Ed. by TRELOAR, P.J. AND SEARLE, M. P.). *Geol. Soc. Spec. Publ.* London 74, 265–276.
- STECK, A., EPARD, J.L., VANNAY, J.C., HUNZIKER, J., GIRARD, M., MORARD, A. & ROBYR, M. 1998: Geological transect across the Tso Moriri and Spiti areas – The nappe structures of the Tethys Himalaya. *Eclogae geol. Helv.* 91, 103–121.
- THONI, M. 1977: Geology, Structural Evolution and Metamorphic Zoning in the Kulu Valley (Himachal Himalayas, India) with Special reference to the Reversed Metamorphism. *Mitt. Ges. Geol. Bergbaustud. Österr.* 24, 125–187.
- VALDYIA, K.S. 1995: Proterozoic sedimentation and Pan-African geodynamic development in the Himalaya. *J. Precambrian Res.* 74, 35–55.
- VANNAY, J.C. 1993: Géologie des chaînes du Haut-Himalaya et du Pir Panjal au Haut-Lahul (NW Himalaya, Inde): Paléogéographie et tectonique. *Mém. Géol. Lausanne* 16, 1–148.
- VANNAY, J.C. & STECK, A. 1995: Tectonic evolution of the High Himalaya in Upper Lahul (NW Himalaya, India). *Tectonics* 14, 253–263.
- VANNAY, J.C. & GASEMANN, B. 1998: Inverted metamorphism in the High Himalaya of Himachal Pradesh (NW India): Phase equilibria versus thermobarometry. *Schweiz. Mineral. Petrogr. Mitt.* 78, 107–132.

Manuscript received August 13, 1997

Revision accepted October 8, 1998

Plate 1. Geological map and sections of the Spiti valley-eastern Lahul-Parvati valley traverse in the High Himalaya of northern Himachal Pradesh, established on the basis of an original 1:25000 scale survey. Geographical basis: satellite imagery SPOT 205-285 of 24. 8. 1986, SPOT 205-286/0 of 10. 10. 1994, SPOT 206-285/0 of 24. 8. 1986 and LANDSAT 147-38.0 of 25. 10. 1989.

# Tethyan Himalaya and High Himalayan Crystalline

Kulling Fm. (Upper Permian)	Siltstones, sandstones, shales, limestones, marls
Gamschikidam Fm. (Upper Permian)	Conglomerates, sandstones
Po Fm. (Middle to Upper Carboniferous)	Siltstones, sandstones, shales, limestones, marls
Lipak Fm. (Lower Carboniferous)	Limestones, dolomites, marls, sandstones, gypsum, shales
Muth Fm. (Middle Devonian)	Quartz sandstones
Thaple Fm. (Middle Ordovician)	Sandstones, siltstones, shales, dolomites
Karsu Fm. (Lower Cambrian)	Siltstones, greywackes, sandstones, dolomites
Hauaman Tibbu intrusion (Lower Ordovician)	Granites, granodiorites, orthogneiss
Mafic intrusions	Olivine gabbros, amphibolites

Phe Fm.  
(Precambrian to Lower Cambrian)

Siltstones, greywackes, sandstones
Slates, phyllites
Phyllites, garnet-bearing two-mica schists, biotite schists
Garnet, kyanite and/or sillimanite-bearing two-mica schists and schists
Chlorite- and biotite schists (D <sub>1</sub> shear zones)
Carbonaceous graphitic quartzites
Contact metamorphic zone

Bl in First appearance of biotite  
Gr in First appearance of garnet  
Thrust fault  
Normal fault  
Strike-slip fault

## Lesser Himalayan Sequence

Mélange zone	Phyllites, calcoschists and lenses of quartzite
Boring Group	Quartzite Chlorite- and biotite schists, phyllites

